

**Author Response to Referee #1 (Dr. Andreas Zuend) of “Influence of Organic Compound Functionality on Aerosol Hygroscopicity: Dicarboxylic Acids, Alkyl-Substituents, Sugars and Amino Acids”**

Aleksandra Marsh<sup>1</sup>, Rachael E. H. Miles<sup>1</sup>, Grazia Rovelli<sup>1</sup>, Alexander G. Cowling<sup>1</sup>, Lucy Nandy<sup>2</sup>, Cari S. Dutcher<sup>2</sup> and Jonathan. P Reid<sup>1</sup>

<sup>1</sup> School of Chemistry, University of Bristol, Bristol, BS8 1TS, UK

<sup>2</sup> Department of Mechanical Engineering, University of Minnesota, 111 Church Street SE, Minneapolis, MN 55455, USA

*Correspondence to:* Jonathan. P. Reid j.p.reid@bristol.ac.uk

The authors would like to thank the referee for their supportive comments and the additional suggestions they have made for minor revision. We respond to these comments below.

*Referee Comment:* P5, Eq. (5): correct the symbol for saturation vapour pressure (currently  $\rho^\circ$  “rho”) to  $p^\circ$ . This would be a more typical choice, would be in agreement with the expression given by Rovelli et al (2016) and avoids use of rho which stands for density in Eq. (2). Also, on line 15, correct spelling of “Fuchs-Sutugin” (only one t).

*Response:* Both of these changes have been made on page 5.

*Referee Comment:* P5, line 5. (Related to the response to my initial comment P 7, l. 2): “When referring to gradient in the text, we are referring to the gradient in water partial pressure and we believe this is correct. We do not refer to a gradient formed from (RH-aw). To be consistent with our previous publications, we have removed the subscript i entirely from the equation but not replaced it with w.”

*The revised sentence reads:* “In this equation, the gradient in water partial pressure is the difference between the RH and  $a_w$ , the instantaneous water activity at the droplet surface.”

*This remains a confusing description of what the equation actually states (and a more fitting description is given in Rovelli et al). First, “the difference between the RH and  $a_w$ ” (i.e.  $RH - a_w$ ) is simply not a (mathematical) gradient; rather it is a difference. A gradient is for example a difference per unit distance or its equivalent in partial differential form, but it is not simply a difference as implied in the statement. Second, “the difference between the RH and  $a_w$ ” is not the gradient in water (vapour) partial pressure and does not directly represent it, even though there exist similar mass flux expressions with differences in partial pressures or differences in vapour densities as part of the formula. Both gradients as well as differences in water vapour partial pressures carry units different from  $RH - a_w$ . Third, from the given statement it is unclear to what “the instantaneous water activity at the droplet surface” refers to: should it refer to RH or to  $a_w$ ? This needs to be clarified in the text as well as pointing out that RH in this equation refers to  $RH_\infty$ , the RH in the surrounding gas phase sufficiently far away from the droplet surface ( $S_\infty$  in Rovelli et al.).*

*Response:* We apologise to the lack of clarity remaining in this sentence and have now reworded it to read: “In this equation, the difference in water partial pressure between infinite distance and the droplet surface, which drives diffusional mass transport in the gas phase, is quantified by the difference between the RH and the instantaneous water activity at the droplet surface,  $a_w$ , respectively. This difference, a fraction of 1, should be considered in combination with the saturation vapour pressure  $p^\circ$  which appears in the denominator of the first bracketed term in the equation, giving the true difference in vapour pressure between infinite distance and the droplet surface.”

*Referee Comment: P10, line 29: I suggest to modify the new sentence to read: “Hence thermodynamic model predictions for amino acids were generated using E-AIM, Model III (Clegg et al., 1998), using the standard UNIFAC model including certain modified main group interaction parameters introduced by Peng et al. (2001).” This modification is more clear in that it does not imply that Peng et al. parameterized the whole UNIFAC model (they only modified a small subset of main group interaction parameters).*

Response: This has been added as suggested.

*Referee Comment: P12, line 15 (related to Referee Comment: P12, l. 27: “Molecular structures presented in Fig. 10 are the open chain form, which must be used during modelling using UNIFAC.”; Why “must”? AIOMFAC also allows you to use the cyclic structure of sugars in aqueous solution, e.g. glucopyranose instead of glucose, if desired.*

*“Cyclic sugar structures do not appear to be available on AIOMFAC-web. Amended P11 L27 to read ‘Molecular structures presented in Fig. 10 are the open chain form, which must be used during modelling using AIOMFAC-web.’”*

*I do not understand how the authors come to that “which must be used” conclusion about the availability of cyclic sugar structures in AIOMFAC-web. AIOMFAC-web allows you to select from a wide range of organic subgroups and there is no problem in choosing those subgroups referring to cyclic sugar structures to define an organic compound (using the option “Define Subgroups” on the input form for organic compounds). There are even examples given in the “Predefined List” input option, e.g. for D-mannopyranose,  $(\text{CH}_2^{\text{[OH]}})(\text{CH}^{\text{[OH]}})_4(\text{CHO}^{\text{[ether]}})(\text{OH})_5$ , the cyclic structure equivalent of the open-chain form of mannose. The manuscript text should be corrected and the authors may want to check whether replacing the open chain forms in Fig. 10 by equivalent cyclic sugar structures would lead to significantly different model curves.*

Response: We are very sorry for this misunderstanding, we were not initially aware of how to represent these sugars in their cyclic form in AIOMFAC-web but the referee’s comment has been helpful at correcting this. Predictions for galactose and xylose have now been generated in their cyclic forms and the results are summarised in the Table below, also included in the Supplementary Information. An additional Figure (S40.0) has been provided in the supplementary information to clarify the difference between the open chain and cyclic predictions for these two compounds. However, we have not added these predictions to Figure 10 - we feel that the addition of further curves would make the figure too cluttered. UNIFAC predictions for trehalose are in its cyclic form.

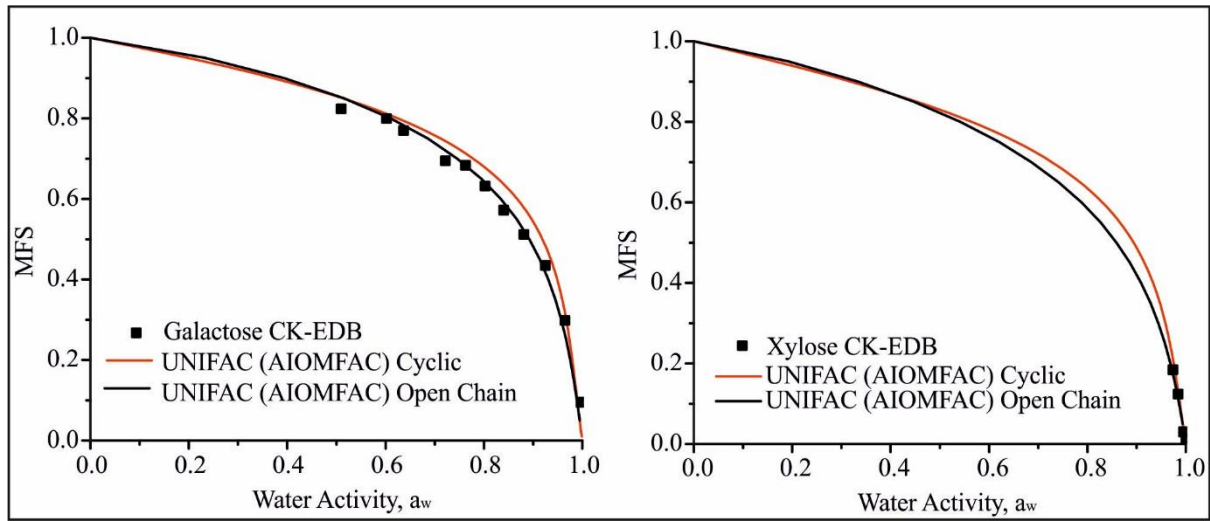
**Table S40.0: Table of UNIFAC groups for cyclic and open chain galactose and xylose.**

Compound	Open Chain (In Manuscript)	Cyclic
Galactose	$\text{CHO}(\text{CH}_1^{\text{[OH]}})_4\text{CH}_2^{\text{[alc]}}(\text{OH})_5$	$(\text{CH}^{\text{[alc]}})_4(\text{CH}_2^{\text{[OH]}})(\text{CHO}^{\text{[ether]}})(\text{OH})_4$
Xylose	$(\text{CH}_2(\text{OH}))_3\text{CH}_2^{\text{[alc]}}\text{CHO}(\text{OH})_4$	$(\text{CH}^{\text{[OH]}})_4(\text{CHO}^{\text{[ether]}})(\text{OH})_4$

Further, we have deleted P12 L15-16: ‘Which must be used during modelling with AIOMFAC-web.’

We have added P12 L15-16: ‘Molecular structures presented in Fig. 10 are the open chain form for galactose and xylose and trehalose is represented using its cyclic form. Comparison of predictions for the open chain and cyclic structural forms for xylose and galactose are shown in Figure S40.0’

**Figure S40.0 Galactose and Xylose CK-EDB data as a function of MFS and water activity compared with predictions for both cyclic and open chain UNIFAC group thermodynamic predictions.**



# Influence of Organic Compound Functionality on Aerosol Hygroscopicity: Dicarboxylic Acids, Alkyl-Substituents, Sugars and Amino Acids

Aleksandra Marsh<sup>1</sup>, Rachael E. H. Miles<sup>1</sup>, Grazia Rovelli<sup>1</sup>, Alexander G. Cowling<sup>1</sup>, Lucy Nandy<sup>2</sup>,  
5 Cari S. Dutcher<sup>2</sup> and Jonathan. P Reid<sup>1</sup>

<sup>1</sup> School of Chemistry, University of Bristol, Bristol, BS8 1TS, UK

<sup>2</sup> Department of Mechanical Engineering, University of Minnesota, 111 Church Street SE, Minneapolis, MN 55455, USA

Correspondence to: Jonathan. P. Reid j.p.reid@bristol.ac.uk

10  
**Abstract.** Hygroscopicity data for 36 organic compounds including amino acids, organic acids, alcohols and sugars is determined using a Comparative Kinetics Electrodynamic Balance (CK-EDB). The CK-EDB employs an electric field to trap charged aqueous droplets in a temperature and relative humidity (RH) controlled chamber. The dual micro dispenser set up allows for sequential trapping of probe and sample droplets for accurate determination of droplet water activities from 0.45 to  
15 > 0.99. Here, we validate and benchmark the CK-EDB for the homologous series of straight chain dicarboxylic acids (oxalic – pimelic) with measurements in better agreement with UNiversal quasichemical Functional group Activity Coefficients (UNIFAC) predictions than the original data used to parametrise UNIFAC. Further, a series of increasingly complex organic compounds, with subtle changes to molecular structure and branching, are used to rigorously assess the accuracy of predictions by UNIFAC, which does not explicitly account for molecular structure. We show that the changes in hygroscopicity that result  
20 from increased branching and chain length are poorly represented by UNIFAC, with UNIFAC under-predicting hygroscopicity. Similarly, amino acid hygroscopicity is under-predicted by UNIFAC predictions, a consequence of the original data used in the parametrisation of the molecular subgroups. New hygroscopicity data are also reported for a selection of alcohols and sugars and show variable levels of agreement with predictions.

## 1. Introduction

25 The hygroscopicity of an aerosol can be defined as the capacity of an aerosol particle to absorb water and quantifies the equilibrium partitioning of water between the gas and condensed phases (Krieger et al., 2012). Aerosol hygroscopic growth impacts directly on the radiative balance of the atmosphere, with the size and refractive index of aerosol particles influencing their light scattering and absorption cross-sections (Ravishankara et al., 2015;Moise et al., 2015). Similarly, the hygroscopic response of aerosol impacts on the transport of chemical components in the environment and on atmospheric chemical  
30 composition through heterogeneous chemistry and cloud chemistry with implications for air quality (Akimoto, 2003;Farmer et al., 2015;Hallquist et al., 2009). The activation of cloud condensation nuclei (CCN) to form cloud droplets is governed by

hygroscopic response as well as aerosol size distribution, leading to the indirect effect of aerosols on climate (Farmer et al., 2015;Lohmann and Feichter, 2005). Furthermore, hygroscopic growth on inhalation can influence the depth of penetration of aerosol into the respiratory system, with consequences for the impact of ambient aerosol and particulate matter on rates of morbidity and mortality (Haddrell et al., 2015;Pöschl and Shiraiwa, 2015). Thus, an improved characterisation and  
5 quantification of the hygroscopic response of ambient aerosol is important for more accurate predictions of the radiative forcing of aerosol, their impact on air quality and their consequences for human health.

Atmospheric aerosol are composed of a plethora of inorganic and organic species from a diverse range of biogenic and anthropogenic sources including inorganic salts, sulphates, nitrates, metals and organic compounds, such as acids, alcohols,  
10 amino acids and sugars (Baltensperger, 2016;Seinfeld and Pankow, 2003;Zhang et al., 2015). Organic species can dominate ambient fine aerosol mass (particles < 1µm in diameter) and have varying degrees of oxidation, molecular mass, hygroscopicity and volatility (Jimenez et al., 2009;McNeill, 2015). Further, the composition of ambient aerosol is constantly changing due to heterogeneous reaction chemistry (Hallquist et al., 2009;Jimenez et al., 2009;Pandis et al., 1995;Ziemann and Atkinson, 2012), varying relative humidity (RH) and temperature (Farmer et al., 2015), and photochemistry (Jacob, 2000;George et al., 2015).

The equilibrium response of an aerosol to changes in ambient RH is described by the Köhler equation, which is a product of the solution water activity (the solute term) and a correction for surface curvature (the Kelvin term) (Wex et al., 2008). The solute term, representing the dependence of the equilibrium water activity on the composition of the solution of inorganic and organic compounds, can be determined from thermodynamic models that represent in detail the non-ideal interactions between  
15 the ionic and neutral species within the solution. Based on parameterisations from experimental data, these models include the Aerosol Inorganic/Organic Mixtures Functional groups Activity Coefficients (AIOMFAC) (Zuend et al., 2008;Zuend et al., 2011), the Extended Aerosol Inorganic Model (Wexler and Clegg, 2002;Clegg et al., 1998), and UManSysProp (Topping et al., 2016) which allow calculation of the activity coefficients that characterise the non-ideality of the aqueous solutions. The key challenges in generating accurate predictions include capturing accurately the non-ideality of solutions, particularly under  
20 very dry conditions/high solute concentrations (Dutcher et al., 2013;Nandy et al., 2016;Ohm et al., 2015), ion-neutral interactions in mixed inorganics/organics (Zuend et al., 2008;Zuend et al., 2011;Losey et al., 2016), the acidity and basicity of solutes (Rindelaub et al., 2016), liquid-liquid phase separation (Zuend and Seinfeld, 2012), solubility (Pajunoja et al., 2015) and the co-condensation of semi-volatile organic compounds (SVOC) with increase in water fraction (Topping et al., 2013). To treat the organic component, AIOMFAC, E-AIM and UManSysProp use the UNiversal quasichemical Functional group  
25 Activity Coefficients (UNIFAC) method developed by Fredenslund et al. (Fredenslund et al., 1975). In this approach, molecules are divided into characteristic molecular subgroups and the activity coefficients derived from group contributions with limited consideration for molecular structure. AIOMFAC-web implements several improved parameters which are detailed by Zuend et al. (2011).

In UManSysProp, compounds are specified using the Simplified Molecular Input Line Entry System (SMILES) which are then converted to UNIFAC groups within the programme. Using these approaches, Petters et al. have shown that the CCN activity of organic compounds can be modelled using group contribution methods (Petters et al., 2016).

5 Despite their accuracy, the use of group contribution methods to predict the water uptake for a larger number of organic components in ambient aerosol is too computationally expensive for inclusion in regional chemical transport and climate models. Reduced parameter models are instead required to represent the thermodynamic properties of ambient organic aerosols.  $\kappa$ -Köhler theory characterises the solute component of hygroscopic growth by a single parameter  $\kappa$  applicable in the limit of dilute aqueous solution aerosol (Kreidenweis et al., 2008; Petters and Kreidenweis, 2007). It must be assumed that the  
10 compounds are fully soluble and the aerosol does not undergo phase separation. The value of  $\kappa$  spans from a value close to 0 for un-hygroscopic/hydrophobic components to a value around 1 for the most hygroscopic inorganic salts (Kreidenweis et al., 2008; Petters and Kreidenweis, 2007). Values are typically determined from sub-saturated hygroscopic growth measurements and reported at the highest accessible RH (Pajunoja et al., 2015). The value of  $\kappa$  can also be inferred from measurements of the critical supersaturation required for CCN activation, a measurement in a super-saturated regime (Carrico et al., 2008).  
15 Further,  $\kappa$  values reported at different RHs can vary significantly and can also differ substantially from measurements in the supersaturated regime, (Hodas et al., 2016). Despite the inherent approximations, reported values of  $\kappa$  provide a way of linking the hygroscopicity of complex ambient aerosol with empirical measurements of chemical functionality such as the level of oxidation, often reported as the ratio O:C from aerosol mass spectrometry measurements (Jimenez et al., 2009; R. Y.-W. Chang et al., 2010). Possible correlations of  $\kappa$  with chemical composition (particularly O:C) have been extensively explored and  
20 reviewed (Rickards et al., 2013; Suda et al., 2014).

Although many ambient measurements of  $\kappa$  have been made, there remains a necessity to rigorously address some of the challenges in quantifying aerosol hygroscopicity through controlled laboratory measurements on well-characterised aerosol of known composition. Dicarboxylic acids from  $C_1 - C_7$  have been studied extensively in the literature and have been used as the  
25 basis for providing revisions of UNIFAC for typical organic components found in the atmosphere (Peng et al., 2001). Further, previous laboratory studies have examined correlations of  $\kappa$  with composition, and have focussed on identifying the influence of certain key functional groups on  $\kappa$ . For example, Suda *et al.* (2014) have studied the systematic impact on  $\kappa$  of hydroxyl, carboxyl, peroxy, nitro and alkene groups of varying carbon chains lengths ( $C_1 - C_{25}$ ) (Suda et al., 2014). However, there remain many gaps in hygroscopicity data for a number of compound classes, including; highly branched dicarboxylic acids,  
30 multifunctional compounds (including ring containing species), amino acids, organo-sulphates and nitro compounds.

We report here a systematic study of the hygroscopicity of a large number of organic compounds (listed in Table 1.) of varying functionality, solubility and molecular weight. This work benefits from the application of a novel electrodynamic balance (EDB) method that offers significant advantages over both alternative single particle techniques and ensemble experimental

5 setups (Rovelli et al., 2016; Davies et al., 2013). Measurements can be made at high water activities (approaching values very close to 1) with a very accurate comparative kinetics method for determining the gas phase RH. The timescale for the measurement to record the whole growth curve is <10 s, sufficiently fast that the growth curves of organic species with vapour pressures of >1 Pa can be measured without significant volatilisation of the organic species. A temperature regulated chamber allows for stable and prolonged temperature control of the trapping region in the range -25°C – +50°C. The use of piezo-electric droplet-on-demand dispensers allows for the use of small sample volumes, allowing measurements on expensive (small amounts) of test compounds or the use of even filter collected samples. Measurements are made on droplets spanning the radius range from 4 – 30 µm, avoiding the additional complexity of correcting the hygroscopic growth measurement for the surface curvature term and providing an unambiguous measurement of the solute term (Rovelli et al., 2016).

10 More specifically, we will present hygroscopic data for 36 organic compounds from 4 distinct compound classes. A series of 17 dicarboxylic acids, with subtle differences to molecular branching and chain length, are used to examine the impact of structural isomerisation on water uptake. Measurements are also presented for a series of amino acids; despite their extensive release from biogenic sources, their hygroscopic properties have yet to be fully characterised (Chan et al., 2005). Although the UNIFAC model predicts water uptake of simple structures reasonably well, we will show that increasing molecular complexity and inclusion of nitrogen containing groups leads to considerably poorer prediction of hygroscopicity. Following an introduction to the methods and materials in Sect. 2, we will present the results for these different compound classes in Sect. 3.

## 2. Methods and Materials

20 Hygroscopicity studies are presented with measurements from a comparative kinetics technique applied in an EDB instrument, (referred to as the comparative kinetics EDB, CK-EDB, below) with electrodes in a concentric cylindrical arrangement. The full experimental details for the CK-EDB have been discussed extensively in previous publications and will only be briefly reviewed here (Rovelli et al., 2016; Davies et al., 2013), along with a discussion of the treatments used for parameterising solution density and refractive index (Cai et al., 2016). Purity and supplier for all compounds is presented in the supplementary information. Further, all measurements presented in this work are taken at 293.15 K. All solutions are prepared using HPLC grade water (VWR Chemicals).

### 2.1 The Comparative Kinetics Electrodynamic Balance

25 The CK-EDB can be used to probe the hygroscopic growth of aerosol particles from low to high water activities (<0.45 to >0.99) with a greater accuracy (<±0.2 % error in water activity at water activities > 0.8 and ±1 % error in water activity at water activities < 0.8) than can be achieved in conventional approaches (Rovelli et al., 2016). The CK-EDB employs an electric field to trap a charged dilute aqueous droplet starting at a water activity > 0.99. The droplet evaporates towards an equilibrium

composition set by the RH of the surrounding gas flow; the RH is determined accurately from an independent measurement of the evaporation profile of a probe droplet of known hygroscopic response (either a pure water droplet or an aqueous sodium chloride solution droplet). The time-dependence in size and composition of the sample droplet (typically over a period of ~10 s) is then used to infer the hygroscopic equilibrium growth curve over the full range in water activities experienced by the droplet during evaporation. The reader is referred to Rovelli et al. (2016) and Davies et al. (2013) for a full description of the method and the analysis.

A pulse voltage is consecutively applied to two droplet dispensers (MicroFab MJ-ABP-01, orifice size 30  $\mu\text{m}$ ) to sequentially generate probe and sample droplets of known starting solute concentration. The droplets are charged by an induction electrode and are trapped within the electric field of the cylindrical electrodes within 100 ms of generation. Thermally regulated water channels through the electrodes and chamber body allow the temperature to be carefully controlled ( $-25^\circ\text{C} - +50^\circ\text{C}$ ) by a refrigerated circulator (F32-ME, Julabo) using a mixture of polyethylene glycol and water. Humidified nitrogen gas flows vertically through the cylindrical electrodes and allows control of the gas phase RH of the chamber (total flow 200  $\text{mL min}^{-1}$  equivalent to a gas velocity of 3  $\text{cm s}^{-1}$ ). Evaporating droplets are illuminated with a 532 nm laser (Laser Quantum Ventus CW laser) and the elastic scattered light is collected using a CCD camera over a range of angles near a scattering angle of  $45^\circ$ . The droplet radius ( $r$ ) is first estimated using the geometric optics approximation (error  $<\pm 1\%$  for droplets  $> 10\ \mu\text{m}$ ) and the angular separation of fringes in the phase function ( $\Delta\varphi$ , radians) (Glantschnig and Chen, 1981),

$$r = \frac{\lambda}{\Delta\varphi} \left( \cos \frac{\varphi}{2} + \frac{n \sin \frac{\varphi}{2}}{\sqrt{1 + n^2 - 2n \cos \frac{\varphi}{2}}} \right)^{-1} \quad (1)$$

where  $n$  is the refractive index of the droplet,  $\lambda$  is the incident laser wavelength and  $\varphi$  is the median observation angle. Initially, during data collection  $n$  is assumed to be that of water. However, this assumption is corrected in subsequent data processing for the change in  $n$  during evaporation; the compositional dependencies of density and  $n$  are described below.

## 2.2. Molar Refraction: Refractive Index and Density Treatments

Solutes in aerosol droplets can reach supersaturated concentrations as water evaporates. Thus, to represent the solution density and refractive index, bulk measurements are insufficient and must be extrapolated to account for the full compositional range, i.e. the entire range in mass fraction of solute, MFS or  $\phi_s$ , from 0 to 1. We have recently provided a comprehensive assessment of the parameterisations that can be used to predict the density and refractive index of supersaturated organic solutions, and we summarise below the recommendations of this study relevant to their application in this work (Cai et al., 2016).

Aqueous solutions of an organic solute are prepared up to the solubility limit of the compound, and the density and refractive index are measured using a vibrating capillary density meter (Mettler Toledo Densito, accuracy  $\pm 0.001\ \text{g.cm}^{-3}$ ) and a

refractometer (Misco Palm Abbe, accuracy  $\pm 0.0001$  at 589 nm), respectively. If the solubility of the organic solute allows measurements above an MFS of  $\sim 0.4$ , a third order polynomial in  $\phi_s^{0.5}$  is fit to the bulk solution density values (where  $\phi_s$  is the MFS). If bulk measurements are limited by solubility to an upper limit in MFS  $< 0.4$ , an ideal mixing treatment is applied to the bulk density values to allow the estimation of the density of the solute,  $\rho_s$ , constraining the bulk data to the equation:

$$5 \quad \frac{1}{\rho_{em}(1-\phi_s)} = \frac{\phi_s}{(1-\phi_s)\rho_s} + \frac{1}{\rho_w} \quad (2)$$

where  $\rho_{em}$  is the mass density of the mixture and  $\rho_w$  the density of water. These two approaches assume that the density of the pure organic solute ( $\rho_s$ ) is not known; under the conditions of aqueous solution aerosol measurements, the density of the solute corresponds to that of the pure sub-cooled melt with most pure organic compounds instead existing in a crystalline form at room temperature. Further details of the density measurements and parameterisations for all systems studied are provided in the Supplementary Information Section.

Once the dependence of solution density on MFS is established, a fit of the bulk solution refractive indices is constrained to follow the molar refraction mixing rule (Liu and Daum, 2008):

$$15 \quad R_e = \left( \frac{n^2-1}{n^2+2} \right) \left( \frac{M_e}{\rho} \right) \quad (3)$$

where  $n$  is the refractive index of the mixture,  $M_e$  the effective molecular weight and  $R_e$  is the molar refraction of the mixture. This allows the estimation of the molar refraction of the pure organic solute, again as a sub-cooled melt. In subsequent use, the molar refraction can be calculated for solutions of any composition,

$$R_e = (1 - x_s)R_w + x_sR_s \quad (4)$$

20 and the value of  $n$  for the solution determined by solving for  $n$  from equation (3). Pure component refractive indices, determined using the molar refraction mixing rule are presented in the Supplementary Information Sections alongside parameterisations of aqueous solution densities and sub-cooled pure component melt densities. Values of aqueous density and refractive index as a function of compound mass fraction are available in the supplementary information in Cai et al. (2016). Further in SI Fig S37.1 we consider the impact of uncertainties in density and refractive index treatments to the measured hygroscopicity, for all compounds shown, the error envelope on hygroscopicity is smaller than the size of the points.

### 2.3. Extraction of Hygroscopicity properties

During the evaporation of an aqueous droplet, the mass flux ( $J$ ) of water can be estimated at each recorded time step from the change in size and the associated density for the known composition of the droplet at that time, starting with a generated droplet of known solution composition. At each time step, the loss in mass is associated solely with loss of water, allowing a calculation of the new MFS and, thus, new values of  $n$  and density. The new value of  $n$  allows a refinement of the estimated radius, with

full details (Davies et al., 2012). The mass flux can then be used to determine the gradient in water partial pressure in the gas phase using an analytical treatment (Kulmala et al., 1993), with

$$I = -4 Sh \pi r (RH - a_w) \left( \frac{RT_\infty}{M \beta_M D r \rho^0(T_\infty) A} + \frac{a_w L^2 M}{R \beta_T K T_\infty^2} \right)^{-1} \quad (5)$$

Deleted:  $\rho^0$

5 which accounts for the limiting influence of heat transport, due to latent heat lost, on the mass flux. In this equation, the difference in water partial pressure between infinite distance and the droplet surface, which drives diffusional mass transport in the gas phase, is quantified by the difference between the RH and the instantaneous water activity at the droplet surface,  $a_w$ , respectively. This difference, a fraction of 1, should be considered in combination with the saturation vapour pressure  $p_s^0$  which appears in the denominator of the first bracketed term in the equation, giving the true difference in vapour pressure between  
 10 infinite distance and the droplet surface. The RH is determined from the probe droplet measurements, as described previously (Rovelli et al., 2016). In this study, the probe droplets are trapped in exactly the same position within the gas flow as the sample droplets which allows the measurement of the RH in situ. The probe droplets are either pure water (for the RH range 80 – 99 %) or aqueous NaCl (for the RH range 50 – 80 %). All quantities in this equation are known apart from  $a_w$  and this can be estimated for every time-step by rearranging the equation to solve for  $a_w$ .  $Sh$  is the Sherwood number, accounting for the  
 15 enhancement in evaporation rate due to the moving gas flow over the droplet, and  $r$  is droplet radius, measured experimentally.  $R$  is the ideal gas constant,  $T_\infty$  is the ambient temperature,  $M$  is the molecular mass of water,  $D$  is the binary diffusion coefficient of water in nitrogen and  $\rho^0$  is the saturation vapour pressure.  $A$  is a correction factor for Stefan flow,  $K$  is thermal conductivity and  $L$  is the latent heat of vaporization of water at  $T_\infty$ . Finally  $\beta_M$  and  $\beta_T$  represent the Fuchs-Sutugin correction factors for mass and heat flux, respectively.

Formatted: Superscript

Deleted: In this equation, the gradient in water partial pressure is the difference between the RH and  $a_w$ , the instantaneous water activity at the droplet surface.

20

It is imperative that the evaporative cooling be accounted for as this suppresses the apparent vapour pressure at any instant, particularly at early time when the mass flux is larger. Indeed, equation (5) explicitly accounts for the latent heat lost from the droplet. At very early times and when evaporating into low RH, the temperature suppression can be sufficient (>3 K) so as to reduce the accuracy of approximations made when deriving equation 5. Under these circumstances, when the temperature  
 25 suppression is larger than this limit, we do not infer equilibrium water activities, but instead only retrieve the equilibrium hygroscopic growth when the temperature suppression is smaller than 3 K. This procedure has been discussed and verified in detail in our earlier work, and the reader is referred to Rovelli et al. (2016) for further details.

Deleted: t

The time-dependent data can also be used to estimate sub-saturated values of  $\kappa$  from (Petters and Kreidenweis, 2007)

$$30 \quad GF = \left( 1 + \kappa \frac{a_w}{1 - a_w} \right)^{\frac{1}{3}} \quad (6)$$

where  $GF$  represents the radius growth factor which is a ratio between the wet droplet radius and dry particle radius. The dry size is estimated from the known starting size of the solution droplet and the starting concentration (MFS) of solutes. Time-

dependencies in radius for a number of compounds with different  $\kappa$  values are shown in Fig. 1(a), illustrating how the CK-EDB experiment can discriminate between compounds of different  $\kappa$  during evaporation. For increasingly hygroscopic aerosol, there is a trend to a final equilibrated size that is larger and the temporal dependence of radius shows a shape that is characterised by less rapid loss of water. A caveat must be noted, however: the profiles do also depend on starting size, solute concentration and the exact RH of the chamber, factors which are all explicitly accounted for in the full quantitative analysis. Values of  $\kappa$  for all compounds studied are reported at  $a_w = 0.95$  in Table 1. It should be recognised that the apparent value of  $\kappa$  varies with the RH at which it is reported (Rickards et al., 2013).

During a typical experiment, measurements of sample and probe droplets are taken sequentially at several steady RHs, typically 50, 60, 70 and 80 % using an aqueous NaCl probe droplet and 80 and 90 % with a water probe droplet. Furthermore, at each measured RH, 10 sample and probe droplets are taken to ensure measurement reproducibility. Final hygroscopicity data is averaged (binned in small steps in RH) and presented as a function of MFS against water activity; full hygroscopicity curves are typically the result of measurements from between 30 – 80 droplets. It must be noted that kappa,  $\kappa$ , values are calculated using all data points before the binning process. In Fig. 1(b) we show typical time-dependencies in radius for a series of aqueous-glycine droplets evaporating into four different RHs. The final hygroscopicity curve for glycine is shown in Fig. 1(c): the large orange points represent data which have been averaged (binned in  $a_w$  steps) from 100's of data points measured from ~50 droplets.

### 3. Results and Discussion

Graphical and tabulated hygroscopicity curves for all 36 compounds studied, UNIFAC predictions, density parametrisations, refractive index values and compound purities are available as Supporting Information. Here, we summarise and compare the behaviour observed for the different classes of chemical compounds studied and consider the trends observed in the value of the parameter  $\kappa$ .

#### 3.1. Hygroscopic Response of Dicarboxylic Acids of Varying Complexity

Structurally similar organic acids were chosen to examine the relationship between the hygroscopicity of binary component aerosol and the degree of carbon-chain branching, chain length and O:C ratio; some of the compounds chosen are identified in Fig. 2(a) and (b). All experimental hygroscopicity data are compared with thermodynamic predictions from the UNIFAC model to assess whether compound hygroscopicity is accurately represented. All calculations for dicarboxylic acids were performed using the AIOMFAC-web model.

As a benchmark test, we consider the homologous series of dicarboxylic acids,  $\text{HOOC}(\text{CH}_2)_n\text{COOH}$ , from oxalic to pimelic acid (i.e. with  $n=0$  to 5) in Fig. 2(a). The UNIFAC model predictions mostly agree closely with experimental observations at

moderate to high water activity with some deviation at lower water activity although pimelic acid is an exception with experimental data deviating significantly from the model prediction. In Fig. 2(b) we compare data from a series of compounds with a malonic acid backbone, but with varying alkyl substituents (methyl, dimethyl and diethyl). The trend towards decreasing hygroscopicity with increasing hydrophobicity (increasing number and length of alkyl substituents) on a mass basis is clear, recognised from observing that there is less water associated with the solution at constant water activity as the molecular weight increases. In addition, the UNIFAC predictions become less accurate as the added substituent becomes larger. The approach used here is particularly valuable for low solubility organic compounds as dilute solutions at high water activity provide the starting point for the measurement. For example, the dry particle size must be measured using a Hygroscopic Tandem Differential Mobility Analyser (HTDMA), necessarily setting a lower limit on the concentration of solutes use when atomising solutions to form aerosol. In addition, the short timescale of the measurement ensures that evaporation of the semi-volatile components, such as these dicarboxylic acids, is avoided.

We compare the measurements reported here with previous data (Peng et al., 2001) in Fig. 3(a)-(d) and Fig S38.1(a)-(d) for the straight chain dicarboxylic acids for which comparison can be made, oxalic, malonic, succinic and glutaric acid. The comparisons made in Fig. 3(a)-(d) act as a form of method validation, extending our previous work; bulk and EDB measurements (Peng et al., 2001) are presented alongside our CK-EDB data and UNIFAC predictions, with good agreement for all systems. Further to this, Fig S38.1(a)-(d) show the dependence on water activity of the difference in MFS ( $\Delta$ MFS) between the current experimental data or the previously published data (Peng et al., 2001) and UNIFAC predictions, allowing a quantitative comparison of the different experimental techniques. For these four straight chain dicarboxylic acids, the average deviations,  $\Delta$ MFS, between UNIFAC predictions and our CK-EDB data ( $a_w$  range 0.5 – 1) and the data of Peng et al. (2001) (up to ~0.9) are  $0.017 \pm 0.017$  and  $-0.0037 \pm 0.065$ . Note that although our data corresponds to a small systematic shift from the UNIFAC model predictions, the spread of data about this mean offset is considerably less than in the previous study and extends to much higher water activity. The differences are summarised in Fig. 4, where the grey shaded area represents the standard deviation from UNIFAC for our measurements of the straight chain carboxylic acids (Fig 3.) and these data are plotted alongside all  $\Delta$ MFS values for all 13 branched dicarboxylic acids studied. Nearly all branched acids deviate more from the UNIFAC predictions than is observed for the straight chain dicarboxylic acids. This confirms our previous observation that the thermodynamic model predictions become increasingly unreliable as branching increases.

To further illustrate this trend in failure to capture the hygroscopicity reliably, we compare a sequence of dicarboxylic acids with carbon backbone length from 3-6 and with a methyl substituent attached in Fig. 5(a). All systems are poorly reproduced by the UNIFAC predictions with a value of  $\Delta$ MFS that is larger than the limit set by straight chain dicarboxylic acids, highlighting the lack of availability in branched chain experimental data to constrain the model. Interestingly, we compare the equilibrium hygroscopic response of a sequence of branched chain dicarboxylic acids in Fig. 5(b) with compounds selected to have the same O:C ratio of 0.57. It is striking that the equilibrium response curves are so similar for these compounds; this is

captured by the similarity in their  $\kappa$  values of 0.065, 0.054, 0.066, 0.064 and 0.060 for diethylmalonic acid, 2,2-dimethyl glutaric acid, 3,3-dimethyl glutaric acid, 3-methyl adipic acid and pimelic acid, respectively. UNIFAC predictions are only possible for two distinct formulaic units with the measurements indicating that these compounds have a higher degree of hygroscopicity than is captured by the model.

5

Hygroscopicity can also be represented as a function of the number of moles of water per mole of solute, shown in Fig. 6(a) for straight chain dicarboxylic acids. This is particularly informative for compounds with similar  $\kappa$  values (similar hygroscopicity), shown in Fig. 6(b)-(c), because the differences in moles of solvating water molecules per mole of solute molecule, should be indicative of molecular structure. For the homologous series of straight chain dicarboxylic acids, a higher water activity is required to achieve the same molar balance of water and solute, Fig. 6(a). For the more hydrophobic branched dicarboxylic acids, an even larger water activity is required, although the curves are notably similar for these compounds which all have the same O:C ratio, Fig. 6(b). Figure 7 compares the experimental number of moles of water per number moles of solute compared with that predicted by UNIFAC for the four compounds with the largest deviation in  $\Delta$ MFS presented in Fig. 4. Rovelli et al. (2016) presented a similar comparison of experimental data and model predictions for inorganic salts, showing remarkable agreement between experimental values and model predictions with all points for all inorganic compounds falling within the  $\pm 0.002$  uncertainty envelope in  $a_{\text{w}}$ , with this uncertainty envelope shown. However, there is a significant deviation from model predictions for the case of the branched dicarboxylic acids presented.

10  
15

In summary, UNIFAC predictions agree well with measurements for simple unbranched dicarboxylic acids with the exception of pimelic acid, although there is an increasing degree of deviation with decreasing water activity. However, as the level of molecular complexity increases through the addition of single or multiple alkyl branches, there is increasing disparity between UNIFAC predictions and measurements.

20

### 3.2. Hygroscopic Response of Amino Acids

A selection of amino acids were chosen for their biological relevance and to represent a wide range of structures and O:C ratios. Nitrogen containing compounds are prevalent in the atmosphere; amino acids contribute to this class of compounds due to their biological origin (Matsumoto and Uematsu, 2005;Barbaro et al., 2015). Recent studies have shown that nitrogen containing compounds react to form brown carbon species, which absorb solar radiation in the UV and visible region. Absorption by brown carbon in cloud droplets leads to water evaporation and cloud dispersion counteracting the aerosol indirect effect (Laskin et al., 2015). Despite their importance as nitrogen containing compounds in the atmosphere, the hygroscopic properties of amino acids are yet to be fully characterised (Chan et al., 2005). Amino acids form zwitterions in solution, which suppresses their vapour pressure and presents challenges in representing them with current thermodynamic models with most models not allowing the inclusion of nitrogen amine containing groups (e.g. AIOMFAC-web). AIOMFAC-web only allows for the inclusion of organonitrate and peroxy acyl nitrate sub groups. [Hence thermodynamic model predictions](#)

25  
30

for amino acids were generated using E-AIM, Model III (Clegg et al., 1998), using the standard UNIFAC model including certain modified main group interaction parameters introduced by Peng et al. (2001). Even then UNIFAC predictions cannot be performed for all the amino acids examined here. In particular, the ring structures found in proline and histidine cannot be represented as subgroups in the current version of E-AIM, although these could be represented with the further parametrisations reported by (Kuramochi et al., 1997b) or (Gupta and Heidemann, 1990).

The equilibrium hygroscopic responses for glycine, DL-alanine, L-valine and L-threonine are shown in Fig. 8(a). These four compounds all contain a similar glycine subunit, but include additional methyl, ethyl and hydroxyl groups. On a MFS scale, the hygroscopic response of these compounds is similar except for L-threonine which is less hygroscopic, an observation that is not expected given the additional hydrophilicity of the hydroxyl substituent. In a similar comparison to that considered in Fig. 5(b), compounds of the same O:C are compared in Fig. 8(b) with equilibrium relationships shown for L-lysine, L-histidine and L-arginine. Lysine ( $\kappa$ , 0.219) is more hygroscopic than histidine ( $\kappa$ , 0.188) and arginine ( $\kappa$ , 0.147), illustrating that compounds with the same O:C can have very different hygroscopic responses, contrary to the observations for dicarboxylic acids. For improved predictions of the amino acids measured, the multilayer adsorption isotherm based model from Dutcher et al. (2013) that includes arbitrary number of adsorbed monolayers is used in Fig. 8(c) and d) to fit to the CK-EDB data. The model uses a power law relationship for aqueous solutions to determine adsorption energy parameter, C of water molecules with a solute by adjusting a single parameter shown in Table S0.2. The model (equation 27 in Dutcher et al. (2013)) is fitted to experimental data for solute molality as a function of water activity, in order to determine the adjustable model parameter. The model predicts solute activities and concentrations across all water activities, by combining short-range adsorption isotherm and long-range Debye-Huckel expressions. The isotherm model results in improvement in MFS predictions when compared to UNIFAC. However, the notable difference in accuracy between the two models is not overly surprising: the isotherm based model of Dutcher et al. 2013 has an adjustable parameter (Table S0.2), while UNIFAC is a fully predictive model.

Figure 9(a) and (b) show comparisons between CK-EDB with available literature data for the hygroscopicity of both glycine and alanine. For glycine (Fig. 9 (a and b)) at high water activity there is good agreement between our CK-EDB data and bulk literature data (Ninni and Meirelles, 2001; Kuramochi et al., 1997a). Further, in Fig. 9 (b) CK-EDB data for alanine agrees with Kuramochi *et al.* (1997). However, there is relatively poor agreement across the entire water activity range between CK-EDB data points from this study for both glycine and alanine with literature data (Chan et al., 2005). The discrepancy arises from the method used by Chan et al. (2005) to identify the 'reference state' to which all growth measurements are compared. For example, for certain systems Chan et al. (2005) have been required to extrapolate from bulk measurements to the highest RH of the droplet measurements. A similar approach is used by Peng et al. (2001) with dicarboxylic acid measurements presented

**Deleted:**

**Deleted:** Hence thermodynamic model predictions for amino acids were generated using E-AIM, using the UNIFAC model with Peng et al. parameterization (Peng et al., 2001) and Model III. (Clegg et al., 1998).

in Fig. 3. However, the bulk data points in this case have sufficient overlap between bulk and aerosol phase measurements to require very little or no extrapolation.

Furthermore, the general trends show that the amino acids are much more hygroscopic than is currently predicted using UNIFAC; indeed, when considering all 10 amino acids included in the SI, all are more hygroscopic than their model predictions suggest (except asparagine). Increased hygroscopicity compared with dicarboxylic acids with similar O:C ratios could be due to the zwitterionic nature of amino acids with their behaviour more similar to that of a salt than an organic species.

### 3.3. Sugars and Alcohols

When retrieving hygroscopic growth curves from the comparative kinetic measurements presented here, it is of critical importance that there is no kinetic impairment to the evaporation of water. For many of the sugars we now consider, it is well established that the diffusion constant of water is strongly dependent on water activity, diminishing by many orders of magnitude and leading to slow diffusion limited release of water under dry conditions (Rickards et al., 2015). Thus, we present data that have been carefully assessed as independent of drying rate, as established by the RH of the gas phase the droplet is drying in. For trehalose, galactose and sorbitol, measurements unimpeded by kinetic limitations have not been possible below 80 % RH, and consequently data presented below 80 % do not average to a consistent series of points.

Equilibrium hygroscopicity curves for the two sugars galactose and xylose, and two sugar alcohols (polyols) erythritol and sorbitol, are shown in Fig. 10. Molecular structures presented in Fig. 10 are the open chain form for galactose and xylose and trehalose is represented using its cyclic form. Comparison of predictions for the open chain and cyclic structural forms for xylose and galactose are shown in Figure S40.0. These have been selected to illustrate the comparable degree of hygroscopic growth for these compounds, all of which have the same O:C ratio of 1, even though they are subtly different in molecular structure and weight. Indeed, their experimental  $\kappa$  values are similar (galactose, 0.134; sorbitol 0.165; erythritol 0.255) and their hygroscopic properties are reasonably well represented by AIOMFAC-web.

**Deleted:** which must be used during modelling using AIOMFAC-web.

### 3.4. Trends in $\kappa$ with O:C Ratio and Molecular Structure

In order to efficiently represent the hygroscopic growth of aerosols in large scale models, it is crucially important that models of low complexity are used to represent aerosol of broad ranging source and chemical complexity. Correlations of the value of the parameter  $\kappa$  with surrogate measures of ambient aerosol composition such as O:C have been considered (Duplissy et al., 2011; Massoli et al., 2010). We consider the trends arising from the results presented here in the variation in  $\kappa$  with degree of substitution and functional group identity. In Fig. 11(a), we compare the values of  $\kappa$  for the homologous series of dicarboxylic acids and their branched derivatives. Clearly, both increased chain length and increased branching lead to greater hydrophobicity and lower hygroscopicity. Overall trends in hygroscopicity, as represented by the dependence of MFS on water activity, can be fit to the power law model from Dutcher et al. 2013 (Table S0.1) and we show the upper and lower bounds for

compounds from each class (amino acids, organic acids, sugars and alcohols) in Fig. 11(b). This clearly illustrates that the amino acids are more hygroscopic than the majority of the other compounds studied.

Further, we consider in Fig. 12(a) the variation in  $\kappa$  with O:C ratio for all of the compounds examined here. The variation in  $\kappa$  with O:C ratio for the organic acids, sugars and alcohols is well-described (within the uncertainties) by the parametrisation provided by Rickards *et al.* (2013). However, the trend for the sequence of amino acid compounds shows that they are considerably more hygroscopic than comparable dicarboxylic acids with the same or similar O:C ratios. For example succinic acid and glycine have the same O:C ratio of 1 but with experimental  $\kappa$  values of 0.198, and 0.671 respectively. This illustrates the additional complexity in representing hygroscopicities with a simple single parameter model when multi-functional compounds are present, likely to be typical of the composition of atmospheric aerosol. Compounds with the same O:C ratio can have  $\kappa$  values that span from very low hygroscopicity (less than 0.05) to very high hygroscopicity (approaching 0.4), as is seen for compounds with an O:C around 0.6. Fig. 12(b) shows the correlation between  $\kappa$  values determined in this study and calculated  $\kappa$  values from UManSysProp (Topping *et al.*, 2016) using the hygroscopic growth factors [organic systems] model with density calculated using (Girolami, 1994). During the calculations the particle was assumed to have a dry diameter of 1000 nm and surface tension of 72 mNm<sup>-1</sup>. Although there is a reasonably clear correlation between experimentally determined  $\kappa$  values and calculated  $\kappa$ , it is also clear that the value can be over-estimated by as much as a factor of 2. Further, UManSysProp predictions can also lead to an underestimation of  $\kappa$  for a limited number of compounds, including valine, histidine, and glutaric and methyl succinic acid.

The supplementary information provides tabulated hygroscopicity data for all compounds measured in this study, it also details compound purities, density and refractive index parametrisations for all compounds.

#### 4. Conclusions

In conclusion we have presented equilibrium hygroscopicity data and density and refractive index parametrisations for 36 organic compounds of varying functionality, molecular weight and O:C ratio. Of these compounds straight chain dicarboxylic acids (C<sub>2</sub>–C<sub>5</sub>) were found to be in better agreement with UNIFAC than the initial data used to parametrise UNIFAC (Peng *et al.*, 2001). Equilibrium hygroscopicity curves of increasingly branched dicarboxylic acids are not well predicted by UNIFAC. Additionally amino acid thermodynamic model predictions are not in agreement with experimental observations. The discernible differences in hygroscopicity for different compound classes shown in both hygroscopicity curves in Fig. 13(b) and  $\kappa$  values in Fig. 12(a) offers the potential for future modelling methods to be built on relationships between compound classes and O:C and N:C ratios. Predictive tools considering these very general and smooth relationships would be much less computationally expensive than current group contribution methods and thus could be incorporated into climate models.

## Acknowledgements

REHM and JPR acknowledge support from the Natural Environment Research Council through grant NE/N006801/1. AM acknowledges the EPSRC for support through DTA funding. GR acknowledges the Italian Ministry of Education for the award of a PhD studentship. CSD and LN acknowledge support from the National Science Foundation through Grant Number 1554936. Young Chul Song from the University of Bristol is acknowledged for CK-EDB measurement for the compound Erythritol, data used in this work.

## References

- Akimoto, H.: Global Air Quality and Pollution, *Science*, 302, 1716-1719, doi:10.1126/science.1092666, 2003.
- 10 Baltensperger, U.: Spiers Memorial Lecture Introductory lecture: chemistry in the urban atmosphere, *Farad. Discuss.*, 189, 9-29, doi:10.1039/C6FD00065G, 2016.
- Barbaro, E., Zangrando, R., Vecchiato, M., Piazza, R., Cairns, W. R. L., Capodaglio, G., Barbante, C., and Gambaro, A.: Free amino acids in Antarctic aerosol: potential markers for the evolution and fate of marine aerosol, *Atmos. Chem. Phys.*, 15, 5457-5469, doi:10.5194/acp-15-5457-2015, 2015.
- 15 Cai, C., Miles, R. E. H., Cotterell, M. I., Marsh, A., Rovelli, G., Rickards, A. M. J., Zhang, Y.-h., and Reid, J. P.: Comparison of Methods for Predicting the Compositional Dependence of the Density and Refractive Index of Organic-Aqueous Aerosols, *J. Phys. Chem. A*, 120, 6604-6617, doi:10.1021/acs.jpca.6b05986, 2016.
- Carrico, C. M., Petters, M. D., Kreidenweis, S. M., Collett, J. L., Engling, G., and Malm, W. C.: Aerosol hygroscopicity and cloud droplet activation of extracts of filters from biomass burning experiments, *J Geophys Res Atmos*, 113, doi:10.1029/2007JD009274, 2008.
- 20 Chan, M. N., Choi, M. Y., Ng, N. L., and Chan, C. K.: Hygroscopicity of Water-Soluble Organic Compounds in Atmospheric Aerosols, *Environ. Sci. Technol.*, 39, 1555-1562, doi:10.1021/es049584l, 2005.
- Clegg, S. L., Brimblecombe, P., and Wexler, A. S.: Thermodynamic Model of the System  $H^+-NH_4^+-SO_4^{2-}-NO_3^- -H_2O$  at Tropospheric Temperatures, *J. Phys. Chem. A*, 102, 2137-2154, doi:10.1021/jp973042r, 1998.
- 25 Davies, J. F., Haddrell, A. E., and Reid, J. P.: Time-Resolved Measurements of the Evaporation of Volatile Components from Single Aerosol Droplets, *Aerosol Sci Tech*, 46, 666-677, doi:10.1080/02786826.2011.652750, 2012.
- Davies, J. F., Haddrell, A. E., Rickards, A. M. J., and Reid, J. P.: Simultaneous Analysis of the Equilibrium Hygroscopicity and Water Transport Kinetics of Liquid Aerosol, *Anal. Chem.*, 85, 5819-5826, doi:10.1012/ac4005502, 2013.
- 30 Duplissy, J., DeCarlo, P. F., Dommen, J., Alfarra, M. R., Metzger, A., Barmadimos, I., Prevot, A. S. H., Weingartner, E., Tritscher, T., Gysel, M., Aiken, A. C., Jimenez, J. L., Canagaratna, M. R., Worsnop, D. R., Collins, D. R., Tomlinson, J., and Baltensperger, U.: Relating hygroscopicity and composition of organic aerosol particulate matter, *Atmos. Chem. Phys.*, 11, 1155-1165, doi:10.5194/acp-11-1155-2011, 2011.
- Dutcher, C. S., Ge, X., Wexler, A. S., and Clegg, S. L.: An Isotherm-Based Thermodynamic Model of Multicomponent Aqueous Solutions, Applicable Over the Entire Concentration Range, *J. Phys. Chem. A*, 117, 3198-3213, doi:10.1021/jp310860p, 2013.
- 35 Farmer, D. K., Cappa, C. D., and Kreidenweis, S. M.: Atmospheric Processes and Their Controlling Influence on Cloud Condensation Nuclei Activity, *Chem. Rev.*, 115, 4199-4217, doi:10.1021/cr5006292, 2015.
- Fredenslund, A., Jones, R. L., and Prausnitz, J. M.: Group-contribution estimation of activity coefficients in nonideal liquid mixtures, *AIChE Journal*, 21, 1086-1099, doi:10.1002/aic.690210607, 1975.
- 40 George, C., Ammann, M., D'Anna, B., Donaldson, D. J., and Nizkorodov, S. A.: Heterogeneous Photochemistry in the Atmosphere, *Chem. Rev.*, 115, 4218-4258, doi:10.1021/cr500648z, 2015.
- Girolami, G. S.: A Simple "Back of the Envelope" Method for Estimating the Densities and Molecular Volumes of Liquids and Solids, *Journal of Chemical Education*, 71, 962-964, doi:10.1021/ed071p962, 1994.
- 45 Glantschnig, W. J., and Chen, S.-H.: Light scattering from water droplets in the geometrical optics approximation, *Appl. Opt.*, 20, 2499-2509, doi:10.1364/AO.20.002499, 1981.

- Gupta, R. B., and Heidemann, R. A.: Solubility Models for Amino-Acids and Antibiotics, *Aiche Journal*, 36, 333-341, DOI 10.1002/aic.690360303, 1990.
- Haddrell, A. E., Davies, J. F., and Reid, J. P.: Dynamics of Particle Size on Inhalation of Environmental Aerosol and Impact on Deposition Fraction, *Environ. Sci. Technol.*, 49, 14512-14521, doi:10.1021/acs.est.5b01930, 2015.
- 5 Hallquist, M., Wenger, J. C., Baltensperger, U., Rudich, Y., Simpson, D., Claeys, M., Dommen, J., Donahue, N. M., George, C., Goldstein, A. H., Hamilton, J. F., Herrmann, H., Hoffmann, T., Iinuma, Y., Jang, M., Jenkin, M. E., Jimenez, J. L., Kiendler-Scharr, A., Maenhaut, W., McFiggans, G., Mentel, T. F., Monod, A., Prévôt, A. S. H., Seinfeld, J. H., Surratt, J. D., Szmigielski, R., and Wildt, J.: The formation, properties and impact of secondary organic aerosol: current and emerging issues, *Atmos. Chem. Phys.*, 9, 5155-5236, doi:10.5194/acp-9-5155-2009, 2009.
- 10 Hodas, N., Zuend, A., Schilling, K., Berkemeier, T., Shiraiwa, M., Flagan, R. C., and Seinfeld, J. H.: Discontinuities in hygroscopic growth below and above water saturation for laboratory surrogates of oligomers in organic atmospheric aerosols, *Atmos Chem Phys*, 16, 12767-12792, 10.5194/acp-16-12767-2016, 2016.
- Hori, M., Ohta, S., Murao, N., and Yamagata, S.: Activation capability of water soluble organic substances as CCN, *J. Aerosol Sci.*, 34, 419-448, doi:10.1016/S0021-8502(02)00190-8, 2003.
- 15 Huff-Hartz, K. E. H., Tischuk, J. E., Chan, M. N., Chan, C. K., Donahue, M. N., and Pandis, S. N.: Cloud condensation nuclei activation of limited solubility organic aerosol, *Atmos. Environ.*, 40, 605-617, doi:10.1016/j.atmosenv.2005.09.076, 2006.
- Jacob, D. J.: Heterogeneous chemistry and tropospheric ozone, *Atmos. Environ.*, 34, 2131-2159, doi:10.1016/S1352-2310(99)00462-8, 2000.
- Jimenez, J. L., Canagaratna, M. R., Donahue, N. M., Prevot, A. S. H., Zhang, Q., Kroll, J. H., DeCarlo, P. F., Allan, J. D., Coe, H., Ng, N. L., Aiken, A. C., Docherty, K. S., Ulbrich, I. M., Grieshop, A. P., Robinson, A. L., Duplissy, J., Smith, J. D., Wilson, K. R., Lanz, V. A., Hueglin, C., Sun, Y. L., Tian, J., Laaksonen, A., Raatikainen, T., Rautiainen, J., Vaattovaara, P., Ehn, M., Kulmala, M., Tomlinson, J. M., Collins, D. R., Cubison, M. J., E., Dunlea, J., Huffman, J. A., Onasch, T. B., Alfarra, M. R., Williams, P. I., Bower, K., Kondo, Y., Schneider, J., Drewnick, F., Borrmann, S., Weimer, S., Demerjian, K., Salcedo, D., Cottrell, L., Griffin, R., Takami, A., Miyoshi, T., Hatakeyama, S., Shimojo, A., Sun, J. Y., Zhang, Y. M., Dzepina, K., Kimmel, J. R., Sueper, D., Jayne, J. T., Herndon, S. C., Trimborn, A. M., Williams, L. R., Wood, E. C., Middlebrook, A. M., Kolb, C. E., Baltensperger, U., and Worsnop, D. R.: Evolution of Organic Aerosols in the Atmosphere, *Science*, 326, 1525-1529, doi:10.1126/science.1180353, 2009.
- 20 Koehler, K. A., Kreidenweis, S. M., DeMott, P. J., Prenni, A. J., Carrico, C. M., Ervens, B., and Feingold, G.: Water activity and activation diameters from hygroscopicity data – Part II: Application to organic species, *Atmos. Chem. Phys.*, 6, 795-809, doi:10.5194/acp-6-795-2006, 2006.
- 30 Kreidenweis, S. M., Petters, M. D., and DeMott, P. J.: Single-parameter estimates of aerosol water content, *Environ. Res. Lett.*, 3, doi:10.1088/1748-9326/3/3/035002, 2008.
- Krieger, U. K., Marcolli, C., and Reid, J. P.: Exploring the complexity of aerosol particle properties and processes using single particle techniques, *Chem. Soc. Rev.*, 41, 6631-6662, doi:10.1039/c2cs35082c, 2012.
- 35 Kulmala, M., Vesala, T., and Wagner, P.: An Analytical Expression For the Rate of Binary Condensational Particle Growth, *Proc. R. Soc. London. A*, 441, 689-605, 1993.
- Kumar, P. P., Broekhuizen, K., and Abbatt, J. P. D.: Organic acids as cloud condensation nuclei: Laboratory studies of highly soluble and insoluble species, *Atmos. Chem. Phys.*, 3, 509-520, doi:10.5194/acp-3-509-2003, 2003.
- 40 Kuramochi, H., Noritomi, H., Hoshino, D., and Nagahama, K.: Measurements of Vapor Pressures of Aqueous Amino Acid Solutions and Determination of Activity Coefficients of Amino Acids, *J. Chem. Eng. Data*, 42, 470-474, doi:S0021-9568(96)00113-6, 1997a.
- Kuramochi, H., Noritomi, H., Hoshino, D., and Nagahama, K.: Representation of activity coefficients of fundamental biochemicals in water by the UNIFAC model, *Fluid Phase Equilibria*, 130, 117-132, doi.org/10.1016/S0378-3812(96)03209-8, 1997b.
- 45 Laskin, A., Laskin, J., and Nizkorodov, S. A.: Chemistry of Atmospheric Brown Carbon, *Chem. Rev.*, 115, 4335-4382, doi:10.1021/cr5006167, 2015.
- Liu, Y., and Daum, P. H.: Relationship of refractive index to mass density and self-consistency of mixing rules for multicomponent mixtures like ambient aerosols, *J Aerosol Sci*, 39, 974-986, doi:10.1016/j.jaerosci.2008.06.006, 2008.
- 50 Lohmann, U., and Feichter, J.: Global indirect aerosol effects: a review, *Atmos. Chem. Phys.*, 5, 715-737, doi:1680-7324/acp/2005-5-715, 2005.

- Losey, D. J., Parker, R. G., and Freedman, M. A.: pH Dependence of Liquid–Liquid Phase Separation in Organic Aerosol, *J. Phys. Chem. Lett.*, 7, 3861–3865, doi:10.1021/acs.jpcllett.6b01621, 2016.
- Massoli, P., Lambe, A. T., Ahern, A. T., Williams, L. R., Ehn, M., Mikkilä, J., Canagaratna, M. R., Brune, W. H., Onasch, T. B., Jayne, J. T., Petaja, T., Kulmala, M., Laaksonen, A., Kolb, C. E., Davidovits, P., and Worsnop, D. R.: Relationship between aerosol oxidation level and hygroscopic properties of laboratory generated secondary organic aerosol (SOA) particles, *Geophys. Res. Lett.*, 37, 5, doi:10.1029/2010gl045258, 2010.
- Matsumoto, K., and Uematsu, M.: Free amino acids in marine aerosols over the western North Pacific Ocean, *Atmos. Environ.*, 39, 2163–2170, doi:10.1016/j.atmosenv.2004.12.022, 2005.
- McNeill, V. F.: Aqueous Organic Chemistry in the Atmosphere: Sources and Chemical Processing of Organic Aerosols, *Environ. Sci. Technol.*, 49, 1237–1244, doi:10.1021/es5043707, 2015.
- Moise, T., Flores, J. M., and Rudich, Y.: Optical Properties of Secondary Organic Aerosols and Their Changes by Chemical Processes, *Chem. Rev.*, 115, 4400–4439, doi:10.1021/cr5005259, 2015.
- Nandy, L., Ohm, P. B., and Dutcher, C. S.: Isotherm-Based Thermodynamic Models for Solute Activities of Organic Acids with Consideration of Partial Dissociation, *J. Phys. Chem. A*, 120, 4147–4154, doi: 10.1021/acs.jpca.6b01904, 2016.
- Ninni, L., and Meirelles, A. J. A.: Water Activity, pH and Density of Aqueous Amino Acids Solutions, *Biotechnol. Prog.*, 17, 703–711, doi:10.1021/bp0100427, 2001.
- Ohm, P. B., Asato, C., Wexler, A. S., and Dutcher, C. S.: Isotherm-Based Thermodynamic Model for Electrolyte and Nonelectrolyte Solutions Incorporating Long- and Short-Range Electrostatic Interactions, *The Journal of Physical Chemistry A*, 119, 3244–3252, doi:10.1021/jp512646k, 2015.
- Pajunoja, A., Lambe, A. T., Hakala, J., Rastak, N., Cummings, M. J., Brogan, J. F., Hao, L., Paramonov, M., Hong, J., Prisle, N. L., Malila, J., Romakkaniemi, S., Lehtinen, K. E. J., Laaksonen, A., Kulmala, M., Massoli, P., Onasch, T. B., Donahue, N. M., Riipinen, I., Davidovits, P., Worsnop, D. R., Petäjä, T., and Virtanen, A.: Adsorptive uptake of water by semisolid secondary organic aerosols, *Geophys. Res. Lett.*, 42, 3063–3068, doi:10.1002/2015GL063142, 2015.
- Pandis, S. N., Wexler, A. S., and Seinfeld, J. H.: Dynamics of Tropospheric Aerosols, *J. Phys. Chem.*, 99, 9646–9659, doi:10.1021/j100024a003, 1995.
- Peng, C., Chan, M. N., and Chan, C. K.: The Hygroscopic Properties of Dicarboxylic and Multifunctional Acids, *Environ. Sci. Technol.*, 35, doi:10.1021/es0107531, 2001.
- Petters, M. D., and Kreidenweis, S. M.: A single parameter representation of hygroscopic growth and cloud condensation nucleus activity, *Atmos. Chem. Phys.*, 7, 1961–1971, doi:10.5194/acp-7-1961-2007, 2007.
- Petters, M. D., Kreidenweis, S. M., and Ziemann, P. J.: Prediction of cloud condensation nuclei activity for organic compounds using functional group contribution methods, *Geosci. Model Dev*, 9, 111–124, doi:10.5194/gmd-9-111-2016, 2016.
- Pöschl, U., and Shiraiwa, M.: Multiphase Chemistry at the Atmosphere–Biosphere Interface Influencing Climate and Public Health in the Anthropocene, *Chem. Rev.*, 115, 4440–4475, doi:10.1021/cr500487s, 2015.
- R. Y.-W. Chang, Slowik, J. G., Shantz, N. C., Vlasenko, A., Liggio, J., Sjostedt, S. J., Leitch, W. R., and Abbatt, J. P. D.: The hygroscopicity parameter ( $\kappa$ ) of ambient organic aerosol at a field site, *Atmos. Chem. Phys.*, 10, 5047–5064, doi:10.5194/acp-10-5047-2010, 2010.
- Ravishankara, A. R., Rudich, Y., and Wuebbles, D. J.: Physical Chemistry of Climate Metrics, *Chem. Rev.*, 115, 3682–3703, doi:10.1021/acs.chemrev.5b00010, 2015.
- Rickards, A. M. J., Miles, R. E. H., Davies, J. F., Marshall, F. H., and Reid, J. P.: Measurements of the Sensitivity of Aerosol Hygroscopicity and the  $\kappa$ , *J. Phys. Chem. A*, 117, 14120–14131, doi:10.1021/jp407991n |, 2013.
- Rickards, A. M. J., Song, Y.-C., Miles, R. E. H., Preston, T. C., and Reid, J. P.: Variabilities and uncertainties in characterising water transport kinetics in glassy and ultraviscous aerosol, *Phys Chem Chem Phys*, 17, 10059–10073, doi:10.1039/C4CP05383D, 2015.
- Rindelaub, J. D., Craig, R. L., Nandy, L., Bondy, A. L., Dutcher, C. S., Shepson, P. B., and Ault, A. P.: Direct Measurement of pH in Individual Particles via Raman Microspectroscopy and Variation in Acidity with Relative Humidity, *J. Phys. Chem. A*, 120, 911–917, doi:10.1021/acs.jpca.5b12699, 2016.
- Rovelli, G., Miles, R. E. H., Reid, J. P., and Clegg, S. L.: Accurate Measurements of Aerosol Hygroscopic Growth over a Wide Range in Relative Humidity, *J. Phys. Chem. A*, 120, 4376–4388, doi:10.1021/acs.jpca.6b04194, 2016.
- Seinfeld, J. H., and Pankow, J. F.: Organic Atmospheric Particulate Matter, *Annu. Rev. Phys. Chem.*, 54, 121–140, doi:10.1146/annurev.physchem.54.011002.103756, 2003.

- Suda, S. R., Petters, M. D., Yeh, G. K., Strollo, C., Matsunaga, A., Faulhaber, A., Ziemann, P. J., Prenni, A. J., Carrico, C. M., Sullivan, R. C., and Kreidenweis, S. M.: Influence of Functional Groups on Organic Aerosol Cloud Condensation Nucleus Activity, *Environ. Sci. Technol.*, 48, 10182-10190, doi:10.1021/es502147y, 2014.
- 5 Topping, D., Connolly, P., and McFiggans, G.: Cloud droplet number enhanced by co-condensation of organic vapours, *Nature Geosci.*, 6, 443-446, doi:10.1038/ngeo1809, 2013.
- Topping, D., Barley, M., Bane, M. K., Higham, N., Aumont, B., Dingle, N., and McFiggans, G.: UManSysProp v1.0: an online and open-source facility for molecular property prediction and atmospheric aerosol calculations, *Geosci. Model Dev.*, 9, 899-914, doi:10.5194/gmd-9-899-2016, 2016.
- 10 Wex, H., Stratmann, F., Topping, D., and McFiggans, G.: The Kelvin versus the Raoult Term in the Kohler Equation, *J. Atmos. Sci.*, 65, 4004-4016, doi:10.1175/2008jas2720.1, 2008.
- Wexler, A. S., and Clegg, S. L.: Atmospheric aerosol models for systems including the ions H<sup>+</sup>, NH<sub>4</sub><sup>+</sup>, Na<sup>+</sup>, SO<sub>4</sub><sup>2-</sup>, NO<sub>3</sub><sup>-</sup>, Cl<sup>-</sup>, Br<sup>-</sup>, and H<sub>2</sub>O, *J. Geophys. Res. Atmos.*, 107, ACH 14-11-ACH 14-14, doi:10.1029/2001JD000451, 2002.
- Zhang, R., Wang, G., Guo, S., Zamora, M. L., Ying, Q., Lin, Y., Wang, W., Hu, M., and Wang, Y.: Formation of Urban Fine Particulate Matter, *Chem. Rev.*, 115, 3803-3855, doi:10.1021/acs.chemrev.5b00067, 2015.
- 15 Ziemann, P. J., and Atkinson, R.: Kinetics, products, and mechanisms of secondary organic aerosol formation, *Chem. Soc. Rev.*, 41, 6582-6605, doi:10.1039/C2CS35122F, 2012.
- Zuend, A., Marcolli, C., Luo, B. P., and Peter, T.: A thermodynamic model of mixed organic-inorganic aerosols to predict activity coefficients, *Atmos. Chem. Phys.*, 8, 4559-4593, doi:10.5194/acp-8-4559-2008, 2008.
- 20 Zuend, A., Marcolli, C., Booth, A. M., Lienhard, D. M., Soonsin, V., Krieger, U. K., Topping, D. O., McFiggans, G., Peter, T., and Seinfeld, J. H.: New and extended parameterization of the thermodynamic model AIOMFAC: calculation of activity coefficients for organic-inorganic mixtures containing carboxyl, hydroxyl, carbonyl, ether, ester, alkenyl, alkyl, and aromatic functional groups, *Atmos. Chem. Phys.*, 11, 9155-9206, doi:10.5194/acp-11-9155-2011, 2011.
- Zuend, A., and Seinfeld, J. H.: Modeling the gas-particle partitioning of secondary organic aerosol: the importance of liquid-liquid phase separation, *Atmos. Chem. Phys.*, 12, 3857-3882, doi:10.5194/acp-12-3857-2012, 2012.

25

Tables.

Table 1. Experimentally determined  $\kappa$  values at  $a_w = 0.95$  for all compounds studied at 293.15 K, presented alongside  $\kappa$  values calculated using UManSysProp and the smile string used for this calculation.

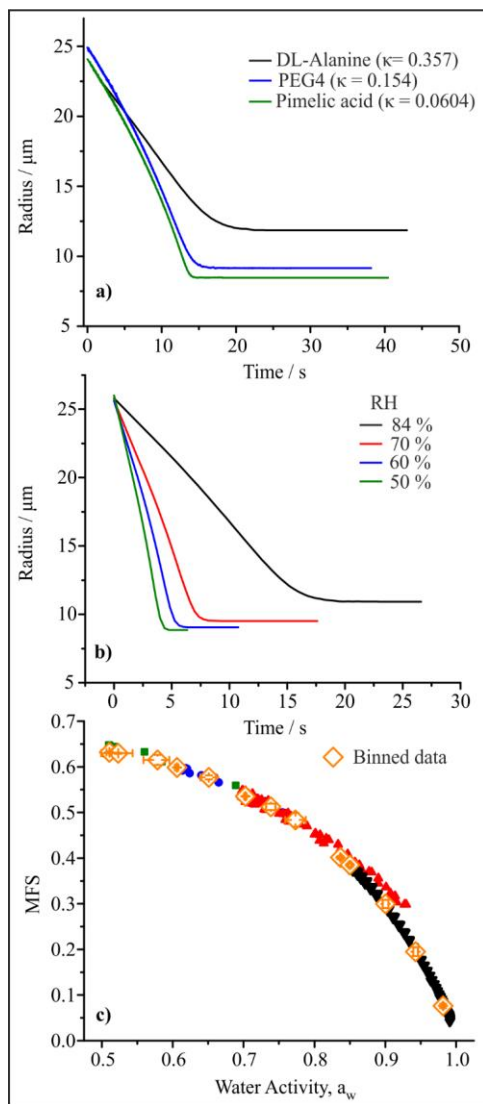
Compound	Average Experimental $\kappa$ Value ( $a_w = 0.95$ )	Standard Deviation in $\kappa$ ( $\pm$ )	UManSysProp Calculated $\kappa$ ( $a_w = 0.95$ )	SMILES String
<i>Amino Acids</i>				
DL-Alanine	0.357	0.010	0.402	<chem>O=C(O)C(N)C</chem>
L-Asparagine	0.187	0.017	0.337	<chem>O=C(N)C[C@H](N)C(=O)O</chem>
L-Aspartic Acid	-	-	0.332	<chem>O=C(O)CC(N)C(=O)O</chem>
L-Arginine	0.147	0.005	0.267	<chem>NC(CCCNC(N)=N)C(O)=O</chem>
Glycine	0.671	0.013	0.621	<chem>C(C(=O)O)N</chem>
L-Histidine	0.188	0.003	0.052	<chem>O=C([C@H](CC1=CNC=N1)N)O</chem>
L-Lysine	0.219	0.007	0.250	<chem>C(CCN)CC(C(=O)O)N</chem>
L-Proline	0.272	0.005	0.273	<chem>OC(=O)C1CCCN1</chem>
L-Threonine	0.235	0.001	0.307	<chem>C[C@H]([C@@H](C(=O)O)N)O</chem>
L-Valine	0.253	0.003	0.136	<chem>CC(C)[C@H](C(=O)O)N</chem>
<i>Carboxylic Acids</i>				
Oxalic Acid	0.409	0.005	0.488	<chem>C(=O)(C(=O)O)O</chem>
Malonic Acid	0.281	0.003	0.362	<chem>O=C(O)CC(=O)O</chem>
Succinic Acid	0.198	0.011	0.252	<chem>C(CC(=O)O)C(=O)O</chem>
Methyl Malonic acid	0.234	0.006	0.252	<chem>CC(C(=O)O)C(=O)O</chem>
Glutaric Acid	0.144	0.005	0.139	<chem>C(CC(=O)O)CC(=O)O</chem>
Methyl Succinic Acid	0.160	0.003	0.138	<chem>CC(CC(=O)O)C(=O)O</chem>
Dimethyl Malonic Acid	0.149	0.002	0.150	<chem>CC(C)(C(=O)O)C(=O)O</chem>
Adipic Acid	0.101	0.004	0.055	<chem>C(CCC(=O)O)CC(=O)O</chem>
2-Methyl Glutaric Acid	0.102	0.005	0.055	<chem>CC(CCC(=O)O)C(=O)O</chem>
3-Methyl Glutaric Acid	0.103	0.006	0.055	<chem>CC(CC(=O)O)CC(=O)O</chem>
2,2-Dimethyl Succinic Acid	0.116	0.009	0.061	<chem>CC(C)(CC(=O)O)C(=O)O</chem>
2,3-Dimethyl Succinic acid	0.130	0.002	0.054	<chem>CC(C(C)C(=O)O)C(=O)O</chem>
Pimelic Acid	0.060	0.003	0.030	<chem>OC(=O)CCCCC(=O)O</chem>

2,2-Dimethyl Glutaric Acid	0.054	0.002	0.032	<chem>CC(C)(CCC(=O)O)C(=O)O</chem>
3-Methyl Adipic Acid	0.064	0.002	0.030	<chem>CC(CCC(=O)O)CC(=O)O</chem>
3,3-Dimethyl Glutaric Acid	0.066	0.003	0.032	<chem>CC(C)(CC(=O)O)CC(=O)O</chem>
Diethyl Malonic Acid	0.065	0.001	0.032	<chem>CCC(CC)(C(=O)O)C(=O)O</chem>
Citric Acid	0.189	0.002	0.192	<chem>OC(=O)CC(O)(C(=O)O)C(=O)O</chem>
Tartaric Acid	0.27	0.006	0.308	<chem>O=C(O)C(O)C(O)C(=O)O</chem>
Sorbitol	0.165	0.003	0.303	<chem>OC([C@H](O)[C@@H](O)[C@H](O)CO)CO</chem>
D-(+)-Trehalose Dihydrate	0.088	0.001	0.151	<chem>C([C@@H]1[C@H]([C@@H]([C@H]([C@@H]1[C@H]([C@H]([C@H](O1)O[C@@H]2[C@@H]([C@H]([C@@H]([C@H](O2)CO))O)O)O)O)O)O</chem>
Galactose	0.134	0.004	0.246	<chem>O[C@H]1[C@@H](O)[C@@H](O)[C@@H](O)[C@@H](O)[C@@H]1O</chem>
Xylose	-	-		
PEG4	0.154	0.004		
PEG3	0.151	0.003		
Erythritol	0.255	0.006	0.380	<chem>OC[C@@H](O)[C@@H](O)CO</chem>

Table 2.  $\kappa$  values available in the literature for dicarboxylic acids.

Compound	Literature $\kappa$
Oxalic acid	0.504 ± 0.044 (Rickards et al., 2013)
Malonic acid	0.44 ± 0.16 (Koehler et al., 2006) 0.227 ± 0.028 (Kumar et al., 2003) 0.292 ± 0.011 (Rickards et al., 2013)
Succinic acid	0.231 ± 0.065 (Hori et al., 2003) 0.216 ± 0.20 (Rickards et al., 2013)
Glutaric acid	0.20 ± 0.08 (Koehler et al., 2006) 0.088 (Huff-Hartz et al., 2006) 0.168 ± 0.30 (Rickards et al., 2013)
Adipic acid	0.096 0.102 ± 0.009 (Kumar et al., 2003) (Rickards et al., 2013)

Figures.



Formatted: Centered

**Fig. 1. (a) Examples of the time-dependent evaporation of aqueous droplets containing compounds with varying  $\kappa$  value evaporating into similar RHs (~82 %). (b) The time-dependence of the radii of droplets of aqueous glycine evaporating into different RHs. (c) Equilibrium hygroscopicity curve for glycine, with binned data points (large open orange diamonds) estimate across the four different experiments at four RHs shown in (b).**

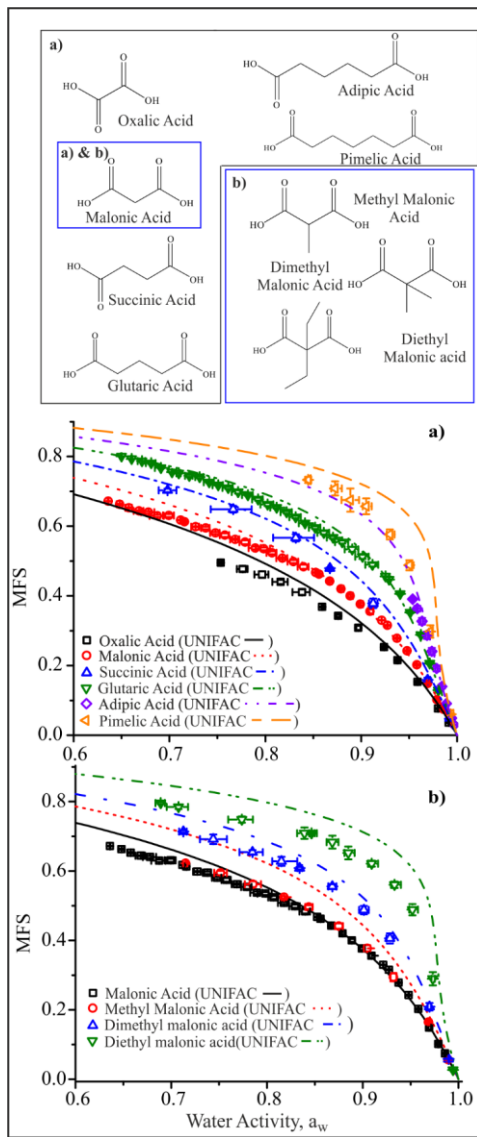


Fig. 2. Equilibrium hygroscopic growth curves are shown in (a) for the homologous series of straight chain dicarboxylic acids and in (b) for dicarboxylic acids with a malonic acid backbone and increasing methyl substitution. UNIFAC prediction using AIOMFAC-web.

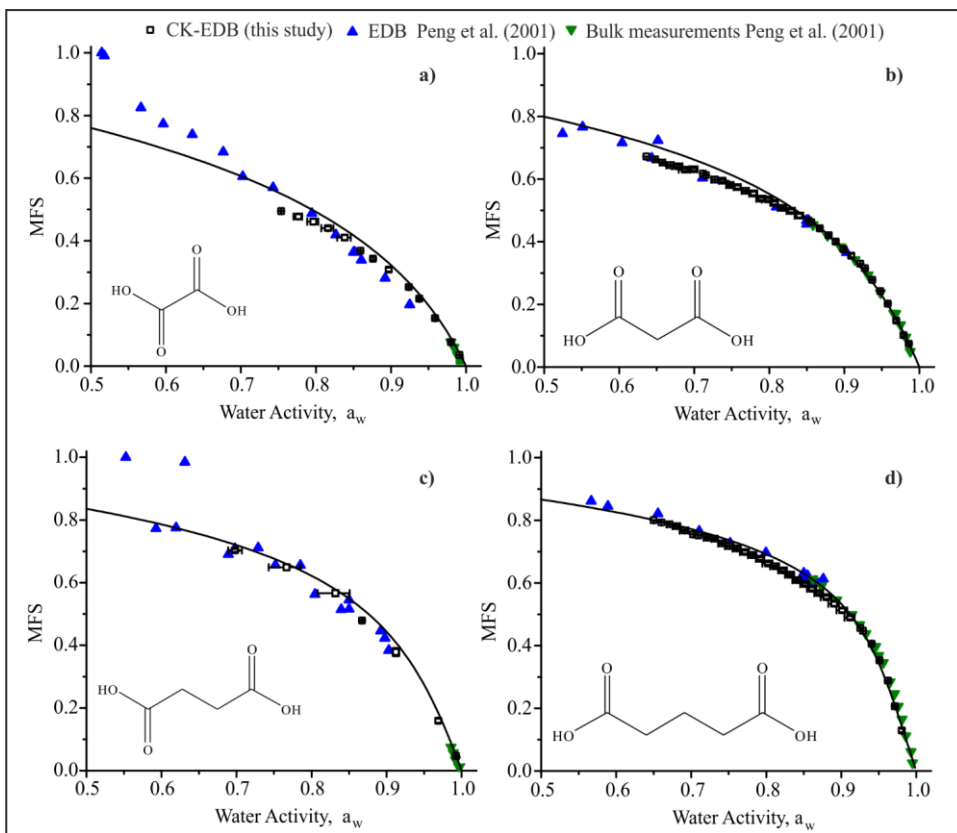


Fig. 3. Hygroscopicity of dicarboxylic acid droplets measured with the CK-EDB (black open squares) compared with the EDB data of Peng *et al.* (2001) (blue up triangles) and bulk measurements (green down triangles) for (a) oxalic acid, (b) malonic acid, (c) succinic acid and (d) glutaric acid. UNIFAC predictions are shown for all compounds (solid black line). UNIFAC prediction using AIOMFAC-web.

5

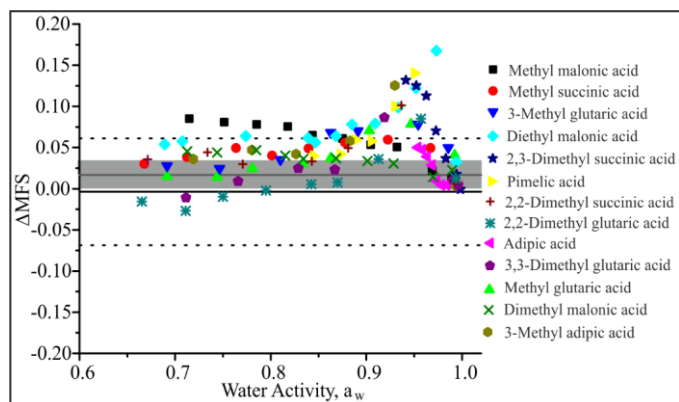
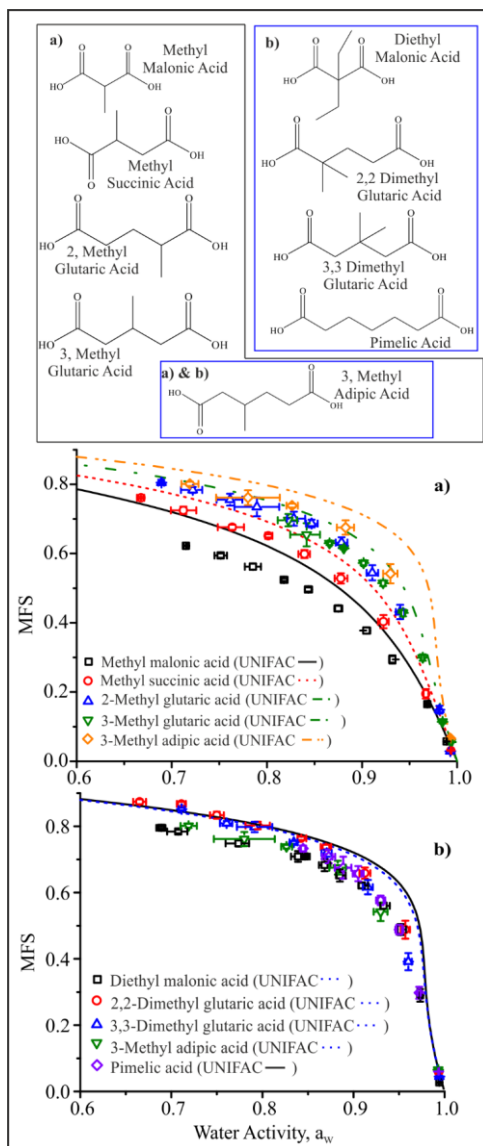


Fig. 4. The difference between the mass fraction of solute from UNIFAC predictions and the CK-EDB data from this study ( $\Delta MFS$ ) for all 13 branched dicarboxylic acids studied. The average in  $\Delta MFS$  for the 4 dicarboxylic acids in Fig. 3 (CK-EDB data, this study) across the whole water activity range is represented with a grey shaded area, the average represented by the dark grey line. Additionally, the average  $\Delta MFS$  (black solid line) and standard deviation (black dashed lines) derived from the Peng et al. (2001) data also shown in Fig. 3.

10

15

20



5 Figure 5. Equilibrium hygroscopicity curves for a series of branched dicarboxylic acids are shown in a). In (b) CK-EDB hygroscopicity curves for a series of dicarboxylic acids with the same O:C ratio of 0.57. UNIFAC prediction using AIOMFAC-web. In b) the AIOMFAC-web prediction for 3-methyl adipic acid,  $[(CH_3)(CH)(CH_2)_3(COOH)_2]$ , 3,3-dimethylglutaric acid,  $[(CH_3)_2(C)(CH_2)_2(COOH)_2]$ , 2,2-dimethylglutaric acid,  $[(CH_3)_2(C)(CH_2)_2(COOH)_2]$  is represented by the blue dashed line. Note that the equilibrium curves for the first 4 compounds are in such close agreement and indistinguishable on this scale that only one curve is shown for clarity. The prediction for pimelic acid  $[(CH_2)_5(COOH)_2]$  is shown as a black solid line.

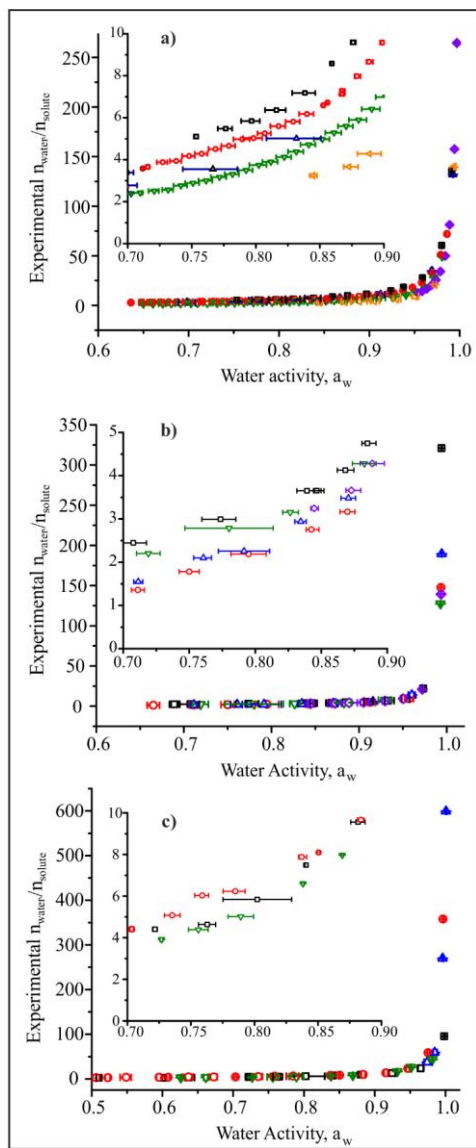


Figure 6. Moles of water, per mole of solute for (a) for straight chain dicarboxylic acids for oxalic (black squares), malonic acid (red circles), succinic acid (blue up triangles), glutaric acid (green down triangles), adipic acid (violet diamonds) and pimelic acid (orange left triangles). In (b) for diethylmalonic acid (black squares), 2,2-dimethyl glutaric acid (red circles), 3,3-dimethyl glutaric acid (blue triangles), 3-methyl adipic acid (pink down triangles) and pimelic acid (green diamonds). And in (c) for galactose (black squares), sorbitol (red circles), xylose (blue down triangles) and erythritol (green down triangles).

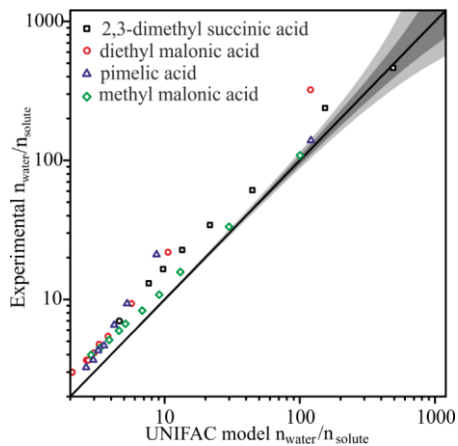


Figure 7. Comparison of the experimentally determined number of moles of water per mole of solute and the value predicted from UNIFAC for the four dicarboxylic acids with the largest deviation from UNIFAC. Shaded regions correspond to error in  $a_w$  of  $\pm 0.001$  (dark shaded grey regions) and  $\pm 0.002$  (light shaded grey regions).

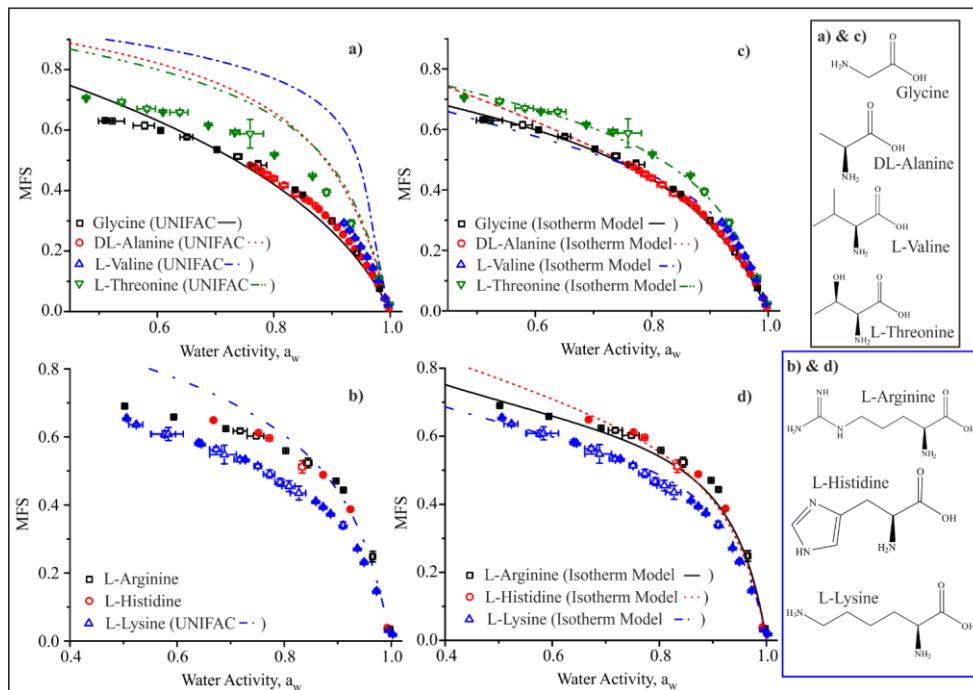


Figure 8. Equilibrium hygroscopicity curves in (a) for structurally similar amino acids with different substituents alongside UNIFAC predictions. In (b) equilibrium hygroscopicity curves of amino acids with the same O:C ratio (0.33) with UNIFAC predictions generated using E-AIM model III. In (c) and (d) the same amino acids as (a) and (b) respectively and are presented alongside thermodynamic predictions using the isotherm model discussed in Dutcher et al. (2013) with coefficients available in Table S0.2.

5

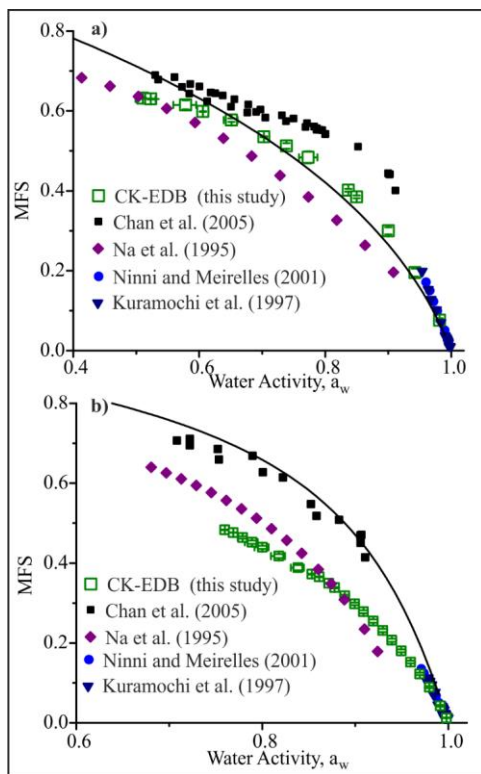


Figure 9. Equilibrium hygroscopicity data for (a) glycine and (b) alanine. The solid black line is the UNIFAC model prediction for alanine and glycine, generated using E-AIM Model III.

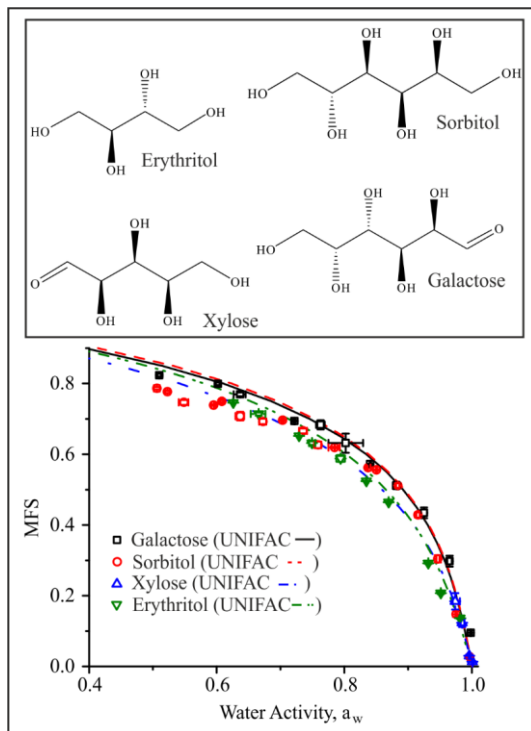


Figure 10. Equilibrium hygroscopicity curves for sugars and alcohols with the same O:C ratio of 1. UNIFAC prediction using AIOMFAC-web.

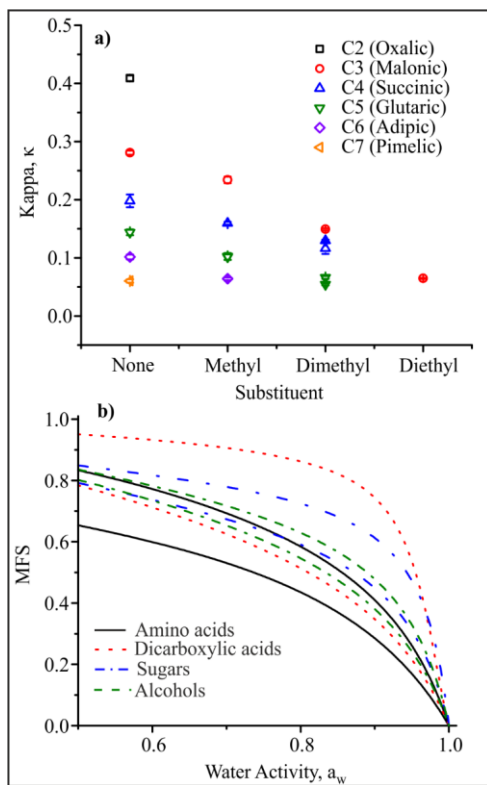


Figure 11. In a)  $\kappa$  values at a water activity of 0.95 are plotted as a function of increasing length of substituent and carbon backbone. In (b) generalised equilibrium hygroscopicity curves are presented as a function of compound class. Upper and lower hygroscopicity limits for each compound class have been fitted using the isotherm model discussed in Dutcher et al. (2013) (coefficients available in Table S0.1).

5

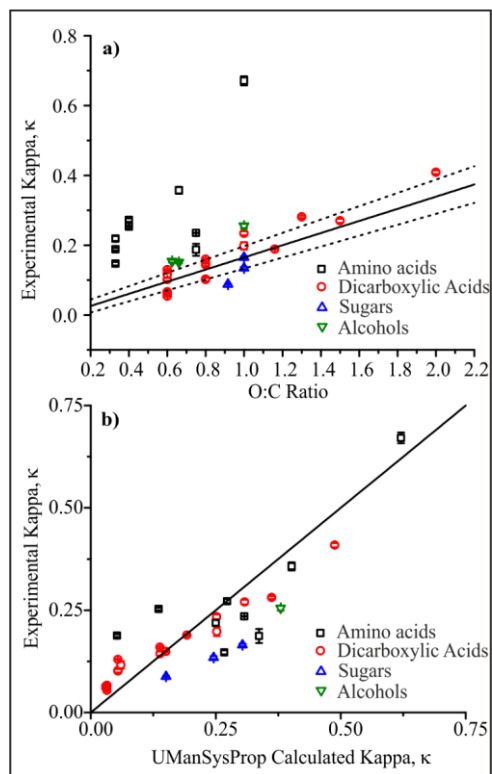


Figure 12. All values of  $\kappa$  for all compound classes presented as a plot of (a)  $\kappa$  vs O:C ratio and (b) as a correlation plot between calculated  $\kappa$  and experimental  $\kappa$ . Errors are indicated but are smaller than some points. In (a) the black solid line overlaid of the form  $\kappa = (0.174 \pm 0.017) \times \text{O:C} - (0.009 \pm 0.015)$ , the parametrisation of Rickards *et al.* (2013), with the black dashed lines showing the upper and lower limits of this parametrisation. In (b) the line represents  $y=x$ .

# Influence of Organic Compound Functionality on Aerosol Hygroscopicity: Dicarboxylic Acids, Alkyl-Substituents, Sugars and Amino Acids

Aleksandra Marsh<sup>1</sup>, Rachael E. H. Miles<sup>1</sup>, Grazia Rovelli<sup>1</sup>, Alexander G. Cowling<sup>1</sup>, Lucy Nandy<sup>2</sup>, Cari S. Dutcher<sup>2</sup> and Jonathan. P Reid<sup>1</sup>

<sup>1</sup> School of Chemistry, University of Bristol, Bristol, BS8 1TS, UK

<sup>2</sup> Department of Mechanical Engineering, University of Minnesota, 111 Church Street SE, Minneapolis, MN 55455, USA

Correspondence to: Jonathan. P. Reid j.p.reid@bristol.ac.uk

**Table S0** Parameters required for thermodynamic model predictions (\* available from a predefined list). And contents of supplement by page and S number.

Compound	Molar Mass / g.mol <sup>-1</sup>	UNIFAC Structure	Page and S No
DL- Alanine	89.09	CH <sub>3</sub> COOH CHNH <sub>2</sub>	P3 S1
L-Asparagine	132.12	COOH CH <sub>2</sub> CONH <sub>2</sub>	P38 S36
L-Aspartic Acid	133.10	CH <sub>2</sub> (COOH) <sub>2</sub> CHNH <sub>2</sub>	P37 S35
L-Arginine	174.2	-	P4 S2
Glycine	75.06	COOH CHNH <sub>2</sub>	P5 S3
L-Histidine	155.15	-	P6 S4
L-Lysine	146.19	COOH CHNH <sub>2</sub> (CH <sub>2</sub> ) <sub>3</sub> CH <sub>2</sub> NH <sub>2</sub>	P7 S5
L-Proline	115.13	-	P8 S6
L-Threonine	119.12	OH CH <sub>3</sub> CH COOH CHNH <sub>2</sub>	P9 S7
L-Valine	117.15	(CH <sub>3</sub> ) <sub>2</sub> CH COOH CHNH <sub>2</sub>	P10 S8
Oxalic Acid*	90.03	(COOH) <sub>2</sub>	P13 S11
Malonic Acid*	104.062	(COOH) <sub>2</sub> CH <sub>2</sub>	P14 S12
Succinic Acid*	118.09	(COOH) <sub>2</sub> (CH <sub>2</sub> ) <sub>2</sub>	P15 S13
Methyl Malonic acid		(CH <sub>3</sub> )(CH)(COOH) <sub>2</sub>	P19 S17
Glutaric Acid*		(COOH) <sub>2</sub> (CH <sub>2</sub> ) <sub>3</sub>	P16 S14
Methyl Succinic Acid*	132.116	(CH <sub>3</sub> )(CH <sub>2</sub> )(CH)(COOH) <sub>2</sub>	P20 S18
Dimethyl Malonic Acid		(CH <sub>3</sub> ) <sub>2</sub> (C)(COOH) <sub>2</sub>	P36 S34
Adipic Acid*		(COOH) <sub>2</sub> (CH <sub>2</sub> ) <sub>4</sub>	P17 S15
2-Methyl Glutaric Acid*		(CH <sub>3</sub> )(CH <sub>2</sub> ) <sub>2</sub> (CH)(COOH) <sub>2</sub>	P24 S22
3-Methyl Glutaric Acid*	146.14	(CH <sub>3</sub> )(CH <sub>2</sub> ) <sub>2</sub> (CH)(COOH) <sub>2</sub>	P26 S24
2,2-Dimethyl Succinic Acid*		(CH <sub>3</sub> ) <sub>2</sub> (CH <sub>2</sub> )(C)(COOH) <sub>2</sub>	P23 S21
2,3-Dimethyl Succinic acid		(CH <sub>3</sub> ) <sub>2</sub> (CH) <sub>2</sub> (COOH) <sub>2</sub>	P35 S33
Pimelic Acid		(COOH) <sub>2</sub> (CH <sub>2</sub> ) <sub>5</sub>	P18 S16
2,2-Dimethyl Glutaric Acid		(CH <sub>3</sub> ) <sub>2</sub> (CH <sub>2</sub> ) <sub>2</sub> (C)(COOH) <sub>2</sub>	P22 S20
3-Methyl Adipic Acid	160.17	(CH <sub>3</sub> ) <sub>1</sub> (CH <sub>2</sub> ) <sub>3</sub> (CH)(COOH) <sub>2</sub>	P25 S23
3,3-Dimethyl Glutaric Acid		(CH <sub>3</sub> ) <sub>2</sub> (CH <sub>2</sub> ) <sub>2</sub> (C)(COOH) <sub>2</sub>	P27 S25
Diethyl Malonic Acid		(CH <sub>3</sub> ) <sub>2</sub> (CH <sub>2</sub> ) <sub>2</sub> (C)(COOH) <sub>2</sub>	P21 S19
Citric Acid*	192.12	(COOH) <sub>3</sub> (CH <sub>2</sub> ) <sub>2</sub> C <sup>(OH)</sup>	P11 S9
Tartaric Acid	150.09	(COOH) <sub>2</sub> (OH) <sub>2</sub> (CH) <sub>2</sub> <sup>(OH)</sup>	P12 S10
Sorbitol	182.17	(CH <sub>2</sub> <sup>[alc]</sup> ) <sub>2</sub> -(CH <sub>1</sub> <sup>(OH)</sup> ) <sub>4</sub> (OH) <sub>6</sub>	P31 S29
D-(+)-Trehalose Dihydrate	378.33	(CH) (CH <sub>2</sub> <sup>(OH)</sup> ) <sub>8</sub> (CHO <sup>[ether]</sup> ) <sub>3</sub> (OH) <sub>8</sub>	P32 S30

Galactose	180.16	CHO (CH <sub>1</sub> <sup>(OH)</sup> ) <sub>4</sub> CH <sub>2</sub> <sup>(alc)</sup> (OH) <sub>5</sub>	P33 S31
Xylose	150.13	(CH <sub>2</sub> (OH)) <sub>3</sub> CH <sub>2</sub> <sup>(alc)</sup> CHO (OH) <sub>4</sub>	P34 S32
PEG4	194.23	(OH) <sub>2</sub> (CH <sub>2</sub> O) <sub>3</sub> (CH <sub>2</sub> ) <sub>3</sub> (CH <sub>2</sub> <sup>(OH)</sup> ) <sub>2</sub>	P29 S27
PEG3	150.17	(OH) <sub>2</sub> (CH <sub>2</sub> ) <sub>2</sub> (CH <sub>2</sub> O) <sub>2</sub> (CH <sub>2</sub> <sup>(OH)</sup> ) <sub>2</sub>	P28 S26
Erythritol	122.12	(CH <sup>(OH)</sup> ) <sub>2</sub> (CH <sub>2</sub> <sup>(OH)</sup> ) <sub>2</sub> (OH) <sub>4</sub>	P30 S28

**Table S0.1** Fitted parameters for upper and lower MFS vs water activity of compounds in each class, amino and organic acids, sugars and alcohols, as shown in Figure 11b) in the manuscript. The power law coefficient  $P$  is used to calculate energy parameter  $C$  for the first to  $(n - 1)$ th layers, hence  $C_i = (i/n)^P$ , where  $i$  is the layer number and  $n$  is the total number of hydration layers, here  $n = 8$  for all compounds except glycine ( $n = 3$ ) and 2,2-dimethyl glutaric acid ( $n = 16$ ). MSE is a normalized mean-square error, equal to  $\left(\frac{1}{n_p}\right) \sum_{i=1}^{n_p} ((m_{model,i} - m_{data,i}) / (m_{model,i}))^2$ , where  $n_p$  is the number of data points.

Solute	$P$	MSE
Amino acid Upper (Glycine)	-1.934	0.00321
Amino acid Lower (Asparagine)	-0.171	0.04151
Organic acid Upper (Malonic acid)	-0.212	0.00819
Organic acid Lower (2,2 dimethyl glutaric acid)	0.206	0.08315
Sugar Upper (Sorbitol)	-0.522	0.01025
Sugar Lower (Trehalose)	-0.870	0.01687
Alcohol Upper (Erythritol)	-0.238	0.01311
Alcohol Lower (PEG4)	-1.180	0.16205

**Table S0.2** Fitted parameters for nine amino acids. The power law coefficient  $P$  is used to calculate energy parameter  $C$  for the first to  $(n - 1)$ th layers, hence  $C_i = (i/n)^P$ , where  $i$  is the layer number and  $n$  is the total number of hydration layers, here  $n = 8$  for all compounds except glycine ( $n = 3$ ) and threonine ( $n = 5$ ). MSE is a normalized mean-square error, equal to  $\left(\frac{1}{n_p}\right) \sum_{i=1}^{n_p} ((m_{model,i} - m_{data,i}) / (m_{model,i}))^2$ , where  $n_p$  is the number of data points. (Parameter for L-aspartic acid could not be determined due to data range available.)

Solute	$P$	MSE
Alanine	-0.356	0.00051
Asparagine	-0.171	0.04151
Arginine	-0.993	0.04039
Glycine	-1.934	0.00321
Histidine	-0.502	0.02211
Lysine	-1.225	0.00667
Proline	-0.619	0.03764
Threonine	-0.960	0.20107
Valine	-0.892	0.00397

## S1 DL-Alanine Hygroscopicity

**Fig. S1.1:** Hygroscopicity of DL-Alanine (Sigma Aldrich, Purity 99 %) at 293.15 K.

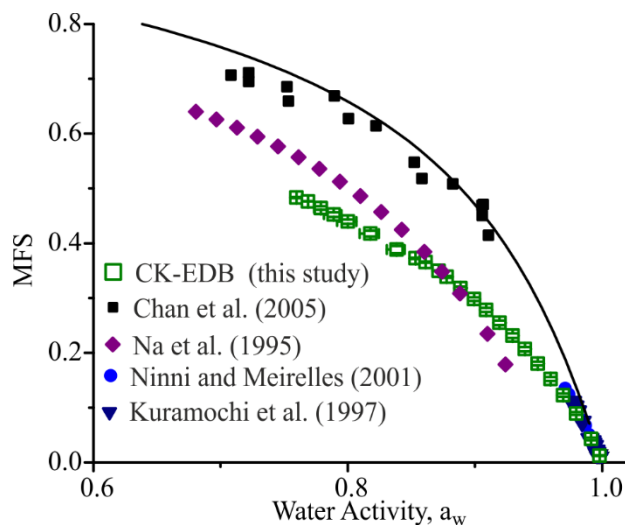


**Table S1.1:** Pure component refractive index ( $n_{\text{melt}}$ ) is determined using molar refraction, assuming ideal mixing for calculation of the melt density ( $\rho_{\text{melt}}$ ), from bulk data available in Cai et al. (2016). The variation of density as a function of the root of solute mass fraction ( $\text{MFS}^{1/2} = x$ ) is represented by polynomial fit parameters. *Upper* and *lower* refer to 95 % confidence limits for fits to experimental data, (Section 2.2 in manuscript).

	$n_{\text{melt}}$	$\rho_{\text{melt}} / \text{g}\cdot\text{cm}^{-3}$	Polynomial fit ( $\rho_{\text{sol}} = a + b_1x + b_2x^2 + b_3x^3$ )			
			a	$b_1$	$b_2$	$b_3$
<i>Best</i>	1.6205	1.4961	999	94.14	-66.93	466.48
<i>Upper</i>	1.6222	1.5042	999	97.38	-76.61	480.88
<i>Lower</i>	1.6188	1.4881	999	90.98	-57.61	452.44

**Table S1.2:** Tabulated experimental data points shown in Fig S1.1.

$a_w$	error $a_w$ (+ve)	error $a_w$ (-ve)	MFS	error MFS
0.75966	0.00182	0.00228	0.48336	8.66E-04
0.76866	1.02E-03	0.00128	0.47642	3.48E-04
0.77876	0.00413	0.00519	0.46428	0.00314
0.78887	0.00613	0.00771	0.45228	0.00412
0.80001	0.00674	0.00847	0.43959	0.00395
0.81774	0.00674	8.47E-03	0.41748	0.00512
0.83836	6.17E-03	7.75E-03	0.38848	6.39E-03
0.85334	0.00473	3.00E-03	0.37246	0.00116
0.86108	0.00116	7.54E-04	0.3655	8.92E-04
0.87144	6.02E-04	4.18E-04	0.34973	5.50E-04
0.87774	0.00139	9.81E-04	0.3386	0.00165
0.88866	0.00217	0.00153	0.31805	0.00274
0.89931	2.66E-03	1.92E-03	0.2981	0.00333
0.9087	0.00257	0.00183	0.27841	0.00381
0.91923	0.00256	0.00191	0.25483	0.00426
0.92957	0.00248	0.00181	0.23142	0.00416
0.93936	0.00243	0.00179	0.20672	0.00392
0.94936	0.00206	1.54E-03	0.18027	0.00361
0.9595	1.95E-03	1.43E-03	0.15211	0.00347
0.96935	1.49E-03	1.11E-03	0.12252	0.003
0.97954	0.00127	9.28E-04	0.08929	0.00254
0.99143	6.34E-04	7.22E-04	0.04259	0.00238

## S2 L-Arginine Hygroscopicity

**Fig S2.1:** Hygroscopicity of L-Arginine, (Acros Organics, Purity > 98 %), at 293.15 K. Open squares, these experiments.

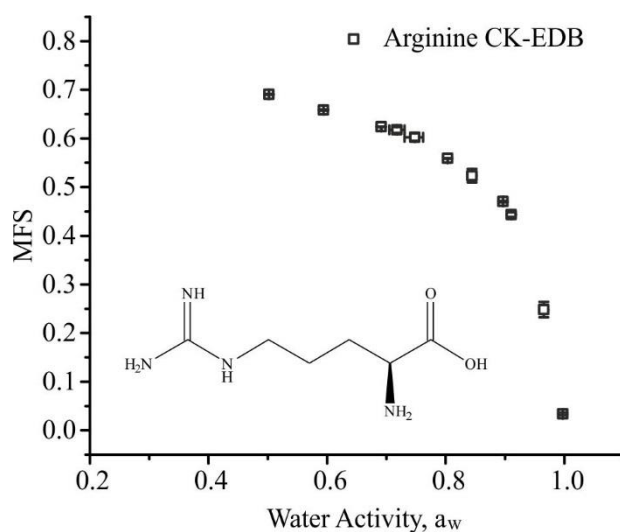


**Table S2.1:** Pure component refractive index ( $n_{\text{melt}}$ ) is determined using molar refraction, assuming ideal mixing for calculation of the melt density ( $\rho_{\text{melt}}$ ), from bulk data available in Cai et al. (2016). The variation of density as a function of the root of solute mass fraction ( $\text{MFS}^{1/2} = x$ ) is represented by polynomial fit parameters. *Upper* and *lower* refer to 95 % confidence limits for fits to experimental data, (Section 2.2 in manuscript).

	$n_{\text{melt}}$	$\rho_{\text{melt}}/\text{g.cm}^{-3}$	Polynomial fit ( $\rho_{\text{sol}} = a + b_1x + b_2x^2 + b_3x^3$ )			
			a	$b_1$	$b_2$	$b_3$
<i>Best</i>	1.637	1.3995	998.6	59.85	28.54	310.48
<i>Upper</i>	1.6382	1.4045	998.6	61.44	24.47	317.9
<i>Lower</i>	1.6358	1.3945	998.6	58.28	32.51	303.13

**Table S2.2:** Tabulated experimental data points shown in Fig S2.1.

$a_w$	error $a_w$ (+ve)	error $a_w$ (-ve)	MFS	error MFS
0.50205	0.00177	0.0021	0.69041	0.00113
0.59399	0.00171	0.00206	0.65822	0.00115
0.69132	0.00127	0.00157	0.62391	1.74E-04
0.71788	0.01297	0.01296	0.61768	0.00607
0.74796	0.0139	0.01716	0.6026	0.00755
0.80315	7.87E-04	0.001	0.55889	4.50E-04
0.84439	0.00739	0.00741	0.52351	0.014
0.89694	0.00128	0.00112	0.47038	0.00138
0.91074	0.00174	0.00175	0.44361	0.00473
0.96538	0.00317	0.00317	0.24814	0.01569
0.99761	5.53E-04	5.28E-04	0.03416	0.00266

### S3 Glycine Hygroscopicity

**Fig S3.1:** Hygroscopicity of Glycine, (Santa Cruz Biotech LTD), at 293.15 K. Solid line standard UNIFAC prediction.

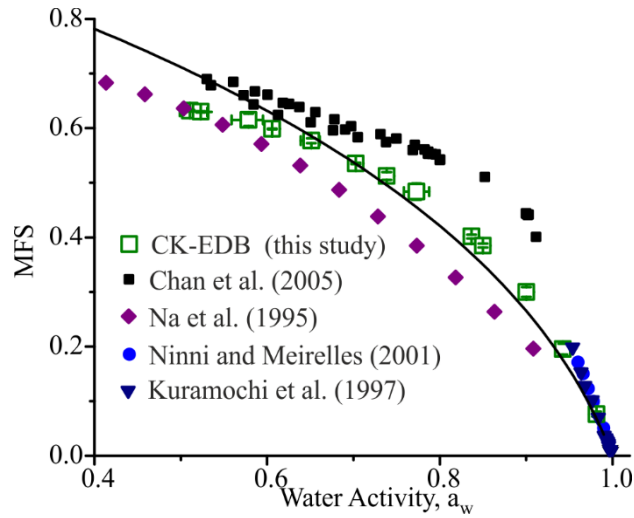


**Table S3.1:** Pure component refractive index ( $n_{melt}$ ) is determined using molar refraction, assuming ideal mixing for calculation of the melt density ( $\rho_{melt}$ ), from bulk data available in Cai et al. (2016). The variation of density as a function of the root of solute mass fraction ( $MFS^{1/2} = x$ ) is represented by polynomial fit parameters. *Upper* and *lower* refer to 95 % confidence limits for fits to experimental data, (Section 2.2 in manuscript).

	$n_{melt}$	$\rho_{melt}/g.cm^{-3}$	Polynomial fit ( $\rho_{sol} = a + b_1x + b_2x^2 + b_3x^3$ )			
			a	$b_1$	$b_2$	$b_3$
<i>Best</i>	1.6634	1.6905	999.47	186.75	-363.66	860.4
<i>Upper</i>	1.6654	1.7006	999.47	192.41	-382.69	883.61
<i>Lower</i>	1.6613	1.6805	999.47	181.22	-345.14	837.67

**Table S3.2:** Tabulated experimental data points shown in Fig S3.1.

$a_w$	error $a_w$ (+ve)	error $a_w$ (-ve)	MFS	error MFS
0.51061	0.00328	0.00389	0.63189	0.00159
0.52315	0.0204	0.02421	0.62993	0.00129
0.57855	0.01673	0.01985	0.61512	0.01113
0.60598	0.00228	0.00276	0.59862	6.15E-04
0.65105	0.00995	0.01205	0.57691	0.00441
0.70256	0.00157	0.00195	0.53551	0.00146
0.73844	0.0068	0.00678	0.51233	0.00686
0.77309	0.01453	0.01453	0.48382	0.01515
0.83663	0.0021	0.00115	0.4015	0.00347
0.84998	0.00206	0.00204	0.38496	0.00336
0.90029	0.00391	0.00391	0.29984	0.00906
0.94266	0.00341	0.00339	0.19519	0.00966
0.98152	0.00147	0.00147	0.07624	0.00455

#### S4 Histidine Hygroscopicity

**Fig S4.1:** Hygroscopicity of L-Histidine, (VWR Chemicals), open symbols, these CC-EDB experiments.

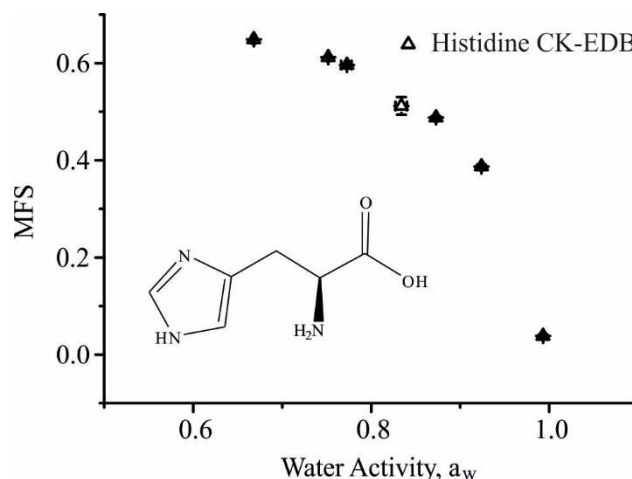


**Table S4.1:** Pure component refractive index ( $n_{melt}$ ) is determined using molar refraction, assuming ideal mixing for calculation of the melt density ( $\rho_{melt}$ ), from bulk data available in Cai et al. (2016). The variation of density as a function of the root of solute mass fraction ( $MFS^{1/2} = x$ ) is represented by polynomial fit parameters. *Upper* and *lower* refer to 95 % confidence limits for fits to experimental data, (Section 2.2 in manuscript).

	$n_{melt}$	$\rho_{melt}/g.cm^{-3}$	Polynomial fit ( $\rho_{sol} = a + b_1x + b_2x^2 + b_3x^3$ )			
			a	$b_1$	$b_2$	$b_3$
<i>Best</i>	1.6892	1.5378	998.9	111.5	-119.61	542.86
<i>Upper</i>	1.6914	1.5462	998.9	115.17	-130.97	558.8
<i>Lower</i>	1.6871	1.5296	998.9	107.98	-108.77	527.49

**Table S4.2:** Tabulated experimental data points shown in **Fig S4.1**.

$a_w$	error $a_w$ (+ve)	error $a_w$ (-ve)	MFS	error MFS
293.15 K				
0.66801	0.00175	0.00214	0.64888	5.85836E-4
0.75174	0.00105	0.00131	0.61182	3.82887E-4
0.77265	0.00527	0.00661	0.59614	0.00177
0.83375	0.0064	0.00643	0.51198	0.01825
0.87281	0.00111	0.00101	0.48826	0.0027
0.9239	8.9548E-4	9.46372E-4	0.38721	0.00439
0.99296	6.37951E-4	6.3374E-4	0.03829	0.00295

## S5 L-Lysine Hygroscopicity

**Fig S5.1:** Hygroscopicity of L-Lysine, (Sigma Aldrich, Purity  $\geq 98\%$ ), at 293.15 K. Open squares, these experiments; solid line, UNIFAC model.

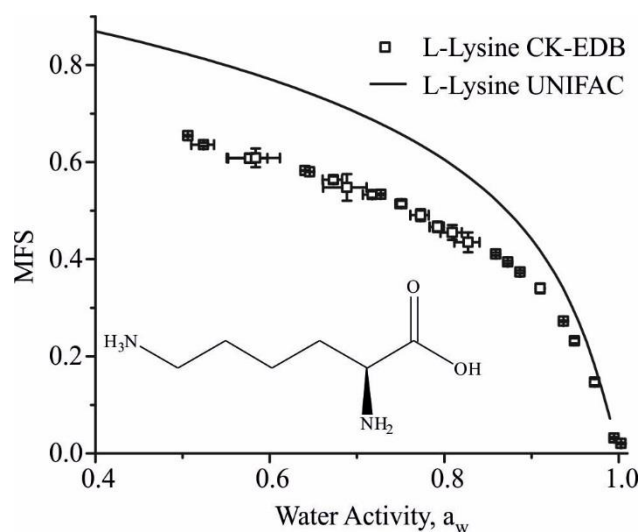


**Table S5.1:** Pure component refractive index ( $n_{melt}$ ) determined using molar refraction where the melt density ( $\rho_{melt}$ ), is determined using a polynomial fit of density to the square root of MFS ( $MFS^{1/2} = x$ ). Bulk values used are available in Cai et al. (2016). *Upper* and *lower* refer to 95 % confidence limits for fits to experimental data.

	$n_{melt}$	$\rho_{melt}/g.cm^{-3}$	Polynomial fit ( $\rho_{sol} = a + b_1x + b_2x^2 + b_3x^3$ )			
			a	$b_1$	$b_2$	$b_3$
<i>Best</i>	1.5586	1.2362	998.2	-15.22	309.14	-56.02
<i>Upper</i>	1.5614	1.2418	998.2	-4.29	271.92	-23.99
<i>Lower</i>	1.5558	1.2306	998.2	-25.93	346.35	-88.05

**Table S5.2:** Tabulated experimental data points shown in Fig S5.1.

$a_w$	error $a_w$ (+ve)	error $a_w$ (-ve)	MFS	error MFS
0.50605	0.00267	0.00316	0.65479	0.00157
0.52404	0.01187	0.01406	0.63621	0.00337
0.57666	0.02059	0.02439	0.60815	0.00948
0.58372	0.02793	0.03308	0.60867	0.01931
0.64049	0.00405	0.00494	0.58275	4.04084E-4
0.64559	0.00205	0.00251	0.57997	4.926E-4
0.67292	0.00999	0.0122	0.56365	0.00675
0.68839	0.0225	0.02735	0.54807	0.02742
0.71755	0.00885	0.01092	0.53328	0.00647
0.72732	0.00179	0.00223	0.53359	0.00179
0.75098	0.0056	0.00696	0.51408	0.00626
0.77291	0.00939	0.01164	0.49095	0.01194
0.79224	0.00736	0.00909	0.46681	0.01099
0.80926	0.01092	0.01352	0.45505	0.01535
0.82751	0.01292	0.01604	0.43489	0.02026
0.85916	0.00152	0.00197	0.41093	0.00309
0.87288	0.00143	0.00143	0.39407	0.00288
0.88688	0.00151	0.00151	0.3739	0.00294
0.90999	0.00294	0.00337	0.33998	0.00983
0.93683	3.20551E-4	3.24824E-4	0.27222	0.00154
0.94931	0.00162	0.00162	0.23179	0.00544
0.97255	0.00147	0.00147	0.14683	0.00623
0.99465	4.49456E-4	4.50168E-4	0.03174	0.0021
1.00277	0.00113	0.00149	0.02039	0.00198

## S6 L-Proline Hygroscopicity

**Figure S6.1:** Hygroscopicity of L-Proline, (Acros Organics, Purity + 99 %), at 293.15 K. Open squares, these experiments.

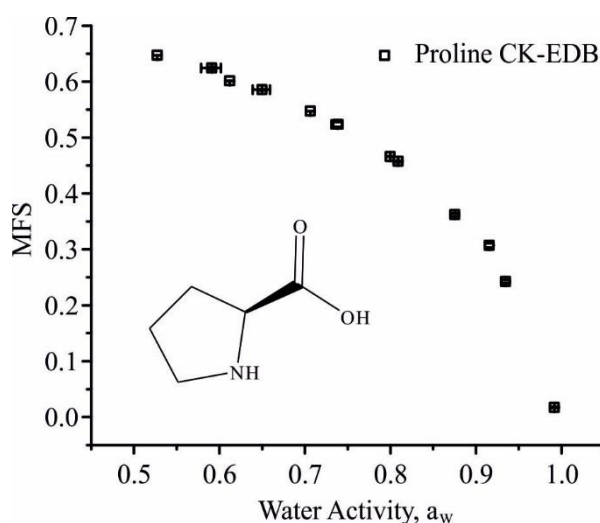


**Table S6.1:** Pure component refractive index ( $n_{melt}$ ) is determined using molar refraction, assuming ideal mixing for calculation of the melt density ( $\rho_{melt}$ ), from bulk data available in Cai et al. (2016). The variation of density as a function of the root of solute mass fraction ( $MFS^{1/2} = x$ ) is represented by polynomial fit parameters. *Upper* and *lower* refer to 95 % confidence limits for fits to experimental data, (Section 2.2 in manuscript).

	$n_{melt}$	$\rho_{melt}/g.cm^{-3}$	Polynomial fit ( $\rho_{sol} = a + b_1x + b_2x^2 + b_3x^3$ )			
			a	$b_1$	$b_2$	$b_3$
<i>Best</i>	1.5948	1.3866	999	55.7	39.01	291
<i>Upper</i>	1.5964	1.3945	999	58.13	32.96	302.44
<i>Lower</i>	1.5932	1.3788	999	53.36	44.73	279.93

**Table S6.2:** Tabulated experimental data points shown in Fig S6.1.

$a_w$	error $a_w$ (+ve)	error $a_w$ (-ve)	MFS	error MFS
0.52739	0.00183	0.00218	0.647	1.53E-04
0.59111	0.01061	0.01264	0.62414	0.00218
0.61213	0.00154	0.00186	0.6013	1.44E-04
0.64995	0.00905	0.01098	0.58549	0.00122
0.70619	9.52E-04	0.00118	0.54716	3.08E-04
0.73823	0.0057	0.00705	0.52349	0.00436
0.79982	7.99E-04	0.00101	0.46617	7.45E-04
0.80883	0.00112	0.00112	0.45742	1.45E-03
0.87515	1.30E-03	0.00103	0.36217	2.56E-03
0.91551	0.00145	0.00184	0.30701	0.00352
0.93455	9.07E-04	9.29E-04	0.24258	0.00279
0.99172	5.01E-04	5.60E-04	0.01734	0.0011

## S7 L-Threonine Hygroscopicity

**Fig S7.1:** Hygroscopicity of L-Threonine, (Acros Organics, Purity 98 %), at 293.15 K. Open squares, these experiments; solid line, UNIFAC model.

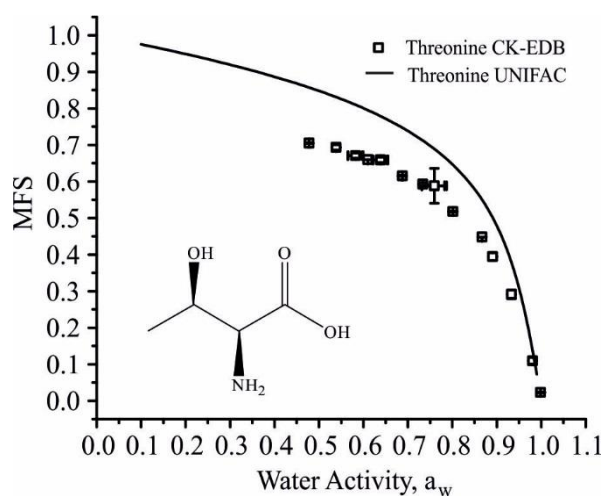


**Table S7.1:** Pure component refractive index ( $n_{melt}$ ) is determined using molar refraction, assuming ideal mixing for calculation of the melt density ( $\rho_{melt}$ ), from bulk data available in Cai et al. (2016). The variation of density as a function of the root of solute mass fraction ( $MFS^{1/2} = x$ ) is represented by polynomial fit parameters. *Upper* and *lower* refer to 95 % confidence limits for fits to experimental data, (Section 2.2 in manuscript).

	$n_{melt}$	$\rho_{melt}/g.cm^{-3}$	Polynomial fit ( $\rho_{sol} = a + b_1x + b_2x^2 + b_3x^3$ )			
			a	$b_1$	$b_2$	$b_3$
<i>Best</i>	1.6185	1.4977	999.4	94.57	-68.14	468.44
<i>Upper</i>	1.6274	1.5403	999.4	112.31	-121.99	546.4
<i>Lower</i>	1.6102	1.4575	999.4	79.24	-23.63	399.69

**Table S7.2:** Tabulated experimental data points shown in Fig S7.1.

$a_w$	error $a_w$ (+ve)	error $a_w$ (-ve)	MFS	error MFS
0.47807	0.00212	0.0025	0.70511	0.00173
0.53888	0.0052	0.0062	0.69319	0.00723
0.58237	0.01442	0.01711	0.67043	0.00714
0.60978	0.00127	0.00154	0.65941	3.88E-04
0.63867	0.01393	0.01689	0.65875	0.00707
0.68779	0.00158	0.00195	0.61529	0.00161
0.73352	0.0081	0.00812	0.59255	0.0041
0.75945	0.02291	0.02781	0.58815	0.04754
0.80118	0.00157	7.31E-04	0.51778	0.00135
0.86674	7.26E-04	4.84E-04	0.44784	3.66E-04
0.89045	0.00426	0.00419	0.39429	0.0104
0.93289	0.00438	0.00418	0.29104	0.01212
0.98064	0.00213	0.00214	0.10966	0.00862
0.99865	7.16E-04	4.45E-04	0.02317	0.00125

## S8 L-Valine Hygroscopicity

**Figure S8.1:** Hygroscopicity of L-Valine, (Sigma Aldrich, Purity  $\geq 98\%$ ), at 293.15 K (blue Open symbols, these CK-EDB experiments; black filled circles, literature data (Kuramochi *et al.*); solid black line, UNIFAC model (293.15 K).

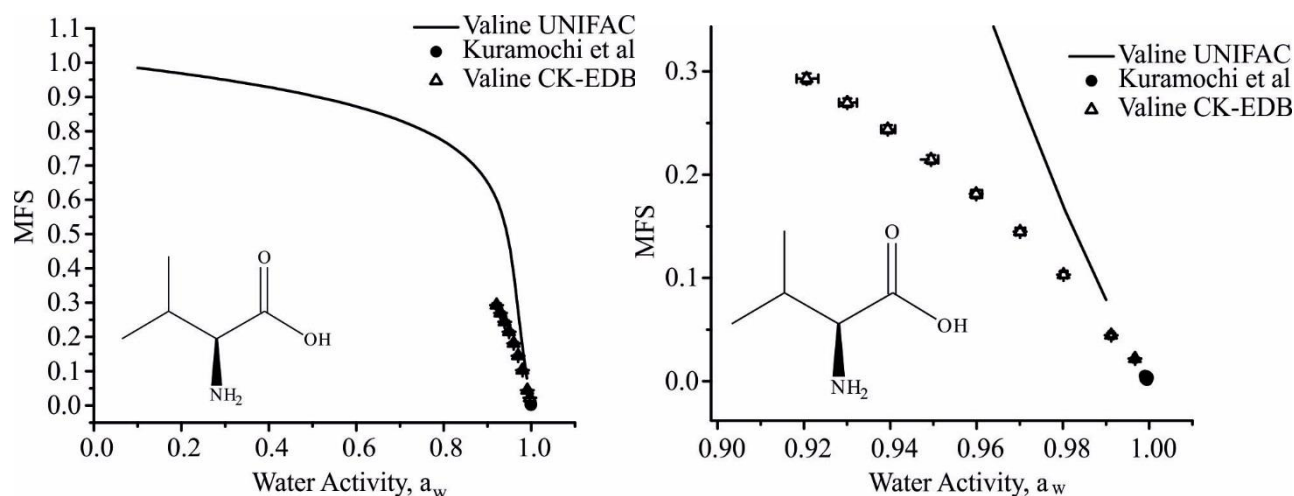


**Table S8.1:** Pure component refractive index ( $n_{melt}$ ) is determined using molar refraction, assuming ideal mixing for calculation of the melt density ( $\rho_{melt}$ ), from bulk data available in Cai *et al.* (2016). The variation of density as a function of the root of solute mass fraction ( $MFS^{1/2} = x$ ) is represented by polynomial fit parameters. *Upper* and *lower* refer to 95 % confidence limits for fits to experimental data, (Section 2.2 in manuscript).

	$n_{melt}$	$\rho_{melt}/g.cm^{-3}$	Polynomial fit ( $\rho_{sol} = a + b_1x + b_2x^2 + b_3x^3$ )			
			a	$b_1$	$b_2$	$b_3$
<i>Best</i>	1.5791	1.2824	998.77	28.73	94.37	159.64
<i>Upper</i>	1.58	1.2872	998.77	29.8	92.82	164.91
<i>Lower</i>	1.5781	1.2776	998.77	27.71	95.81	154.45

**Table S8.2:** Tabulated experimental data points shown in **Fig S8.1**.

$a_w$	error $a_w$ (+ve)	error $a_w$ (-ve)	MFS	error MFS
293.15 K				
0.92062	0.0027	0.00232	0.29295	0.00499
0.93004	2.26E-03	0.00195	0.26962	4.18E-03
0.93941	0.00173	0.00148	0.24396	0.00404
0.94943	0.00169	0.00145	0.21478	0.00403
0.9599	0.00138	0.00118	0.18125	0.00388
0.97008	0.00118	0.00101	0.14482	0.00345
0.98014	8.66E-04	7.41E-04	0.10314	2.94E-03
0.99117	5.34E-04	5.69E-04	0.04451	0.00201
0.99669	4.13E-04	4.57E-04	0.02205	8.65E-04

## S9 Citric Acid Hygroscopicity

**Figure S9.1:** Hygroscopicity of Citric Acid, (Sigma Aldrich, Purity 99 %), at 293.15 K. Open squares, these EDB experiments; solid line, UNIFAC model.

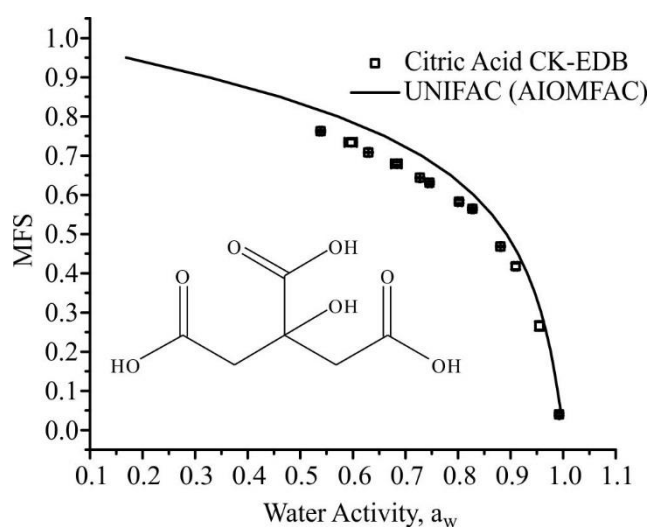


**Table S9.1:** Pure component refractive index ( $n_{melt}$ ) determined using molar refraction where the melt density ( $\rho_{melt}$ ) is determined using a polynomial fit of density to the square root of MFS ( $MFS^{1/2} = x$ ). Bulk values used are available in Cai et al. (2016). *Upper* and *lower* refer to 95 % confidence limits for fits to experimental data.

	$n_{melt}$	$\rho_{melt}/g.cm^{-3}$	Polynomial fit ( $\rho_{sol} = a + b_1x + b_2x^2 + b_3x^3$ )			
			a	$b_1$	$b_2$	$b_3$
<i>Best</i>	1.5054	1.550	998.0	25.0	253.84	273.2
<i>Upper</i>	1.5071	1.5565	998.0	37.88	211.13	309.49
<i>Lower</i>	1.5037	1.5436	998.0	12.11	296.56	236.92

**Table S9.2:** Tabulated experimental data points shown in Fig S9.1.

$a_w$	error $a_w$ (+ve)	error $a_w$ (-ve)	MFS	error MFS
0.53894	0.0024	0.00286	0.76226	0.00233
0.59688	0.01043	0.01244	0.73375	0.00875
0.62961	0.00223	0.00271	0.70793	7.62E-04
0.6837	0.00876	0.01065	0.67914	0.00409
0.72762	0.00123	0.00153	0.64368	0.00135
0.74592	0.00403	0.00404	0.63069	0.00342
0.80229	0.00504	0.0029	0.58246	0.00401
0.82734	0.00237	0.00196	0.56406	0.00314
0.88104	0.00107	0.0012	0.4682	0.00149
0.90968	0.00331	0.00327	0.41761	0.00738
0.95487	0.0028	0.00279	0.26562	0.01165
0.99255	6.21E-04	6.70E-04	0.03973	0.00355

### S10 L-Tartaric Acid Hygroscopicity

**Figure S10.1:** Hygroscopicity of Tartaric Acid, (Sigma Aldrich, Purity  $\geq 99.5\%$ ), at 293.15 K. Open squares, these EDB experiments; solid line, UNIFAC model.

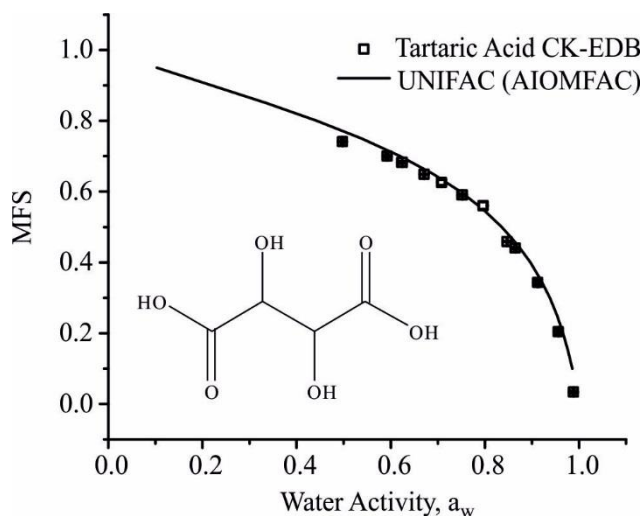


**Table S10.1:** Pure component refractive index ( $n_{melt}$ ) determined using molar refraction where the melt density ( $\rho_{melt}$ ) is determined using a polynomial fit of density to the square root of MFS ( $MFS^{1/2} = x$ ). Bulk values used are available in Cai et al. (2016). *Upper* and *lower* refer to 95 % confidence limits for fits to experimental data.

	$n_{melt}$	$\rho_{melt}/ \text{g.cm}^{-3}$	Polynomial fit ( $\rho_{sol} = a + b_1x + b_2x^2 + b_3x^3$ )			
			a	$b_1$	$b_2$	$b_3$
<i>Best</i>	1.4992	1.6007	999	15.08	325.84	260.78
<i>Upper</i>	1.4996	1.6128	999	29.23	273.11	311.49
<i>Lower</i>	1.4936	1.5886	999	93.2	378.58	210.06

**Table S10.2:** Tabulated experimental data points shown in **Fig S10.1**.

$a_w$	error $a_w$ (+ve)	error $a_w$ (-ve)	MFS	error MFS
0.49764	0.00285	0.00337	0.74075	0.00145
0.59229	0.00275	0.00332	0.70005	0.00184
0.62457	0.00897	0.01082	0.68273	0.00361
0.67107	0.00165	0.00203	0.64893	7.95E-04
0.70799	0.00711	0.00826	0.6255	0.0076
0.75229	0.00853	0.01048	0.59046	0.00337
0.79666	0.00778	0.00946	0.56049	0.00992
0.84739	9.37E-04	5.51E-04	0.45906	0.00122
0.86463	0.00206	0.00206	0.44068	0.00269
0.91248	0.00302	0.00302	0.34362	0.00774
0.95599	0.00217	0.00216	0.20415	0.00789
0.98847	0.00104	0.00105	0.03363	0.00337

## S11 Oxalic Acid Hygroscopicity

**Fig S11.1:** Hygroscopicity of Oxalic Acid, (Sigma Aldrich, Purity 98 %), at 293.15 K. Open squares, these experiments; solid line, UNIFAC model.

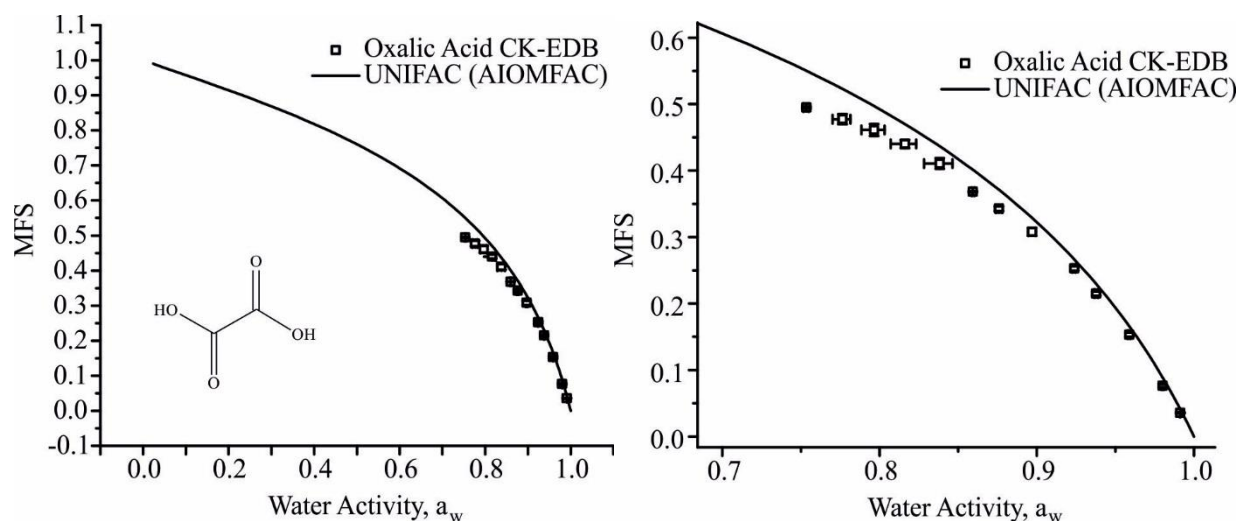


**Table S11.1:** Pure component refractive index ( $n_{melt}$ ) is determined using molar refraction, assuming ideal mixing for calculation of the melt density ( $\rho_{melt}$ ), from bulk data available in Cai et al. (2016). The variation of density as a function of the root of solute mass fraction ( $MFS^{1/2} = x$ ) is represented by polynomial fit parameters. *Upper* and *lower* refer to 95 % confidence limits for fits to experimental data, (Section 2.2 in manuscript).

	$n_{melt}$	$\rho_{melt}/g \cdot cm^{-3}$	Polynomial fit ( $\rho_{sol} = a + b_1x + b_2x^2 + b_3x^3 + b_4x^4 + b_5x^5 + b_6x^6$ )						
			a	$b_1$	$b_2$	$b_3$	$b_4$	$b_5$	$b_6$
<i>Best</i>	1.5167	1.7237	998.4	-14.98	636.47	-1074.2	2603.92	-2596.5	1170.54
<i>Upper</i>	1.5185	1.7403	998.4	-16.27	660.48	-1165.1	2811.06	-2809	1260.66
<i>Lower</i>	1.5149	1.7073	998.4	-13.78	613.65	-989.39	2409.96	-2397.5	1085.84

**Table S11.2:** Tabulated experimental data points shown in **Fig S11.1**.

$a_w$	error $a_w$ (+ve)	error $a_w$ (-ve)	MFS	error MFS
0.75352	0.00146	0.00183	0.49497	0.00148
0.77652	0.00502	0.00629	0.47731	0.0077
0.79664	0.00652	0.00817	0.46116	0.00912
0.81614	0.00716	0.00896	0.44009	0.00613
0.83841	0.00803	0.01005	0.41068	0.00808
0.85938	0.0012	7.60E-04	0.36829	0.00113
0.87602	0.00199	0.00188	0.34275	0.00355
0.89702	0.00235	0.00215	0.30804	0.00596
0.92388	8.50E-04	0.00115	0.25275	0.00331
0.93784	0.00106	0.00106	0.21515	0.00299
0.9589	8.73E-04	8.75E-04	0.15314	0.00313
0.98012	5.72E-04	5.68E-04	0.07645	0.00227
0.99129	2.93E-04	3.54E-04	0.03567	8.98E-04

## S12 Malonic Acid Hygroscopicity

**Figure S12.1:** Hygroscopicity of Malonic Acid, (Sigma Aldrich, Purity 98 %), at 293.15 K. Open squares, these experiments; solid line, UNIFAC model.

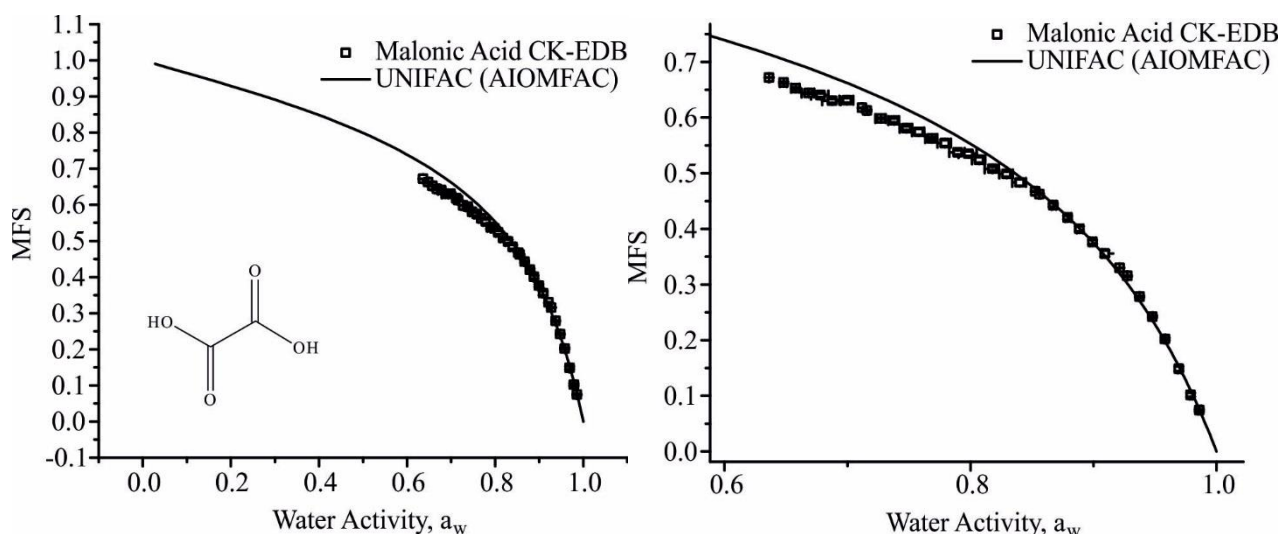


**Table S12.1:** Pure component refractive index determined using molar refraction where the melt density is determined using a polynomial fit of density to the square root of MFS ( $MFS^{1/2} = x$ ). Bulk values used are available in Cai et al. (2016). *Upper* and *lower* refer to 95 % confidence limits for fits to experimental data.

	$n_{melt}$	$\rho_{melt}/g.cm^{-3}$	Polynomial fit ( $\rho_{sol} = a + b_1x + b_2x^2 + b_3x^3$ )			
			a	$b_1$	$b_2$	$b_3$
<i>Best</i>	1.4611	1.4558	997.2	13.47	262.36	182.76
<i>Upper</i>	1.4627	1.4612	997.2	20.7	235.91	207.37
<i>Lower</i>	1.4594	1.4504	997.2	6.24	288.82	158.15

**Table S12.2:** Tabulated experimental data points shown in **Fig S12.1**.

$a_w$	error $a_w$ (+ve)	error $a_w$ (-ve)	MFS	error MFS
0.63613	4.14E-04	5.04E-04	0.6718	1.62E-04
0.64803	0.00253	0.00308	0.66275	0.00161
0.65776	0.00301	0.00367	0.65273	0.00197
0.66822	0.00457	0.00558	0.64421	0.00162
0.67795	0.00624	0.00761	0.64043	0.00324
0.68747	0.00679	0.00828	0.62992	0.00337
0.6994	0.0051	0.00625	0.63085	0.00413
0.7117	4.61E-04	5.72E-04	0.6176	2.85E-04
0.71572	0.00132	0.00164	0.61275	0.00135
0.72728	0.00371	0.00458	0.59849	0.00119
0.73786	0.00398	0.0049	0.59485	0.00362
0.74792	0.00441	0.00544	0.58075	0.00309
0.75777	0.00438	0.00539	0.57442	0.00518
0.76852	0.00437	0.00539	0.56217	0.00227
0.77901	0.00483	0.00595	0.55399	0.00568
0.78948	0.00564	0.00694	0.53743	0.0039
0.79831	0.00665	0.00816	0.53501	0.00406
0.80703	0.00469	0.00576	0.52388	0.00468
0.81779	0.00517	0.00637	0.50809	0.00307
0.82931	0.00495	0.0061	0.49855	0.00449
0.83997	0.00501	0.00616	0.48341	0.0058
0.85259	0.0013	8.20E-04	0.46721	9.32E-04
0.85596	0.00112	6.98E-04	0.46233	0.00114
0.86726	0.00223	0.00146	0.44257	0.00286
0.87898	0.00278	0.00183	0.4203	0.0033
0.8885	0.00291	0.00204	0.4002	0.0044

0.89906	0.00294	0.00205	0.37643	0.00371
0.90919	0.00337	0.00233	0.35563	0.00559
0.9213	1.65E-04	2.03E-04	0.32987	3.33E-04
0.92743	2.61E-04	2.85E-04	0.31545	0.00122
0.93737	3.90E-04	4.01E-04	0.27835	0.00185
0.94793	4.69E-04	4.71E-04	0.24233	0.00205
0.95802	4.67E-04	4.69E-04	0.20227	0.00223
0.96932	0.0018	0.0011	0.14857	0.00427
0.97897	0.00144	8.79E-04	0.10171	0.00358
0.98599	0.00158	9.62E-04	0.07431	0.00205

### S13 Succinic Acid Hygroscopicity

**Fig S13.1:** Hygroscopicity of Succinic Acid, (Sigma Aldrich, Purity 99 %), at 293.15 K. Open squares, these experiments; solid line, UNIFAC model.

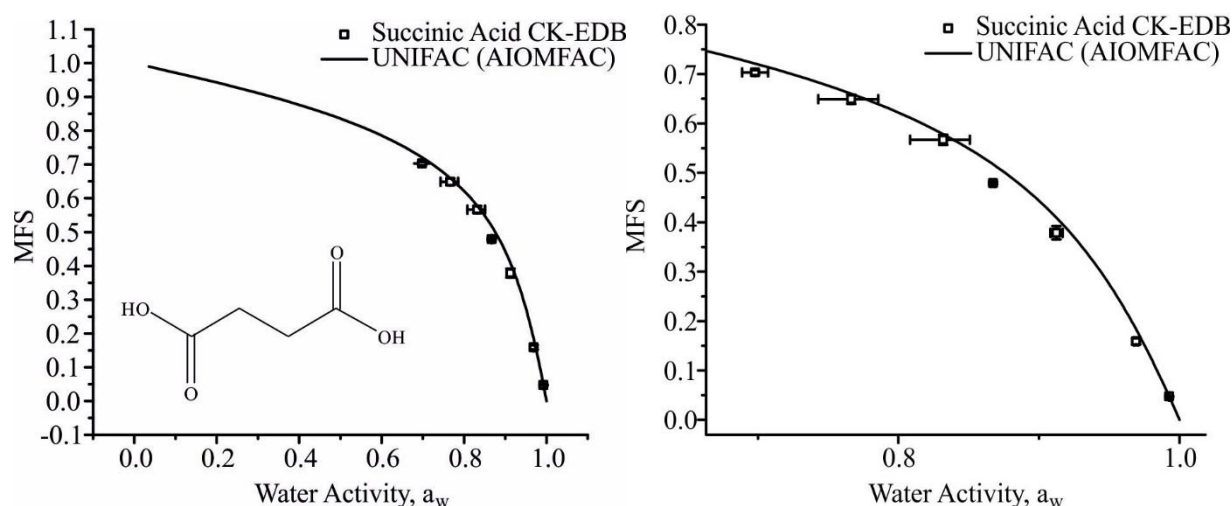


**Table S13.1:** Pure component refractive index ( $n_{\text{melt}}$ ) is determined using molar refraction, assuming ideal mixing for calculation of the melt density ( $\rho_{\text{melt}}$ ), from bulk data available in Cai et al. (2016). The variation of density as a function of the root of solute mass fraction ( $\text{MFS}^{1/2} = x$ ) is represented by polynomial fit parameters. *Upper* and *lower* refer to 95 % confidence limits for fits to experimental data, (Section 2.2 in manuscript).

	$n_{\text{melt}}$	$\rho_{\text{melt}}/\text{g}\cdot\text{cm}^{-3}$	Polynomial fit ( $\rho_{\text{sol}} = a + b_1x + b_2x^2 + b_3x^3 + b_4x^4 + b_5x^5 + b_6x^6$ )						
			a	$b_1$	$b_2$	$b_3$	$b_4$	$b_5$	$b_6$
<i>Best</i>	1.4928	1.4185	998.2	-1.96	324.69	-146.48	426.3	-373.62	191.37
<i>Upper</i>	1.4935	1.4249	998.2	-2.08	329.57	-155.12	447.91	-395.04	201.45
<i>Lower</i>	1.4920	1.4122	998.2	-1.85	319.93	-138.32	405.79	-353.36	181.79

**Table S13.2:** Tabulated experimental data points shown in Fig S13.1.

$a_w$	error $a_w$ (+ve)	error $a_w$ (-ve)	MFS	error MFS
0.69803	0.00919	0.00918	0.70299	0.00502
0.76653	0.0191	0.02355	0.64896	0.00963
0.83176	0.0191	0.02355	0.56672	0.01018
0.86728	0.00142	0.00142	0.47926	0.0025
0.91247	0.00444	0.0044	0.37868	0.01328
0.96915	0.00137	0.00136	0.15909	0.00637
0.99255	3.09E-04	3.16E-04	0.04733	0.00178

## S14 Glutaric Acid Hygroscopicity

**Figure S14.1:** Hygroscopicity of Glutaric Acid, (Sigma Aldrich, Purity 99 %), at 293.15 K. Open squares, these experiments; solid line, UNIFAC model.

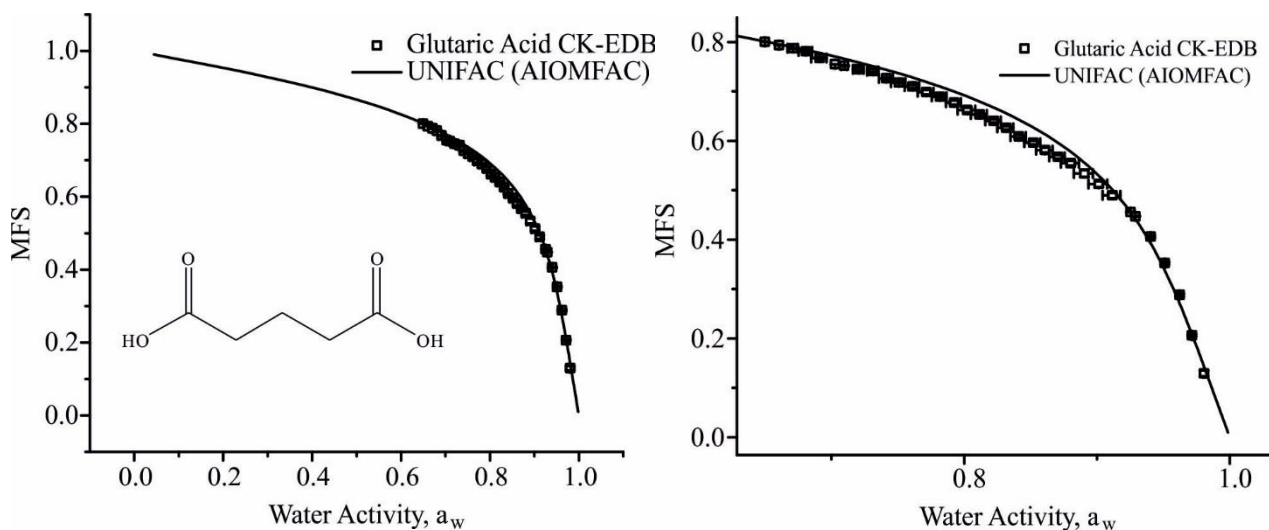


**Table S14.1:** Pure component refractive index ( $n_{melt}$ ) determined using molar refraction where the melt density ( $\rho_{melt}$ ) is determined using a polynomial fit of density to the square root of MFS ( $MFS^{1/2} = x$ ). Bulk values used are available in Cai et al. (2016). *Upper* and *lower* refer to 95 % confidence limits for fits to experimental data.

	$n_{melt}$	$\rho_{melt}/g.cm^{-3}$	Polynomial fit ( $\rho_{sol} = a + b_1x + b_2x^2 + b_3x^3$ )			
			a	b <sub>1</sub>	b <sub>2</sub>	b <sub>3</sub>
<i>Best</i>	1.4655	1.2745	997.5	-1.56	238.79	39.75
<i>Upper</i>	1.4660	1.2760	997.5	0.401	231.59	46.55
<i>Lower</i>	1.4649	1.2729	997.5	-3.53	245.98	32.95

**Table S14.2:** Tabulated experimental data points shown in **Fig S14.1**.

a <sub>w</sub>	error a <sub>w</sub> (+ve)	error a <sub>w</sub> (-ve)	MFS	error MFS
0.64988	4.93E-04	6.03E-04	0.80052	2.01E-04
0.66053	5.88E-04	7.21E-04	0.79339	2.71E-04
0.67122	0.00348	0.00426	0.78724	9.92E-04
0.68089	0.00458	0.00561	0.78134	0.00256
0.69112	0.00522	0.00639	0.76761	0.00226
0.70268	4.02E-04	4.98E-04	0.75519	1.75E-04
0.70969	0.0019	0.00235	0.75207	8.79E-04
0.72069	0.00357	0.00441	0.74499	0.00276
0.73156	0.0038	0.00469	0.74131	0.003
0.74152	0.00467	0.00575	0.72636	0.00217
0.75089	0.00485	0.00598	0.71793	0.00185
0.76119	0.00482	0.00594	0.70997	0.00323
0.77157	0.00535	0.00659	0.69846	0.00478
0.7818	0.00495	0.0061	0.68945	0.00241
0.79242	0.00502	0.00618	0.6775	0.00399
0.80236	5.99E-03	7.39E-03	0.6624	0.00435
0.81173	5.37E-03	6.62E-03	0.65327	0.00271
0.82228	0.00521	0.00642	0.64016	0.00336
0.83171	0.00538	0.00662	0.62617	0.00336
0.84134	0.00521	0.00642	0.60886	0.0028
0.852	0.00538	0.00663	0.59616	0.00364
0.86106	0.00556	0.00684	0.58136	0.00487
0.87055	0.00521	0.00642	0.56748	0.00361
0.88031	0.00617	0.00761	0.5545	0.00465
0.89058	0.00635	0.00785	0.5337	0.00679
0.90142	0.00628	0.00777	0.51244	0.00601

0.91173	0.00596	0.00737	0.48949	0.00523
0.92543	1.50E-04	2.02E-04	0.45608	4.73E-04
0.92905	1.56E-04	1.58E-04	0.44732	6.46E-04
0.94053	3.86E-04	3.86E-04	0.40605	0.00233
0.95111	4.52E-04	4.52E-04	0.35279	0.00256
0.96227	3.42E-04	3.41E-04	0.28818	0.00275
0.97153	3.20E-04	3.20E-04	0.20634	0.00243
0.98066	8.31E-04	8.09E-04	0.12936	0.00558

### S15 Adipic Acid Hygroscopicity

**Figure S15.1:** Hygroscopicity of Adipic Acid, (Sigma Aldrich, Purity 99 %), at 293.15 K. Open squares, these experiments; solid line, UNIFAC model.

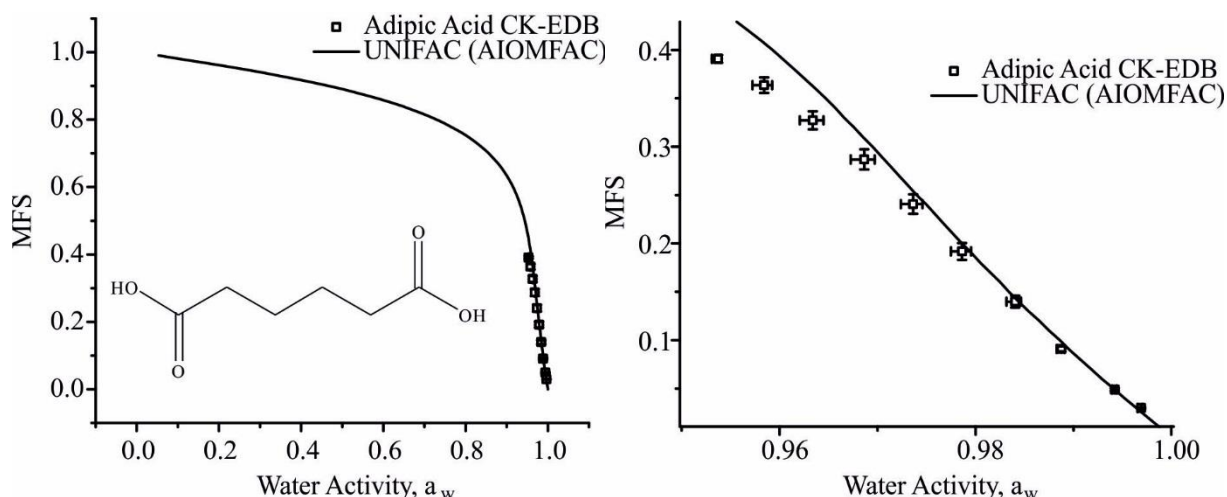


**Table S15.1:** Pure component refractive index ( $n_{\text{melt}}$ ) is determined using molar refraction, assuming ideal mixing for calculation of the melt density ( $\rho_{\text{melt}}$ ), from bulk data available in Cai et al. (2016). The variation of density as a function of the root of solute mass fraction ( $\text{MFS}^{1/2} = x$ ) is represented by polynomial fit parameters. *Upper* and *lower* refer to 95 % confidence limits for fits to experimental data, (Section 2.2 in manuscript).

	$n_{\text{melt}}$	$\rho_{\text{melt}} / \text{g.cm}^{-3}$	Polynomial fit ( $\rho_{\text{sol}} = a + b_1x + b_2x^2 + b_3x^3 + b_4x^4 + b_5x^5 + b_6x^6$ )						
			a	$b_1$	$b_2$	$b_3$	$b_4$	$b_5$	$b_6$
<i>Best</i>	1.5052	1.2897	998.2	-0.483	232.81	-36.78	137.06	-96.59	55.48
<i>Upper</i>	1.5093	1.3192	998.2	-0.705	253.36	-53.41	183.61	-139.01	77.14
<i>Lower</i>	1.5012	1.2614	998.2	-0.323	213.1	-24.73	101.55	-65.53	39.14

**Table S15.2:** Tabulated experimental data points shown in Fig S15.1.

$a_w$	error $a_w$ (+ve)	error $a_w$ (-ve)	MFS	error MFS
0.95373	3.22E-04	6.26E-04	0.39071	0.00391
0.95843	8.35E-04	0.00118	0.36348	0.00812
0.9634	0.0011	0.00133	0.3272	0.00935
0.96865	0.00107	0.00138	0.28685	0.01043
0.97365	9.42E-04	0.00127	0.24062	0.01007
0.97863	9.10E-04	0.00114	0.1917	0.00876
0.98405	5.88E-04	8.82E-04	0.13977	0.00621
0.98877	3.13E-04	4.91E-04	0.09086	0.0027
0.99423	1.80E-04	3.02E-04	0.04898	0.00153
0.99692	1.66E-04	3.62E-04	0.02978	7.74E-04

## S16 Pimelic Acid Hygroscopicity

**Fig S16.1:** Hygroscopicity of Pimelic Acid, (Sigma Aldrich, Purity 99 %), at 293.15 K. Open squares, these experiments; solid line, UNIFAC model.

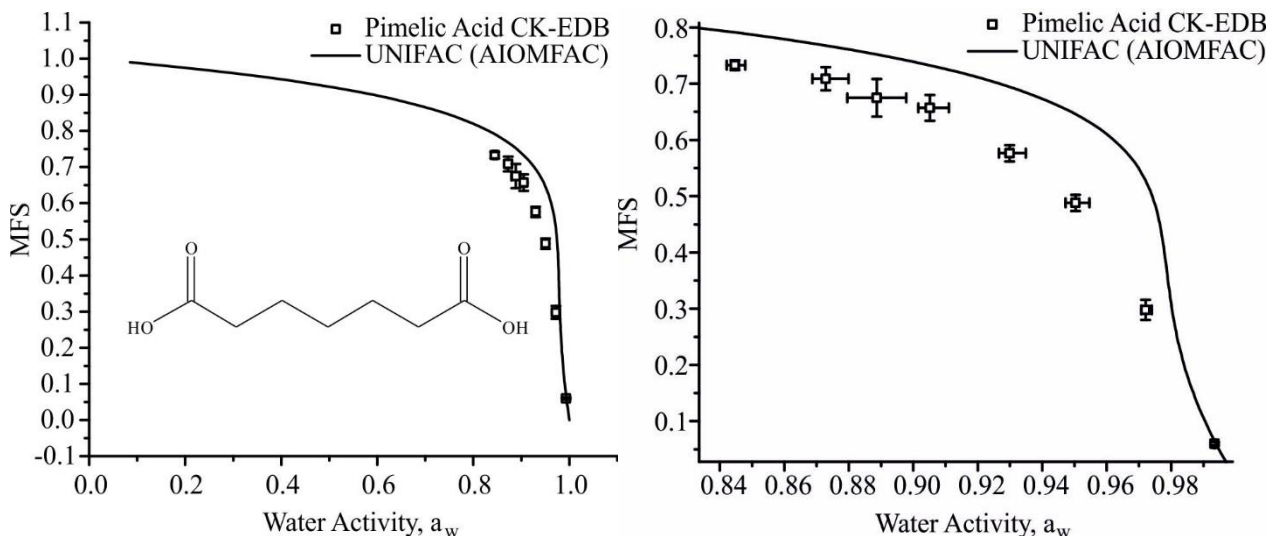


**Table S16.1:** Pure component refractive index ( $n_{\text{melt}}$ ) is determined using molar refraction, assuming ideal mixing for calculation of the melt density ( $\rho_{\text{melt}}$ ), from bulk data available in Cai et al. (2016). The variation of density as a function of the root of solute mass fraction ( $\text{MFS}^{1/2} = x$ ) is represented by polynomial fit parameters. *Upper* and *lower* refer to 95 % confidence limits for fits to experimental data, (Section 2.2 in manuscript).

	$n_{\text{melt}}$	$\rho_{\text{melt}}/\text{g}\cdot\text{cm}^{-3}$	Polynomial fit ( $\rho_{\text{sol}} = a + b_1x + b_2x^2 + b_3x^3 + b_4x^4 + b_5x^5 + b_6x^6$ )						
			a	$b_1$	$b_2$	$b_3$	$b_4$	$b_5$	$b_6$
<i>Best</i>	1.4917	1.2262	998.5	-0.184	188.18	-14.19	67.86	-37.91	23.94
<i>Upper</i>	1.4940	1.2435	998.5	-0.246	200.41	-18.89	83.16	-50.18	30.74
<i>Lower</i>	1.4894	1.2095	998.5	-0.136	176.23	-10.52	55.25	-28.29	18.47

**Table S16.2:** Tabulated experimental data points shown in Fig S16.1.

$a_w$	error $a_w$ (+ve)	error $a_w$ (-ve)	MFS	error MFS
0.84466	0.00317	0.00251	0.73296	0.0087
0.87279	0.00711	0.00413	0.70863	0.02048
0.88863	0.00919	0.00916	0.67508	0.03342
0.90517	0.00585	0.00361	0.65697	0.02274
0.92985	0.00504	0.00334	0.57632	0.01441
0.9503	0.00434	0.00304	0.48806	0.01436
0.97207	0.0019	0.00139	0.29782	0.01787
0.99347	2.49E-04	3.32E-04	0.06002	0.00268

## S17 Methyl Malonic Acid Hygroscopicity

**Fig S17.1:** Hygroscopicity of methyl malonic acid, (Sigma Aldrich, Purity 99 %), at 293.15 K. Open squares, these experiments; solid line, UNIFAC model.

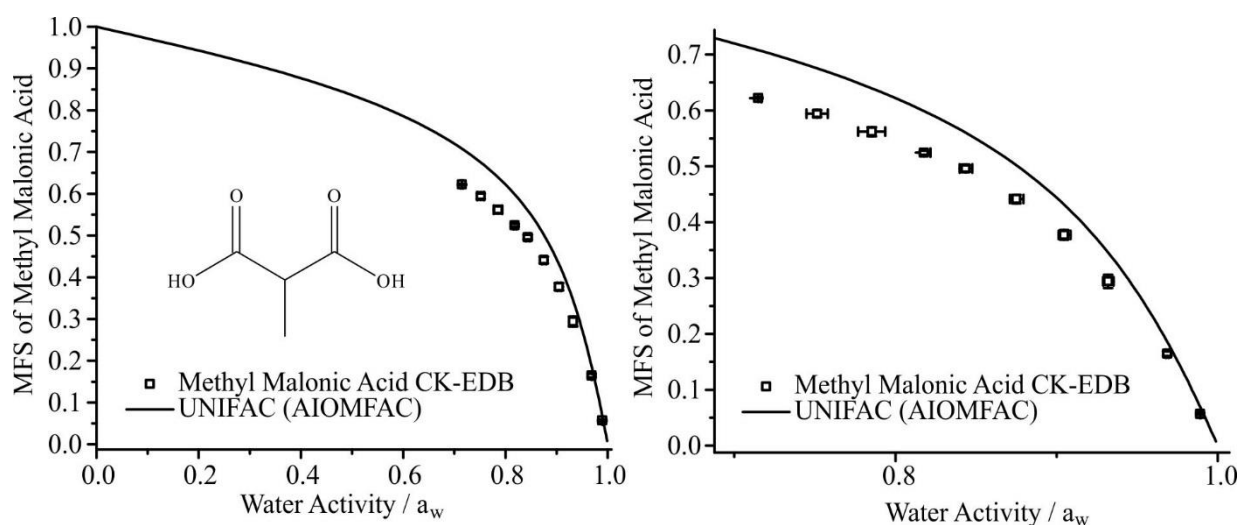


**Table S17.1:** Pure component refractive index ( $n_{\text{melt}}$ ) is determined using molar refraction, assuming ideal mixing for calculation of the melt density ( $\rho_{\text{melt}}$ ), from bulk data available in Cai et al. (2016). The variation of density as a function of the root of solute mass fraction ( $\text{MFS}^{1/2} = x$ ) is represented by polynomial fit parameters. *Upper* and *lower* refer to 95 % confidence limits for fits to experimental data, (Section 2.2 in manuscript).

	$n_{\text{melt}}$	$\rho_{\text{melt}} / \text{g.cm}^{-3}$	Polynomial fit ( $\rho_{\text{sol}} = a + b_1x + b_2x^2 + b_3x^3 + b_4x^4 + b_5x^5 + b_6x^6$ )						
			a	b <sub>1</sub>	b <sub>2</sub>	b <sub>3</sub>	b <sub>4</sub>	b <sub>5</sub>	b <sub>6</sub>
<i>Best</i>	1.4817	1.3876	998.8	-1.45	301.28	-108.73	330.65	-279.56	146.61
<i>Upper</i>	1.4819	1.3902	998.8	-1.49	303.18	-111.53	337.82	-286.56	149.98
<i>Lower</i>	1.4815	1.3851	998.8	-1.42	299.45	-106.09	323.86	-272.94	143.43

**Table S17.2:** Tabulated experimental data points shown in **Fig S17.1**.

a <sub>w</sub>	error a <sub>w</sub> (+ve)	error a <sub>w</sub> (-ve)	MFS	error MFS
0.71493	0.002	0.00248	0.62219	0.00155
0.75141	0.00657	0.00657	0.59428	0.00609
0.78527	0.0084	0.0084	0.562	0.00836
0.81777	0.004	0.00245	0.52434	0.00364
0.84355	0.00409	0.00369	0.49609	0.00573
0.875	0.00438	0.00401	0.44143	0.00784
0.90462	0.00402	0.00333	0.3774	0.00875
0.93201	0.00335	0.00317	0.29413	0.01184
0.96865	8.29E-04	8.90E-04	0.16472	0.0041
0.98911	4.09E-04	4.11E-04	0.05691	0.00203

### S18 Methyl Succinic Acid Hygroscopicity

**Figure S18.1:** Hygroscopicity of methyl succinic acid, (Sigma Aldrich, Purity 99 %), at 293.15 K. Open squares, these experiments; solid line, UNIFAC model.

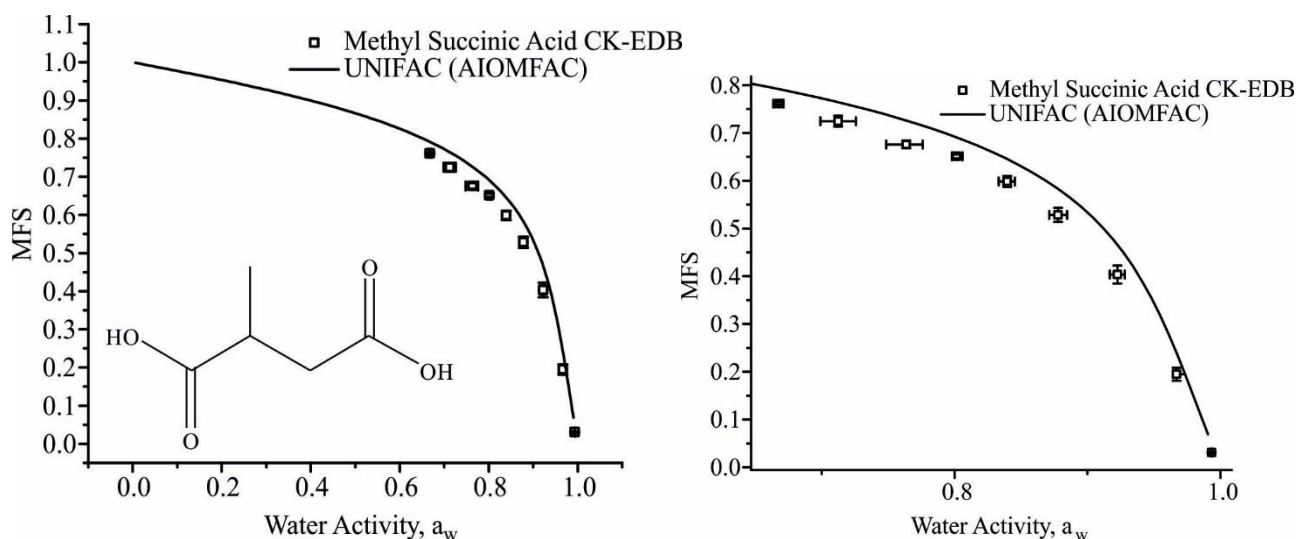


**Table S18.1:** Pure component refractive index ( $n_{melt}$ ) is determined using molar refraction, assuming ideal mixing for calculation of the melt density ( $\rho_{melt}$ ), from bulk data available in Cai et al. (2016). The variation of density as a function of the root of solute mass fraction ( $MFS^{1/2} = x$ ) is represented by polynomial fit parameters. *Upper* and *lower* refer to 95 % confidence limits for fits to experimental data, (Section 2.2 in manuscript).

	$n_{melt}$	$\rho_{melt}/g.cm^{-3}$	Polynomial fit ( $\rho_{sol} = a + b_1x + b_2x^2 + b_3x^3 + b_4x^4 + b_5x^5 + b_6x^6$ )						
			a	$b_1$	$b_2$	$b_3$	$b_4$	$b_5$	$b_6$
<i>Best</i>	1.4779	1.3035	998.2	-0.572	242.3	-43.51	156.55	-114.16	64.69
<i>Upper</i>	1.4784	1.3090	998.2	-0.614	246.13	-46.62	165.26	-122.12	68.76
<i>Lower</i>	1.4774	1.2980	998.2	-0.533	238.48	-40.56	148.19	-106.58	60.79

**Table S18.2:** Tabulated experimental data points shown in Fig S18.1.

$a_w$	error $a_w$ (+ve)	error $a_w$ (-ve)	MFS	error MFS
0.66772	0.00345	0.00424	0.76125	0.00296
0.71234	0.0134	0.0134	0.72476	0.01132
0.7636	0.01237	0.01517	0.67596	0.00785
0.80135	0.00451	0.00326	0.65118	0.00447
0.83951	0.00575	0.00629	0.59855	0.01151
0.87778	0.00688	0.00657	0.52839	0.01469
0.92249	0.00567	0.00567	0.40343	0.01891
0.96705	0.00282	0.00249	0.19484	0.01368
0.99344	3.28E-04	3.47E-04	0.03075	0.00168

### S19 Binary Aqueous Diethylmalonic Acid - Hygroscopicity

**Fig S19.1:** Hygroscopicity of diethylmalonic acid, (Sigma Aldrich, Purity 98 %), at 293.15 K. Open squares, these experiments; solid line, UNIFAC model.

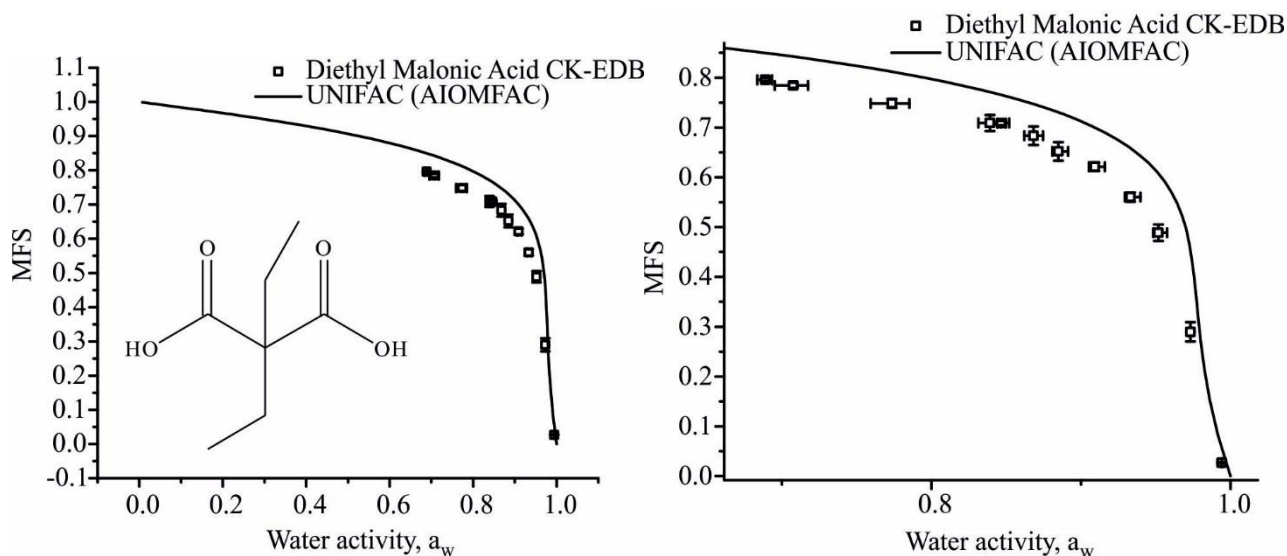


**Table S19.1:** Pure component refractive index ( $n_{melt}$ ) is determined using molar refraction, assuming ideal mixing for calculation of the melt density ( $\rho_{melt}$ ), from bulk data available in Cai et al. (2016). The variation of density as a function of the root of solute mass fraction ( $MFS^{1/2} = x$ ) is represented by polynomial fit parameters. *Upper* and *lower* refer to 95 % confidence limits for fits to experimental data, (Section 2.2 in manuscript).

	$n_{melt}$	$\rho_{melt}/g.cm^{-3}$	Polynomial fit ( $\rho_{sol} = a + b_1x + b_2x^2 + b_3x^3 + b_4x^4 + b_5x^5 + b_6x^6$ )						
			a	$b_1$	$b_2$	$b_3$	$b_4$	$b_5$	$b_6$
<i>Best</i>	1.4854	1.2184	998.2	-0.161	182.82	-12.45	61.98	-33.36	21.37
<i>Upper</i>	1.4858	1.2219	998.2	-0.172	185.32	-13.25	64.69	-35.44	22.55
<i>Lower</i>	1.4850	1.2149	998.2	-0.151	180.32	-11.69	59.36	-31.37	20.24

**Table S19.2:** Tabulated experimental data points shown in **Figure S19.1**.

$a_w$	error $a_w$ (+ve)	error $a_w$ (-ve)	MFS	error MFS
0.68895	0.00441	0.00543	0.79565	0.00315
0.70762	0.01	0.01233	0.78448	0.00548
0.7737	0.01156	0.01425	0.7484	0.00901
0.83916	0.01287	0.00773	0.70902	0.01617
0.84654	0.00329	0.00246	0.70885	0.00435
0.86832	0.00637	0.0062	0.68324	0.01847
0.88499	0.00646	0.00418	0.65203	0.0186
0.90928	0.00665	0.00391	0.62123	0.00847
0.93317	0.00665	0.00374	0.56028	0.00907
0.95177	0.00586	0.00329	0.48861	0.01646
0.97321	0.00199	0.00152	0.28968	0.01912
0.99422	3.23E-04	3.66E-04	0.02697	0.00157

## S20 2,2-Dimethyl Glutaric Acid Hygroscopicity

**Fig S20.1:** Hygroscopicity of 2,2-dimethyl glutaric acid, (Sigma Aldrich, Purity > 98 %), at 293.15 K. Open squares, these experiments; solid line, UNIFAC model.

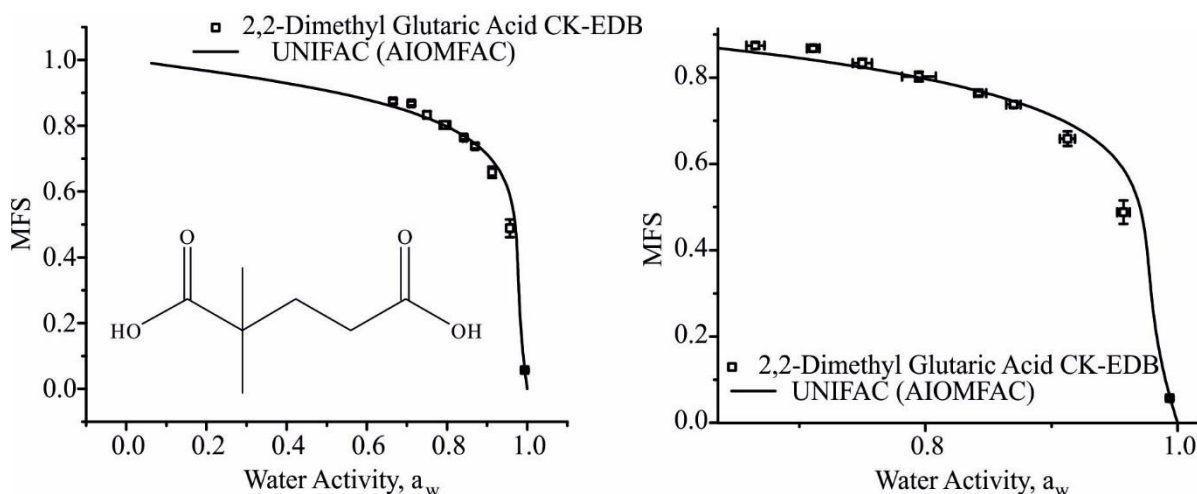


**Table S20.1:** Pure component refractive index ( $n_{\text{melt}}$ ) is determined using molar refraction, assuming ideal mixing for calculation of the melt density ( $\rho_{\text{melt}}$ ), from bulk data available in Cai et al. (2016). The variation of density as a function of the root of solute mass fraction ( $\text{MFS}^{1/2} = x$ ) is represented by polynomial fit parameters. *Upper* and *lower* refer to 95 % confidence limits for fits to experimental data, (Section 2.2 in manuscript).

	$n_{\text{melt}}$	$\rho_{\text{melt}} / \text{g} \cdot \text{cm}^{-3}$	Polynomial fit ( $\rho_{\text{sol}} = a + b_1x + b_2x^2 + b_3x^3 + b_4x^4 + b_5x^5 + b_6x^6$ )						
			a	b <sub>1</sub>	b <sub>2</sub>	b <sub>3</sub>	b <sub>4</sub>	b <sub>5</sub>	b <sub>6</sub>
<i>Best</i>	1.4881	1.2225	998.2	-0.174	185.75	-13.39	65.16	-35.81	22.76
<i>Upper</i>	1.4884	1.2248	998.2	-0.181	187.39	-13.93	67	-37.24	23.57
<i>Lower</i>	1.4878	1.2201	998.2	-0.166	184.04	-12.83	63.28	-34.36	21.94

**Table S19.2:** Tabulated experimental data points shown in **Fig S20.1**.

a <sub>w</sub>	error a <sub>w</sub> (+ve)	error a <sub>w</sub> (-ve)	MFS	error MFS
0.66522	0.00707	0.00713	0.87406	0.00722
0.71105	0.00493	0.00494	0.8677	0.00654
0.74996	0.00758	0.00758	0.83334	0.01058
0.79488	0.01337	0.01338	0.80256	0.01126
0.84249	0.00573	0.00389	0.76365	0.00522
0.86987	0.00563	0.00574	0.73768	0.00728
0.91262	0.00592	0.00605	0.65854	0.01692
0.95695	0.00508	0.00491	0.48805	0.02723
0.99362	3.59E-04	3.74E-04	0.05685	0.00348

## S21 2,2-Dimethyl Succinic Acid Hygroscopicity

**Fig S21.1:** Hygroscopicity of 2,2-dimethyl succinic acid, (Sigma Aldrich, Purity 99 %), at 293.15 K. Open squares, these experiments; solid line, UNIFAC model.

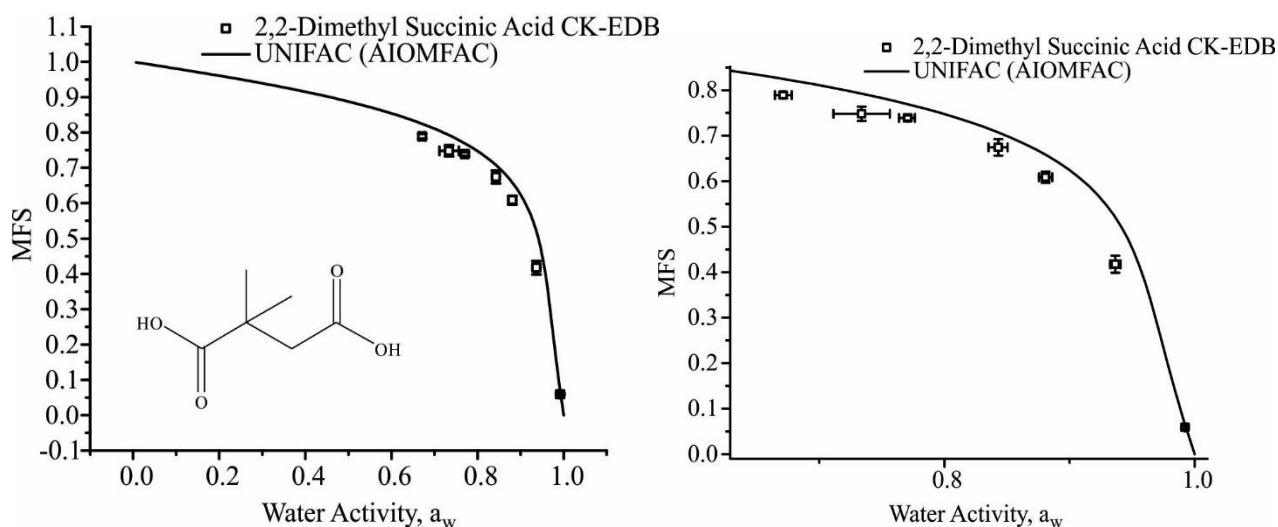


**Table S21.1:** Pure component refractive index ( $n_{\text{melt}}$ ) is determined using molar refraction, assuming ideal mixing for calculation of the melt density ( $\rho_{\text{melt}}$ ), from bulk data available in Cai et al. (2016). The variation of density as a function of the root of solute mass fraction ( $\text{MFS}^{1/2} = x$ ) is represented by polynomial fit parameters. *Upper* and *lower* refer to 95 % confidence limits for fits to experimental data, (Section 2.2 in manuscript).

	$n_{\text{melt}}$	$\rho_{\text{melt}} / \text{g} \cdot \text{cm}^{-3}$	Polynomial fit ( $\rho_{\text{sol}} = a + b_1x + b_2x^2 + b_3x^3 + b_4x^4 + b_5x^5 + b_6x^6$ )						
			a	$b_1$	$b_2$	$b_3$	$b_4$	$b_5$	$b_6$
<i>Best</i>	1.4889	1.2710	997.9	-0.382	220.13	-29.13	114.09	-76.29	44.68
<i>Upper</i>	1.4897	1.2776	997.9	-0.419	224.73	-31.96	122.4	-83.53	48.48
<i>Lower</i>	1.4880	1.2644	997.9	-0.347	215.51	-26.48	106.23	-69.5	41.09

**Table S21.2:** Tabulated experimental data points shown in **Fig S21.1**

a <sub>w</sub>	error a <sub>w</sub> (+ve)	error a <sub>w</sub> (-ve)	MFS	error MFS
0.6713	0.00663	0.00663	0.78921	0.00655
0.73389	0.02256	0.02256	0.74829	0.01579
0.77076	0.00564	0.00705	0.73908	0.00579
0.84308	0.00747	0.00776	0.67413	0.01818
0.88089	0.00536	0.00529	0.60846	0.01212
0.9367	0.00425	0.00424	0.41751	0.01893
0.99244	4.24E-04	5.93E-04	0.05911	0.00313

## S22 2-Methyl Glutaric Acid Hygroscopicity

**Fig S22.1:** Hygroscopicity of 2-methyl glutaric acid, (Sigma Aldrich, Purity 98 %), at 293.15 K. Open squares, these experiments; solid line, UNIFAC model.

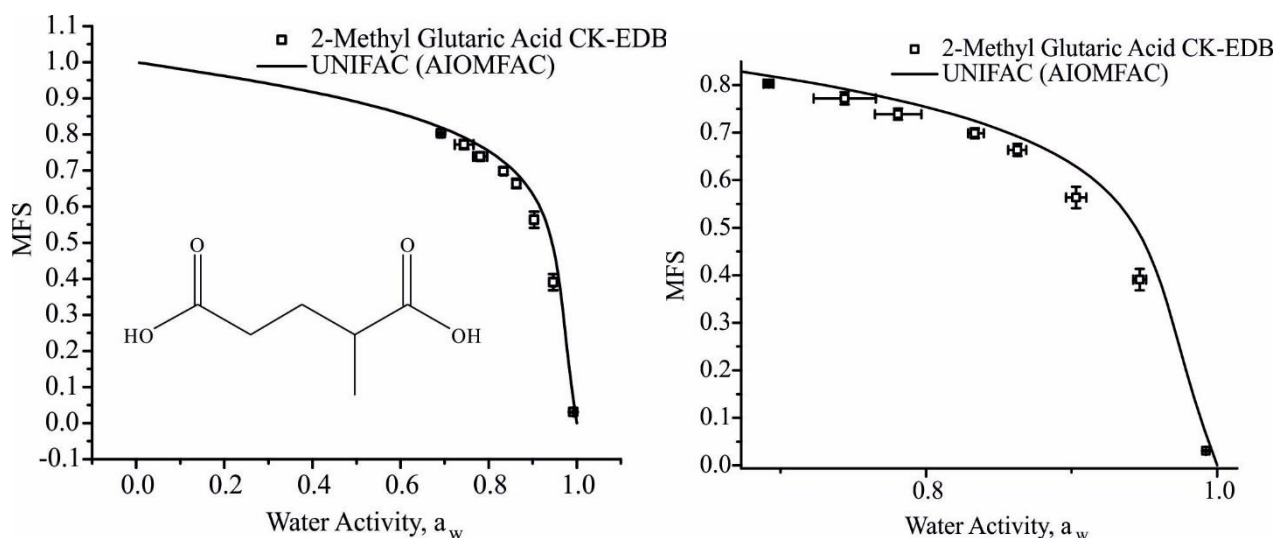


**Table S22.1:** Pure component refractive index ( $n_{melt}$ ) is determined using molar refraction, assuming ideal mixing for calculation of the melt density ( $\rho_{melt}$ ), from bulk data available in Cai et al. (2016). The variation of density as a function of the root of solute mass fraction ( $MFS^{1/2} = x$ ) is represented by polynomial fit parameters. *Upper* and *lower* refer to 95 % confidence limits for fits to experimental data, (Section 2.2 in manuscript).

	$n_{melt}$	$\rho_{melt}/g.cm^{-3}$	Polynomial fit ( $\rho_{sol} = a + b_1x + b_2x^2 + b_3x^3 + b_4x^4 + b_5x^5 + b_6x^6$ )						
			a	$b_1$	$b_2$	$b_3$	$b_4$	$b_5$	$b_6$
<i>Best</i>	1.4866	1.2585	997.6	-0.319	211.59	-24.4	99.95	-64.16	38.24
<i>Upper</i>	1.4873	1.2648	997.6	-0.350	216	-26.78	107.1	-70.26	41.49
<i>Lower</i>	1.4858	1.2522	997.6	-0.290	207.17	-22.18	93.17	-58.44	35.17

**Table S22.2:** Tabulated experimental data points shown in Fig S22.1

$a_w$	error $a_w$ (+ve)	error $a_w$ (-ve)	MFS	error MFS
0.68925	0.00271	0.00334	0.80479	0.00208
0.72204	0.01005	0.01239	0.78383	0.00857
0.76123	0.01296	0.01422	0.75567	0.01704
0.78959	0.02339	0.02377	0.73478	0.02713
0.82836	0.01185	0.00726	0.70077	0.02018
0.84699	0.00634	0.00601	0.68658	0.01104
0.8785	0.00611	0.00622	0.63205	0.01527
0.91076	0.00612	0.00583	0.54437	0.02194
0.94004	0.00438	0.00438	0.4312	0.02071
0.98128	4.79E-04	0.0012	0.14884	0.0113
0.99285	2.24E-04	2.25E-04	0.02928	0.00106

### S23 3-Methyl Adipic Acid Hygroscopicity

**Fig S23.1:** Hygroscopicity of 3-methyl adipic acid, (Sigma Aldrich, Purity 99 %), at 293.15 K. Open squares, these experiments; solid line, UNIFAC model.

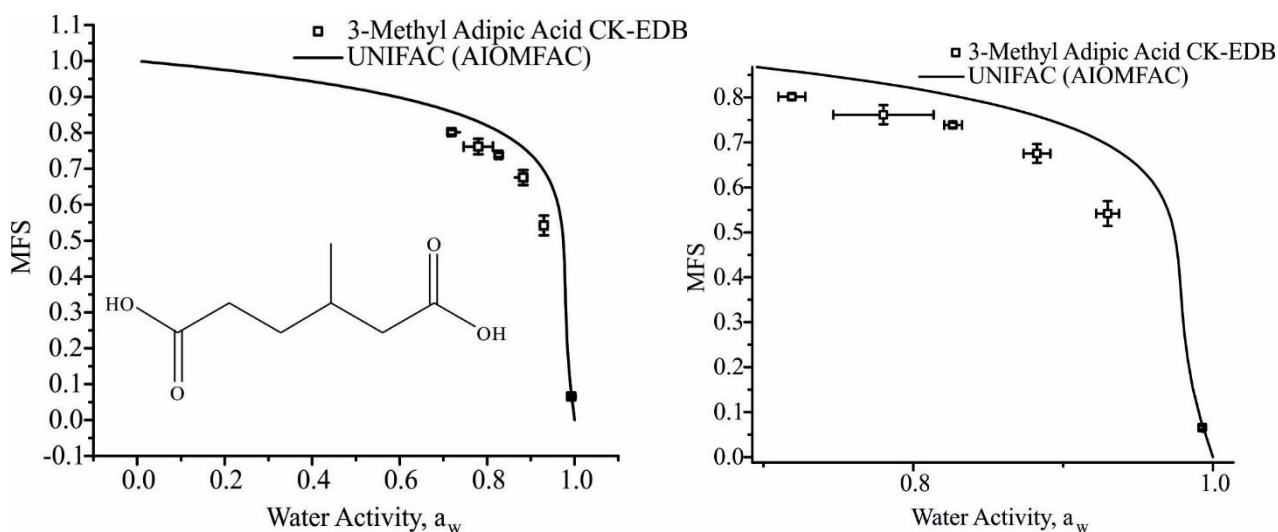


**Table S23.1:** Pure component refractive index ( $n_{melt}$ ) is determined using molar refraction, assuming ideal mixing for calculation of the melt density ( $\rho_{melt}$ ), from bulk data available in Cai et al. (2016). The variation of density as a function of the root of solute mass fraction ( $MFS^{1/2} = x$ ) is represented by polynomial fit parameters. *Upper* and *lower* refer to 95 % confidence limits for fits to experimental data, (Section 2.2 in manuscript).

	$n_{melt}$	$\rho_{melt}/g.cm^{-3}$	Polynomial fit ( $\rho_{sol} = a + b_1x + b_2x^2 + b_3x^3 + b_4x^4 + b_5x^5 + b_6x^6$ )						
			a	$b_1$	$b_2$	$b_3$	$b_4$	$b_5$	$b_6$
<i>Best</i>	1.4865	1.2141	999.0	-0.147	179.19	-11.33	58.11	-30.42	19.69
<i>Upper</i>	1.4878	1.2243	999.0	-0.176	186.48	-13.59	65.86	-36.34	23.06
<i>Lower</i>	1.4852	1.2041	999.0	-0.121	171.99	-9.4	51.21	-25.33	16.75

**Table S23.2:** Tabulated experimental data points shown in Fig S23.1.

$a_w$	error $a_w$ (+ve)	error $a_w$ (-ve)	MFS	error MFS
0.71902	0.00897	0.00897	0.80154	0.00624
0.78015	0.03348	0.03347	0.7615	0.02149
0.82646	0.00615	0.00574	0.73848	0.00556
0.88266	0.00886	0.00907	0.67532	0.02097
0.92986	0.00748	0.00771	0.54185	0.02748
0.993	2.61E-04	3.72E-04	0.06527	0.00354

### S24 3-Methyl Glutaric Acid Hygroscopicity

**Fig S24.1:** Hygroscopicity of 3-methyl glutaric acid, (Sigma Aldrich, Purity 99 %), at 293.15 K. Open squares, these experiments; solid line, UNIFAC model.

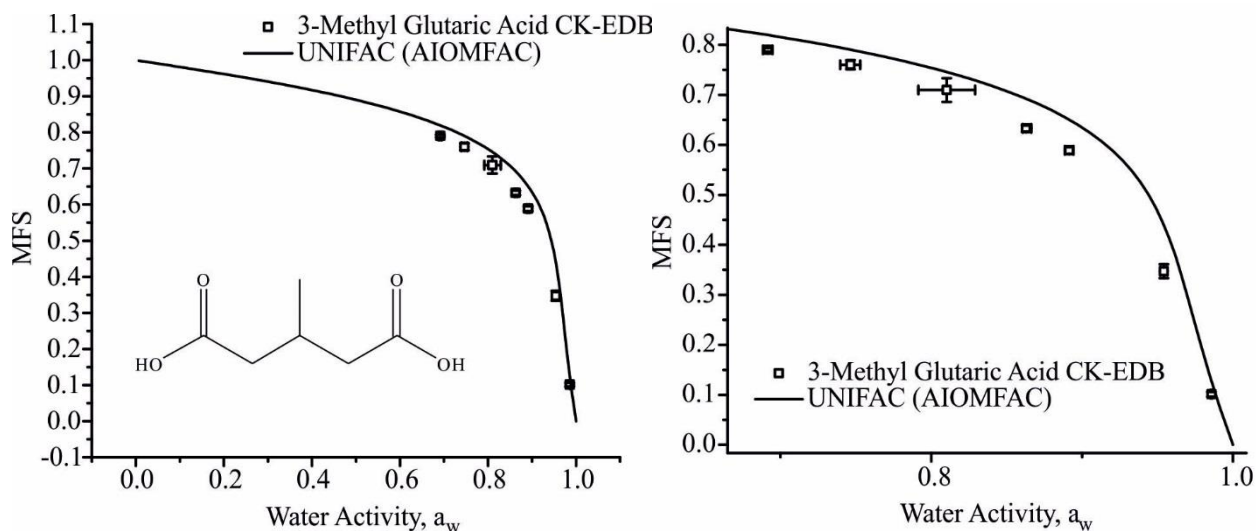


**Table SI.24.1:** Pure component refractive index ( $n_{\text{melt}}$ ) is determined using molar refraction, assuming ideal mixing for calculation of the melt density ( $\rho_{\text{melt}}$ ), from bulk data available in Cai et al. (2016). The variation of density as a function of the root of solute mass fraction ( $\text{MFS}^{1/2} = x$ ) is represented by polynomial fit parameters. *Upper* and *lower* refer to 95 % confidence limits for fits to experimental data, (Section 2.2 in manuscript).

	$n_{\text{melt}}$	$\rho_{\text{melt}} / \text{g} \cdot \text{cm}^{-3}$	Polynomial fit ( $\rho_{\text{sol}} = a + b_1x + b_2x^2 + b_3x^3 + b_4x^4 + b_5x^5 + b_6x^6$ )						
			a	$b_1$	$b_2$	$b_3$	$b_4$	$b_5$	$b_6$
<i>Best</i>	1.4819	1.2498	997.9	-0.277	205.29	-21.26	90.32	-56.07	33.89
<i>Upper</i>	1.4822	1.2531	997.9	-0.292	207.6	-22.37	93.74	-58.92	35.43
<i>Lower</i>	1.4816	1.2466	997.9	-0.264	203.04	-20.22	87.1	-53.39	32.44

**Table S24.2:** Tabulated experimental data points shown in **Fig S24.1**.

$a_w$	error $a_w$ (+ve)	error $a_w$ (-ve)	MFS	error MFS
0.69173	0.00299	0.00334	0.79013	0.0038
0.74649	0.00642	0.00683	0.76025	0.00932
0.81013	0.01887	0.01884	0.70959	0.02367
0.86283	0.00343	0.00213	0.63276	0.00618
0.89131	0.00283	0.00283	0.58884	0.00675
0.95411	0.00246	0.00245	0.3472	0.01394
0.98567	6.06E-04	6.09E-04	0.10123	0.00477

### S25 3, 3-Dimethyl Glutaric Acid Hygroscopicity

**Fig S25.1:** Hygroscopicity of 3, 3-dimethyl glutaric acid, (Sigma Aldrich, Purity 98 %), at 293.15 K. Open squares, these experiments; solid line, UNIFAC model.

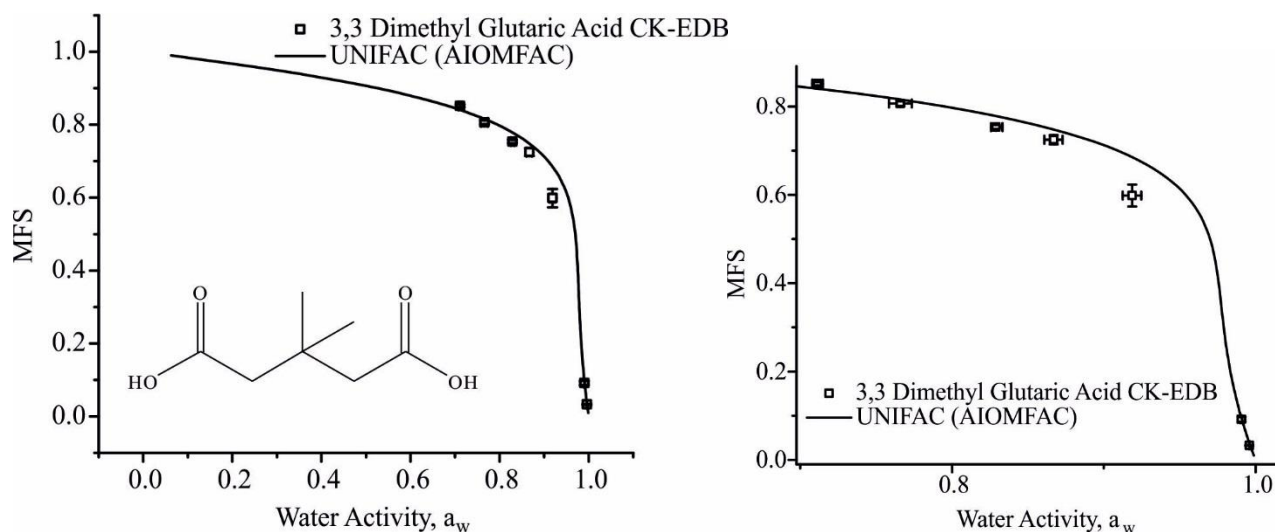


**Table S25.1:** Pure component refractive index ( $n_{melt}$ ) is determined using molar refraction, assuming ideal mixing for calculation of the melt density ( $\rho_{melt}$ ), from bulk data available in Cai et al. (2016). The variation of density as a function of the root of solute mass fraction ( $MFS^{1/2} = x$ ) is represented by polynomial fit parameters. *Upper* and *lower* refer to 95 % confidence limits for fits to experimental data, (Section 2.2 in manuscript).

	$n_{melt}$	$\rho_{melt}/g.cm^{-3}$	Polynomial fit ( $\rho_{sol} = a + b_1x + b_2x^2 + b_3x^3 + b_4x^4 + b_5x^5 + b_6x^6$ )						
			a	$b_1$	$b_2$	$b_3$	$b_4$	$b_5$	$b_6$
<i>Best</i>	1.4903	1.2206	998.3	-0.167	184.33	-12.92	63.58	-34.59	22.07
<i>Upper</i>	1.4906	1.2231	998.3	-0.175	186.11	-13.5	65.55	-36.11	22.93
<i>Lower</i>	1.4900	1.2182	998.3	-0.160	182.61	-12.38	61.74	-33.18	21.27

**Table S25.2:** Tabulated experimental data points shown in **Fig S25.1**.

$a_w$	error $a_w$ (+ve)	error $a_w$ (-ve)	MFS	error MFS
0.71132	0.00345	0.00345	0.85176	0.00384
0.76078	0.006	0.00743	0.80912	0.00721
0.79151	0.01941	0.01942	0.79788	0.01562
0.83444	0.00416	0.00451	0.75169	0.00421
0.87055	0.00543	0.00565	0.71882	0.0105
0.91582	0.00545	0.00564	0.61641	0.02163
0.96018	0.00389	0.00389	0.39161	0.02576
0.99443	2.18E-04	2.83E-04	0.04485	0.00225

## S26. PEG3 Hygroscopicity

**Fig S26.1:** Hygroscopicity of PEG3, at 293.15 K. Open squares, these experiments; solid line, UNIFAC model.

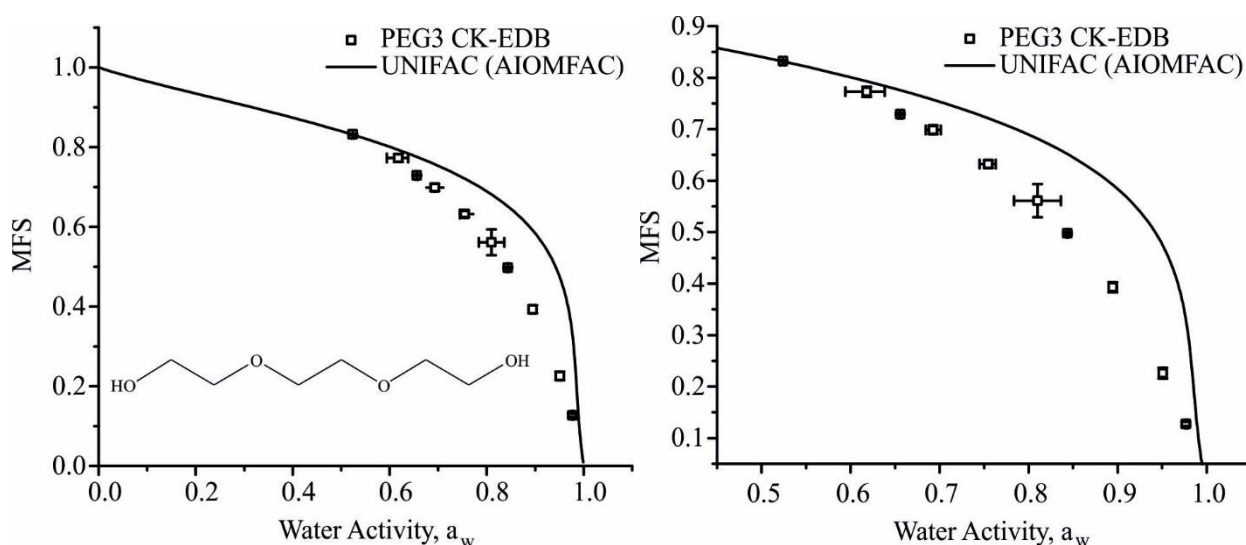


**Table S26.1:** Measured values of pure component melt density ( $\rho_{\text{melt}}$ ) and refractive index ( $n_{\text{melt}}$ ) (PEG3 is liquid), presented with parameterisation for solution measurements of density where  $x$  is the square root of MFS ( $\text{MFS}^{1/2} = x$ ). *Upper* and *lower* refer to 95 % confidence limits for fits to experimental data. Upper and lower limit on refractive index and density are determined by the error in the refractometer and by the densitometer respectively.

	$n_{\text{melt}}$	$\rho_{\text{melt}} / \text{g.cm}^{-3}$	Polynomial fit ( $\rho_{\text{sol}} = a + b_1x + b_2x^2 + b_3x^3$ )			
			$a$	$b_1$	$b_2$	$b_3$
<i>Best</i>	1.4551	1.109	999.97	-75.75	431.63	-246.73
<i>Upper</i>	1.4552	1.122	999.97	-0.198	268.11	-144.15
<i>Lower</i>	1.4550	1.096	999.97	-151.31	595.15	-349.31

**Table S26.2:** Tabulated experimental data points shown in **Fig S26.1**.

$a_w$	error $a_w$ (+ve)	error $a_w$ (-ve)	MFS	error MFS
0.524	0.0024	0.00286	0.83232	0.00127
0.61806	0.02008	0.02389	0.77269	0.0098
0.65597	0.00198	0.00242	0.72923	0.00152
0.69291	0.00856	0.00856	0.69867	0.0088
0.75489	8.16E-03	0.01	0.63211	7.82E-03
0.81001	0.0263	0.0263	0.56113	0.03211
0.84347	0.00123	0.00119	0.49753	0.00229
0.89472	0.00416	0.00414	0.39303	0.01004
0.95087	3.07E-03	3.07E-03	0.22603	0.01048
0.97688	0.00201	0.00112	0.12742	0.00393

## S27. PEG4 Hygroscopicity

**Fig S27.1:** Hygroscopicity of PEG4, at 293.15 K. Open squares, these CC-EDB experiments; solid line, UNIFAC model; blue line UManSysProp; red line adsorption isotherm model from Dutcher.

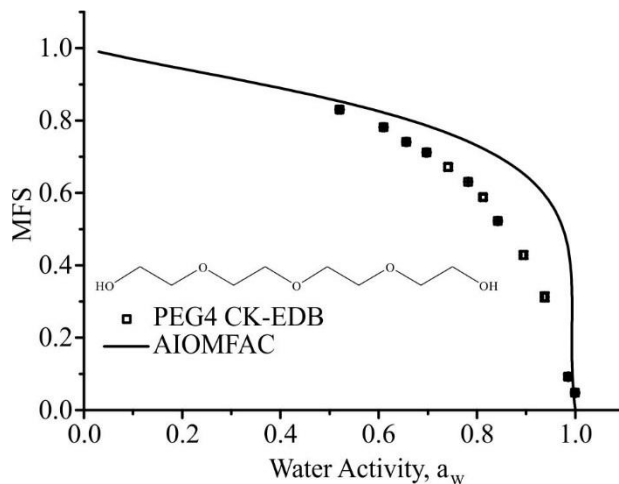


**Table S27.1:** Measured values of pure component melt density ( $\rho_{\text{melt}}$ ) and refractive index ( $n_{\text{melt}}$ ) (PEG4 is liquid), presented with parameterisation for solution measurements of density where  $x$  is the square root of MFS ( $\text{MFS}^{1/2} = x$ ). *Upper* and *lower* refer to 95 % confidence limits for fits to experimental data. Upper and lower limit on refractive index and density are determined by the error in the refractometer and by the densitometer respectively.

	$n_{\text{melt}}$	$\rho_{\text{melt}} / \text{g.cm}^{-3}$	Polynomial fit ( $\rho_{\text{sol}} = a + b_1x + b_2x^2 + b_3x^3$ )			
			a	$b_1$	$b_2$	$b_3$
<i>Best</i>	1.4589	1.1271	999.97	-37.39	296.85	-130.68
<i>Upper</i>	1.4590	1.13412	999.97	-9.65	235.84	-92.25
<i>Lower</i>	1.4588	1.12338	999.97	-65.13	357.86	-169.11

**Table S27.2:** Tabulated experimental data points shown in **Fig S27.1**.

$a_w$	error $a_w$ (+ve)	error $a_w$ (-ve)	MFS	error MFS
0.52052	0.00336	0.00399	0.83006	8.065E-4
0.60966	0.00229	0.00278	0.78149	8.220E-4
0.65636	0.00166	0.00204	0.74058	0.00177
0.69735	0.00172	0.00212	0.71195	0.00154
0.74132	0.00556	0.00685	0.67145	0.00929
0.78212	6.975E-4	8.803E-4	0.63073	8.501E-4
0.81258	0.00536	0.00535	0.58791	0.00759
0.84243	0.00132	0.00111	0.52225	0.00213
0.89453	0.00427	0.00448	0.42827	0.01048
0.93766	0.00385	0.00376	0.31263	0.01217
0.98571	0.0013	0.00127	0.0918	0.00662
0.99969	0.00143	0.00156	0.0475	0.00252

## S28 Erythritol Hygroscopicity

**Fig S28.1:** Hygroscopicity of erythritol (Sigma Aldrich 99 %), at 293.15 K. Open squares, these experiments; solid line, UNIFAC model.

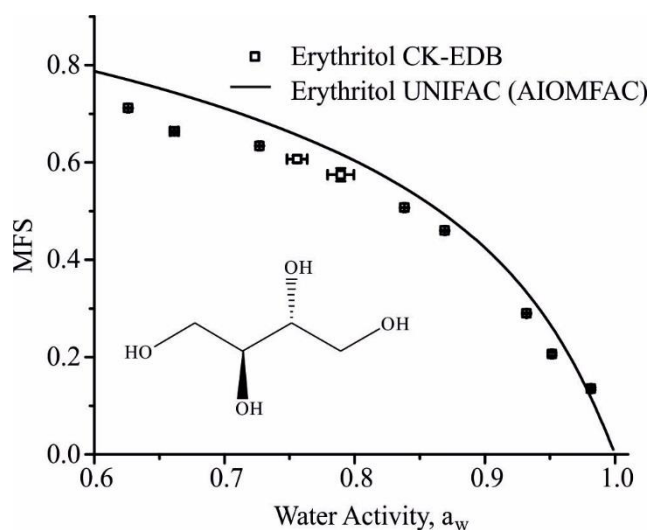


**Table S28.1:** Pure component refractive index ( $n_{\text{melt}}$ ) is determined using molar refraction, assuming ideal mixing for calculation of the melt density ( $\rho_{\text{melt}}$ ), from bulk data available in Cai et al. (2016). The variation of density as a function of the root of solute mass fraction ( $\text{MFS}^{1/2} = x$ ) is represented by polynomial fit parameters. *Upper* and *lower* refer to 95 % confidence limits for fits to experimental data, (Section 2.2 in manuscript).

	$n_{\text{melt}}$	$\rho_{\text{melt}} / \text{g}\cdot\text{cm}^{-3}$	Polynomial fit ( $\rho_{\text{sol}} = a + b_1x + b_2x^2 + b_3x^3$ )			
			a	$b_1$	$b_2$	$b_3$
<i>Best</i>	1.5211	1.3754	998.6	58.46	37.98	278.66
<i>Upper</i>	1.5388	1.3813	998.6	60.21	33.79	286.94
<i>Lower</i>	1.5204	1.3695	998.6	56.75	42.03	27.049

**Table S28.2:** Tabulated experimental data points shown in **Fig S28.1**.

$a_w$	error $a_w$ (+ve)	error $a_w$ (-ve)	MFS	error MFS
0.62602	8.77112E-4	0.00107	0.71188	6.08334E-4
0.66147	0.0027	0.0033	0.66395	0.00226
0.72692	0.00104	0.00129	0.6342	6.57702E-4
0.75582	0.00775	0.00777	0.60723	0.00739
0.78929	0.01009	0.0101	0.57499	0.01315
0.83827	7.77253E-4	0.001	0.50705	9.72437E-4
0.86916	7.13427E-4	6.96511E-4	0.46004	0.00138
0.93195	2.64028E-4	3.52642E-4	0.28987	0.00175
0.95145	7.53773E-4	7.52526E-4	0.20621	0.00312
0.9815	5.76107E-4	5.56581E-4	0.13503	0.00279

## S29 Sorbitol Hygroscopicity

**Fig S29.1:** Hygroscopicity of sorbitol (Sigma Aldrich  $\geq 98\%$ ), at 293.15 K. Open squares, these experiments; solid line, UNIFAC model. Data taken at RHs lower than indicated by the dashed black line show increased error in hygroscopicity retrieval due to the imposition of a kinetic limitation on water transport.

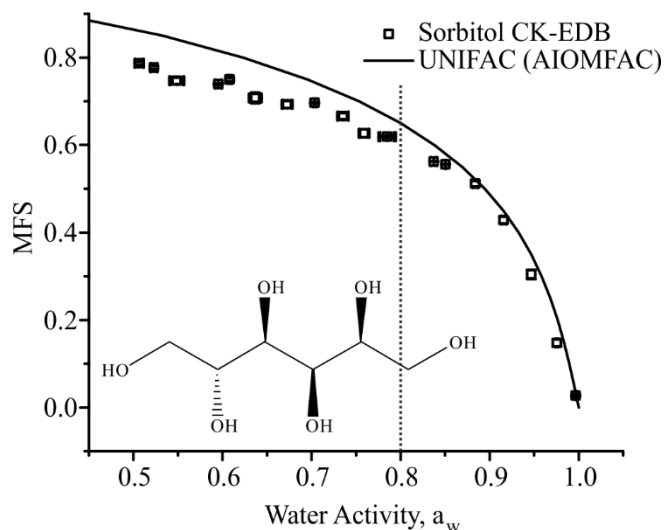


**Table S29.1:** Pure component refractive index ( $n_{\text{melt}}$ ) determined using molar refraction where the melt density ( $\rho_{\text{melt}}$ ) is determined using a polynomial fit of density to the square root of MFS ( $\text{MFS}^{1/2} = x$ ). Bulk values used are available in Cai et al. (2016). *Upper* and *lower* refer to 95 % confidence limits for fits to experimental data.

	$n_{\text{melt}}$	$\rho_{\text{melt}}/\text{g}\cdot\text{cm}^{-3}$	Polynomial fit ( $\rho_{\text{sol}} = a + b_1x + b_2x^2 + b_3x^3$ )			
			a	$b_1$	$b_2$	$b_3$
<i>Best</i>	1.5244	1.4231	997.8	8.6	286.1	130.7
<i>Upper</i>	1.5267	1.4333	997.8	24.74	234.56	175.54
<i>Lower</i>	1.5220	1.4128	997.8	-7.6	337.59	85.83

**Table S29.2:** Tabulated experimental data points shown in **Fig S29.1**.

$a_w$	error $a_w$ (+ve)	error $a_w$ (-ve)	MFS	error MFS
0.50647	0.00432	0.00512	0.78667	0.00341
0.52291	0.0031	0.00369	0.7771	0.00307
0.54873	0.00705	0.00838	0.74672	0.00731
0.59535	0.00322	0.00389	0.73916	0.00193
0.60809	0.0019	0.0023	0.74976	0.00343
0.63682	0.00605	0.00728	0.70773	0.01216
0.67255	0.00497	0.00601	0.69271	0.00773
0.7035	0.00148	0.00183	0.69648	0.00163
0.73531	0.00619	0.00619	0.66608	0.00694
0.75896	0.00493	0.00599	0.62673	0.00941
0.78492	0.00775	0.00958	0.61901	0.00237
0.83722	0.00384	0.0025	0.56241	9.55991E-4
0.85049	9.622E-4	8.165E-4	0.5556	0.00118
0.88386	0.00262	0.0027	0.51154	0.00629
0.91574	0.00253	0.00266	0.4286	0.0076
0.94681	0.00245	0.00245	0.30429	0.01053
0.97555	0.0014	0.00139	0.14769	0.00774
0.99655	0.00112	6.78573E-4	0.02751	0.00293

### S30 D-(+)-Trehalose Dihydrate Hygroscopicity

**Fig S30.1:** Hygroscopicity of D-(+)-trehalose dihydrate (Sigma Aldrich  $\geq 99\%$ ), at 293.15 K. Open squares, these experiments; solid line, UNIFAC model. Data taken at RHs lower than indicated by the dashed black line show increased error in hygroscopicity retrieval due to the imposition of a kinetic limitation on water transport.

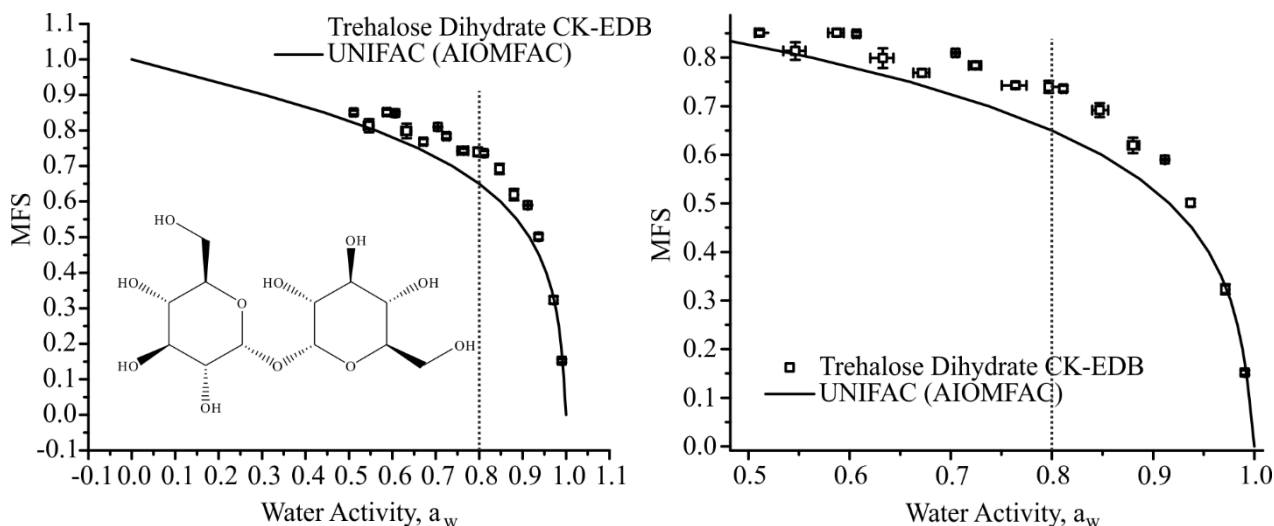


**Table S30.1:** Pure component refractive index ( $n_{\text{melt}}$ ) determined using molar refraction where the melt density ( $\rho_{\text{melt}}$ ) is determined using a polynomial fit of density to the square root of MFS ( $\text{MFS}^{1/2} = x$ ). Bulk values used are available in Cai et al. (2016). *Upper* and *lower* refer to 95 % confidence limits for fits to experimental data.

	$n_{\text{melt}}$	$\rho_{\text{melt}}/\text{g}\cdot\text{cm}^{-3}$	Polynomial fit ( $\rho_{\text{sol}} = a + b_1x + b_2x^2 + b_3x^3$ )			
			a	$b_1$	$b_2$	$b_3$
<i>Best</i>	1.5193	1.4682	997.8	8.2	284.3	177.8
<i>Upper</i>	1.5211	1.4734	997.8	11.6	269.79	194.19
<i>Lower</i>	1.5175	1.4629	997.8	4.87	298.84	161.43

**Table S30.2:** Tabulated experimental data points shown in **Fig S30.1**.

$a_w$	error $a_w$ (+ve)	error $a_w$ (-ve)	MFS	error MFS
0.51123	0.00397	0.0047	0.8511	0.00561
0.54636	0.01007	0.01196	0.81364	0.01816
0.5873	0.007	0.00844	0.85121	0.00732
0.60689	0.00263	0.00319	0.84879	0.00386
0.63303	0.01031	0.01244	0.79889	0.02031
0.67154	0.00716	0.00861	0.76858	0.00766
0.70479	0.00212	0.00262	0.80977	0.00199
0.72437	0.00577	0.00642	0.78413	0.00669
0.76384	0.01102	0.01364	0.743	0.00611
0.79679	0.00422	0.00225	0.7399	0.01219
0.81122	0.00282	0.00195	0.73624	0.0059
0.84712	0.00837	0.00721	0.69205	0.01427
0.88007	0.00598	0.00498	0.61945	0.01589
0.9118	5.25851E-4	5.4066E-4	0.58998	0.00159
0.93698	0.00204	0.00204	0.50101	0.00792
0.97142	0.00151	0.00149	0.3233	0.01015
0.99054	4.05516E-4	4.09208E-4	0.15195	0.00476

### S31. Galactose Hygroscopicity

**Fig S31.1:** Hygroscopicity of (Sigma Aldrich  $\geq 99\%$ ), at 293.15 K. Open squares, these experiments; solid line, UNIFAC model. Data taken at RHs lower than indicated by the dashed black line show increased error in hygroscopicity retrieval due to the imposition of a kinetic limitation on water transport.

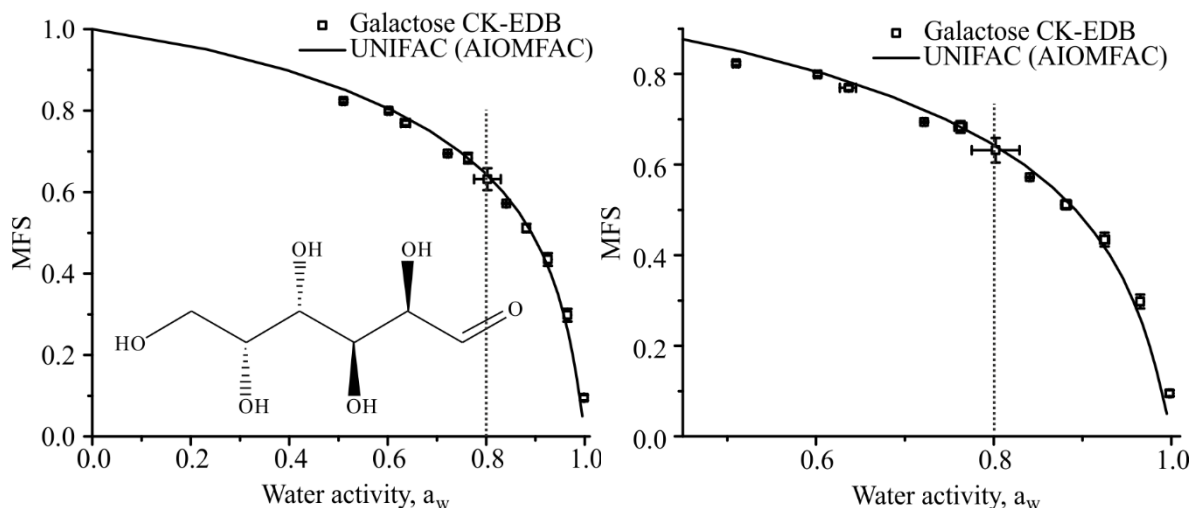


**Table SI.31.1:** Pure component refractive index ( $n_{\text{melt}}$ ) is determined using molar refraction, assuming ideal mixing for calculation of the melt density ( $\rho_{\text{melt}}$ ), from bulk data available in Cai et al. (2016). The variation of density as a function of the root of solute mass fraction ( $\text{MFS}^{1/2} = x$ ) is represented by polynomial fit parameters. *Upper* and *lower* refer to 95 % confidence limits for fits to experimental data, (Section 2.2 in manuscript).

	$n_{\text{melt}}$	$\rho_{\text{melt}}/\text{g.cm}^{-3}$	Polynomial fit ( $\rho_{\text{sol}} = a + b_1x + b_2x^2 + b_3x^3$ )			
			a	$b_1$	$b_2$	$b_3$
<i>Best</i>	1.5885	1.6306	997.36	403.27	83.09	150.11
<i>Upper</i>	1.5892	1.6351	996.67	165.3	-284.07	752.22
<i>Lower</i>	1.5878	1.6261	997.37	399.69	83.4	145.36

**Table S31.2:** Tabulated experimental data points shown in **Fig S31.1**.

$a_w$	error $a_w$ (+ve)	error $a_w$ (-ve)	MFS	error MFS
0.50996	0.00287	0.0034	0.82372	0.00382
0.60189	0.00267	0.00323	0.7993	0.00405
0.63684	0.00839	0.01012	0.76963	0.0055
0.72183	0.0016	0.00199	0.69438	0.00194
0.76282	0.00662	0.00694	0.68348	0.01289
0.80226	0.02704	0.02704	0.6317	0.02723
0.84064	0.00138	8.91966E-4	0.572	0.00141
0.88152	0.00559	0.00561	0.51157	0.01025
0.92485	0.00483	0.00491	0.43437	0.01532
0.96504	0.00377	0.00374	0.29773	0.01536
0.99822	0.00115	7.88489E-4	0.09505	0.00656

### S32 Xylose Hygroscopicity

**Fig S32.1:** Hygroscopicity of (Sigma Aldrich  $\geq 99\%$ ), at 293.15 K. Open squares, these experiments; solid line, UNIFAC model.

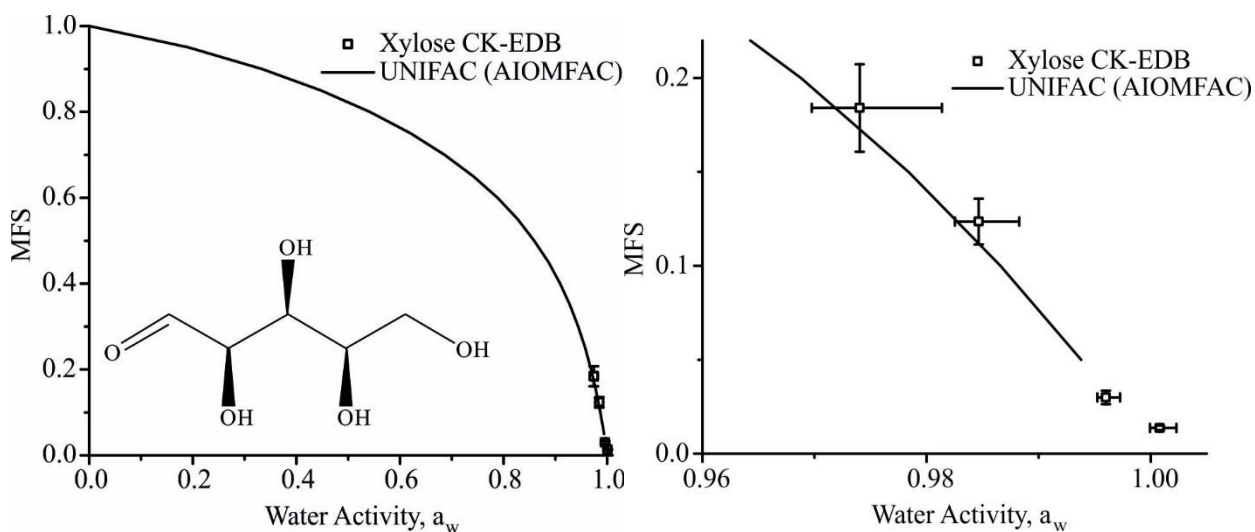


**Table S32.1:** Pure component refractive index ( $n_{\text{melt}}$ ) is determined using molar refraction, assuming ideal mixing for calculation of the melt density ( $\rho_{\text{melt}}$ ), from bulk data available in Cai et al. (2016). The variation of density as a function of the root of solute mass fraction ( $\text{MFS}^{1/2} = x$ ) is represented by polynomial fit parameters. *Upper* and *lower* refer to 95 % confidence limits for fits to experimental data, (Section 2.2 in manuscript).

	$n_{\text{melt}}$	$\rho_{\text{melt}}/\text{g}\cdot\text{cm}^{-3}$	Polynomial fit ( $\rho_{\text{sol}} = a + b_1x + b_2x^2 + b_3x^3$ )			
			a	$b_1$	$b_2$	$b_3$
<i>Best</i>	1.5615	1.5626	996.73	127.69	-163.53	597.09
<i>Upper</i>	1.5619	1.5653	996.74	126.37	-159.45	591.57
<i>Lower</i>	1.5611	1.5598	996.72	128.97	-167.5	602.42

**Table S32.2:** Tabulated experimental data points shown in **Fig S32.1**.

$a_w$	error $a_w$ (+ve)	error $a_w$ (-ve)	MFS	error MFS
0.97404	0.00732	0.00429	0.1841	0.0233
0.98465	0.00361	0.00212	0.12356	0.01215
0.996	0.00127	7.43479E-4	0.02995	0.00361
1.00081	0.00148	8.71845E-4	0.01372	0.0012

### S33 2,3-Dimethyl Succinic Acid Hygroscopicity

**Fig S33.1:** Hygroscopicity of 2,3-dimethyl succinic acid (Sigma Aldrich  $\geq 99\%$ ), at 293.15 K. Open squares, these experiments; solid line, UNIFAC model. (Density treatment for 2,2-dimethyl succinic acid used.)

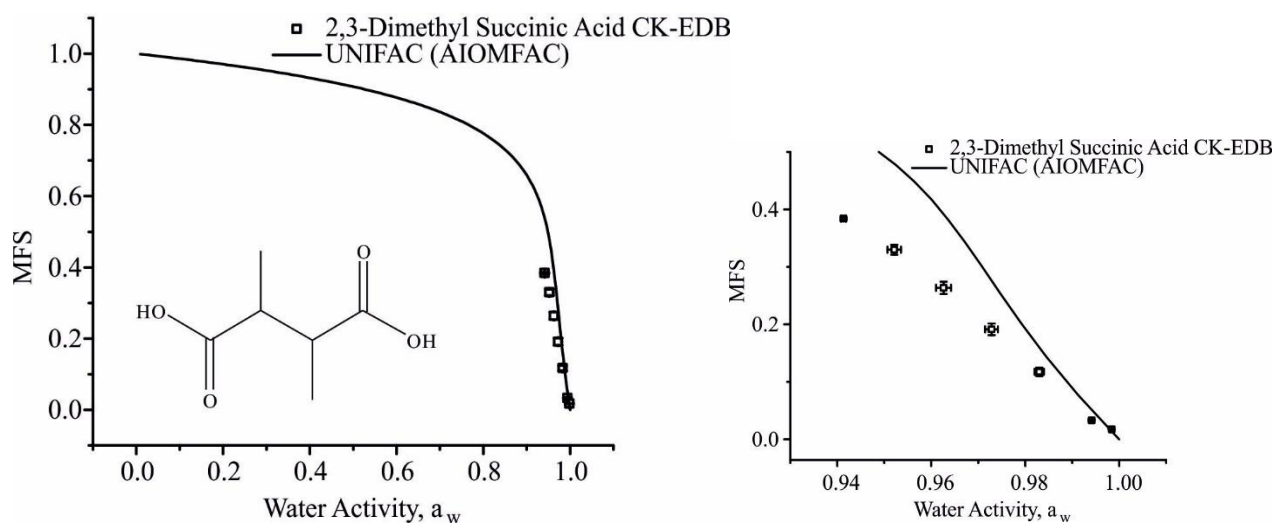


**Table S33.2:** Tabulated experimental data points shown in Fig S33.1.

$a_w$	error $a_w$ (+ve)	error $a_w$ (-ve)	MFS	error MFS
0.94132	5.11673E-4	5.12405E-4	0.38395	0.00207
0.95214	0.00144	0.00144	0.32979	0.00859
0.96262	0.00159	0.00159	0.26369	0.01065
0.97285	0.00138	0.00138	0.19135	0.01011
0.98303	0.001	0.001	0.11733	0.00731
0.99417	2.09751E-4	2.24291E-4	0.03301	0.00121
0.99844	2.59195E-4	4.09162E-4	0.01724	4.61378E-4

### S34 Dimethyl Malonic Acid Hygroscopicity

**Figure S34.1:** Hygroscopicity of (Sigma Aldrich 98 %), at 293.15 K. Open squares, these experiments; solid line, UNIFAC model. (Density treatment for methyl succinic acid used.)

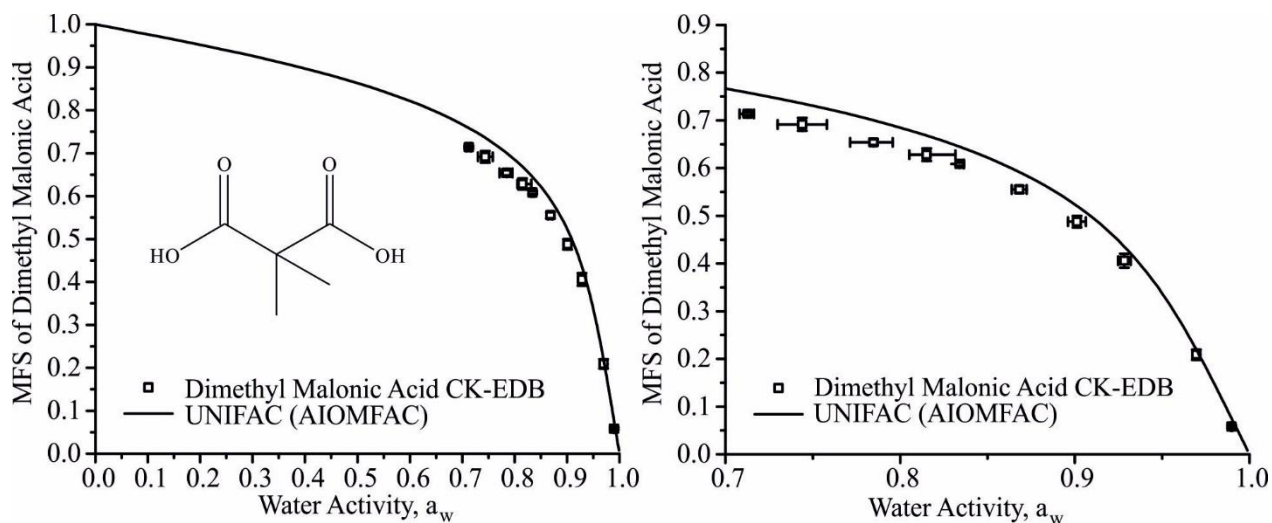


**Table S34.2:** Tabulated experimental data points shown in **Figure S34.1**.

$a_w$	error $a_w$ (+ve)	error $a_w$ (-ve)	MFS	error MFS
0.71262	0.00362	0.00449	0.7136	0.00301
0.744	0.0141	0.0141	0.69155	0.01343
0.78481	0.01088	0.01348	0.65412	0.00614
0.81516	0.01647	0.00985	0.62813	0.01311
0.83412	0.00246	0.00229	0.60844	0.00357
0.86818	0.00422	0.00426	0.5554	0.00729
0.90119	0.00509	0.00506	0.48761	0.01203
0.92833	0.00366	0.00365	0.40593	0.01475
0.96965	0.00157	0.00194	0.2089	0.01089
0.9897	4.75033E-4	4.76981E-4	0.05824	0.00271

### S35 Aspartic Acid Hygroscopicity

**Fig S35.1:** Hygroscopicity of aspartic acid (Sigma Aldrich  $\geq 99\%$ ), at 293.15 K. Open squares, these experiments; solid line, UNIFAC model. (Density treatment for alanine used)

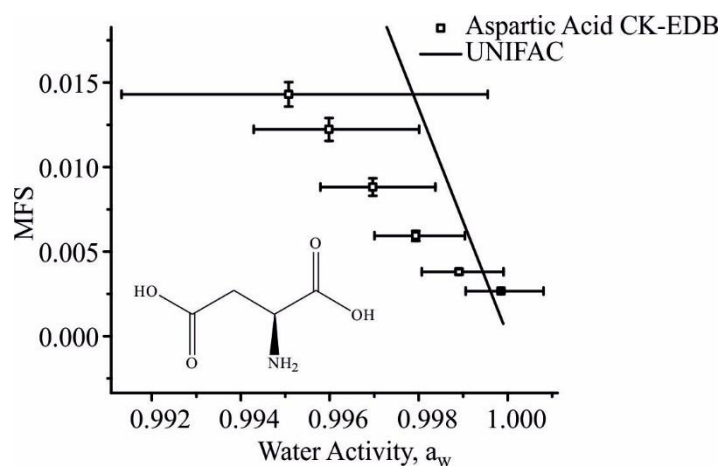


**Table S35.1:** Tabulated experimental data points shown in **Fig S35.1**.

$a_w$	error $a_w$ (+ve)	error $a_w$ (-ve)	MFS	error MFS
0.99507	0.00448	0.00375	0.01431	7.18E-04
0.99599	0.00202	0.0017	0.01223	6.83E-04
0.99697	0.00141	0.00118	0.00882	5.15E-04
0.99793	0.00111	9.28E-04	0.00594	3.01E-04
0.99891	0.001	8.39E-04	0.00381	1.64E-04
0.99985	9.52E-04	7.98E-04	0.00266	8.72E-05

### S36 Asparagine Hygroscopicity

**Fig S36.1:** Hygroscopicity of asparagine (Sigma Aldrich  $\geq 98\%$ ), at 293.15 K. Open squares, these experiments; solid line, UNIFAC model. (Density treatment for alanine used)

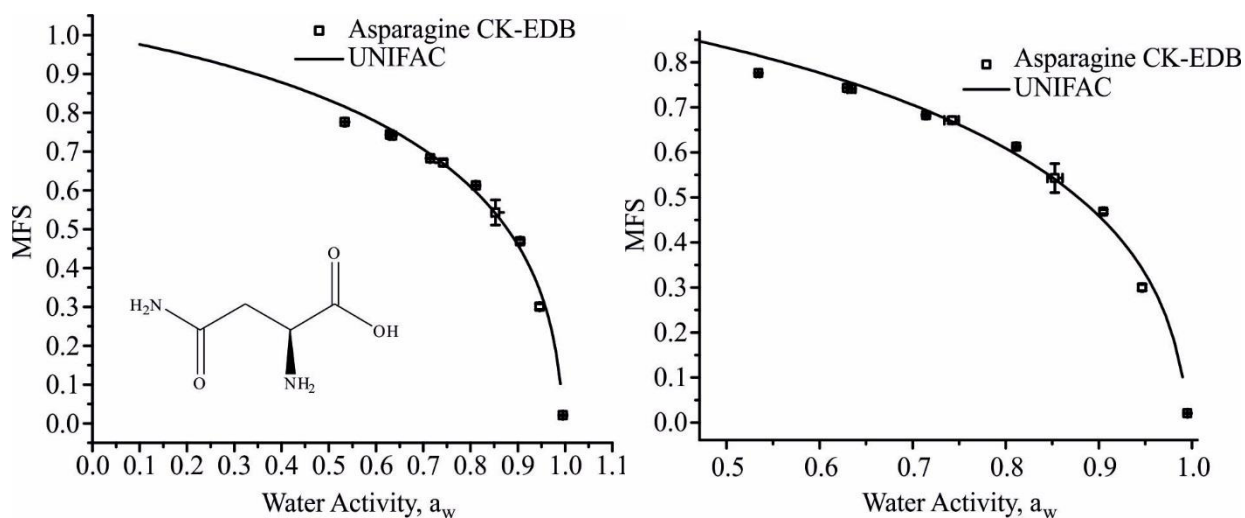
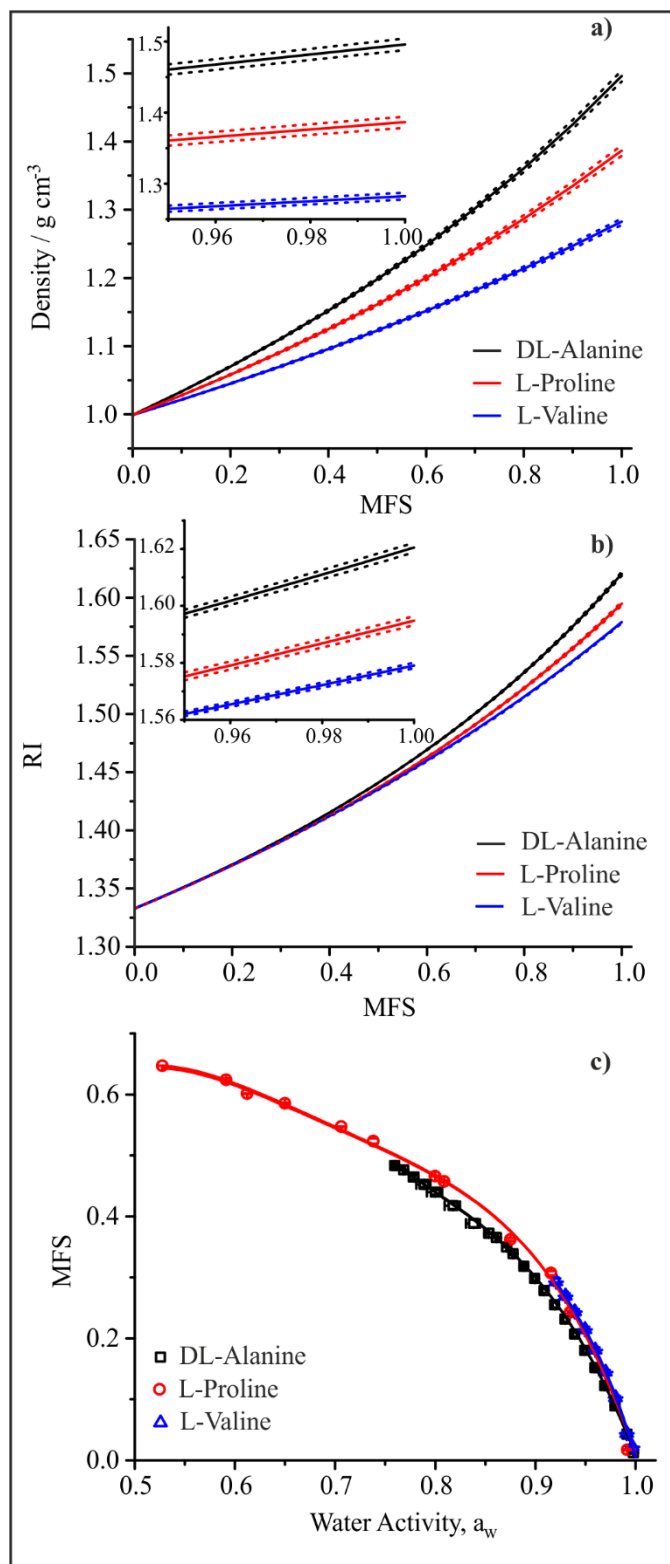


**Table S36.1:** Tabulated experimental data points shown in **Figure S36.1**.

$a_w$	error $a_w$ (+ve)	error $a_w$ (-ve)	MFS	error MFS
0.53409	0.00178	0.00213	0.77577	0.00129
0.62935	0.00189	0.0023	0.74326	0.00101
0.63444	0.00381	0.00465	0.74081	0.00101
0.71441	0.00113	0.0014	0.68254	0.00175
0.74237	0.007	0.00854	0.67146	0.00782
0.81123	8.45796E-4	8.49613E-4	0.61254	0.00185
0.85278	0.00812	0.00813	0.54286	0.03203
0.9048	0.00102	9.46055E-4	0.46853	0.00454
0.94641	0.00108	0.0011	0.3002	0.00693
0.9951	2.80427E-4	2.96722E-4	0.02083	0.00124

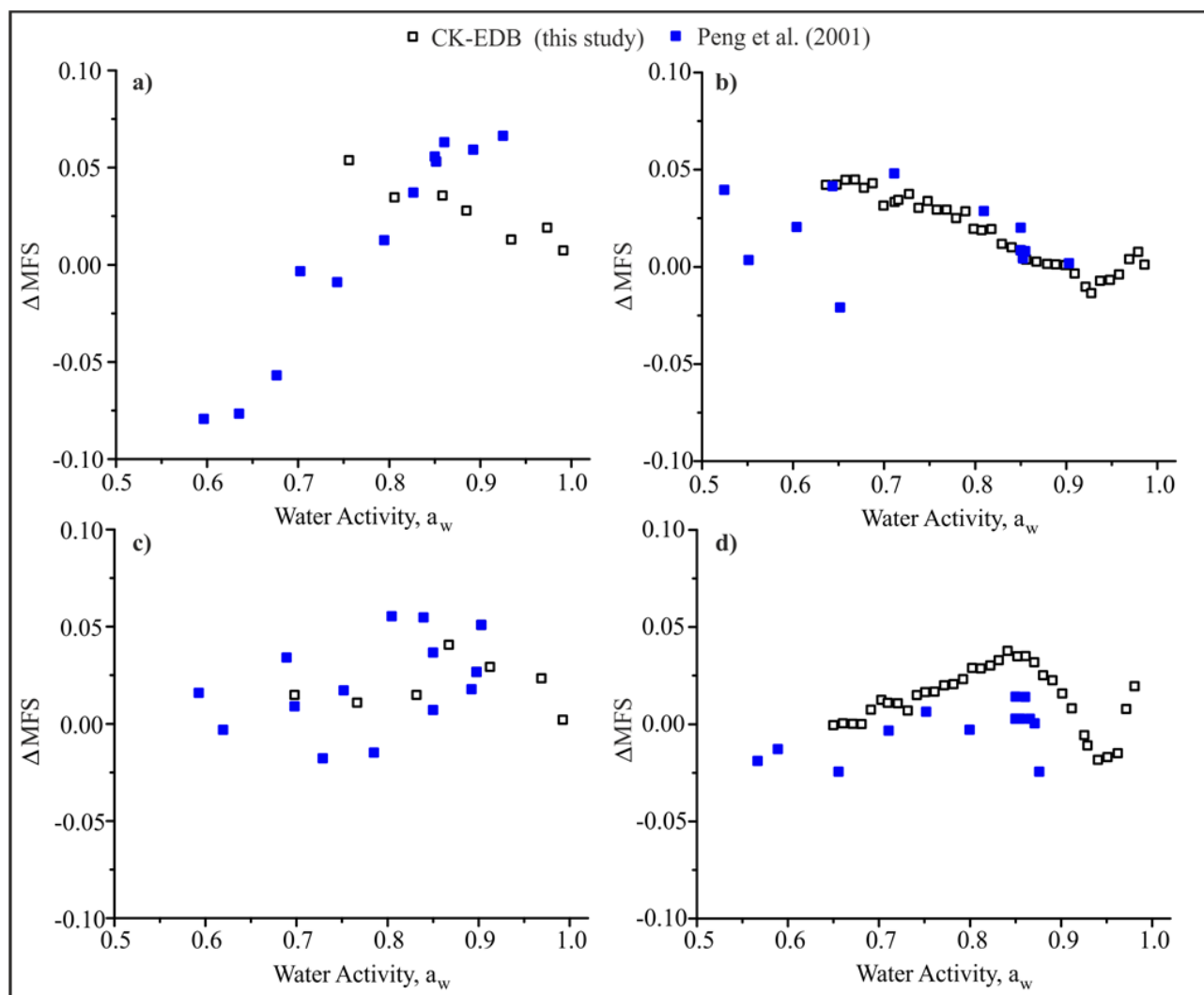
### S37 Errors in Density and Refractive Index Parametrisations and their Impact on Hygroscopicity

**Fig S37.1** Parametrisation for (a) density based on ideal mixing and bulk measured values for density up to the solubility limit and (b) refractive index predicted beyond the solubility limit using molar refraction. In both (a) and (b) dashed lines indicate the uncertainty envelope in the parametrisations. All bulk experimental values of aqueous density and refractive index are available in the supplementary information of Cai et al. (2016). In (c) measured equilibrium hygroscopicity curves are presented with upper and lower error envelope arising from the uncertainties in density and refractive index which is too small to be obvious.



### S38 $\Delta$ MFS for Simple Straight Chain Dicarboxylic Acids

Fig S38.1 The difference in mass fraction of solute ( $\Delta$ MFS) between values predicted by UNIFAC and experimental values (a) oxalic acid, (b) malonic acid, (c) succinic acid and (d) glutaric acid.



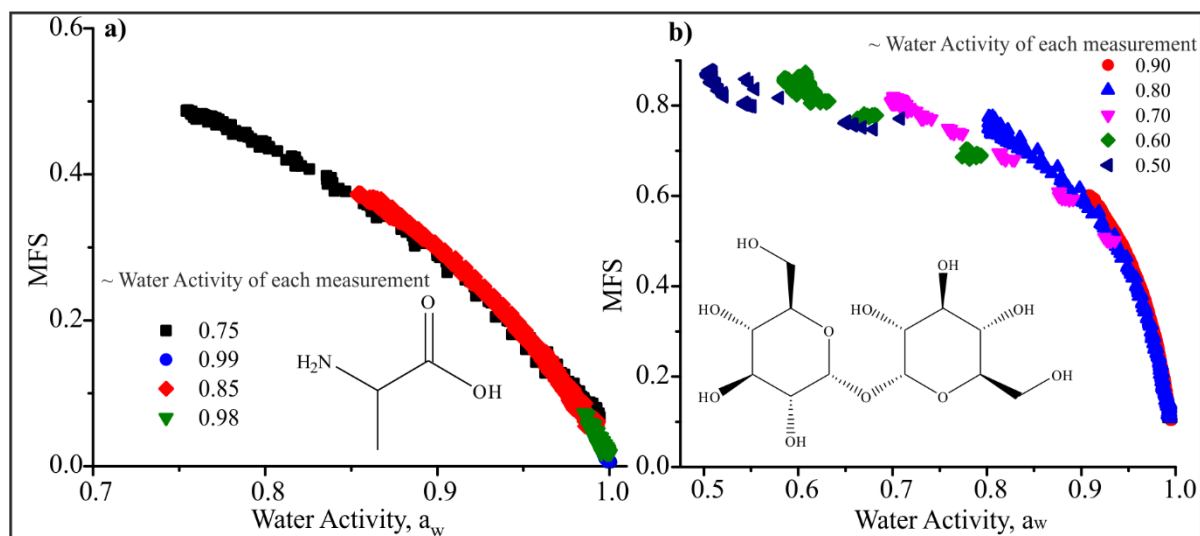
### S39 Viscosity, Diffusion Constant and Timescale of Diffusional Mixing

The kinetic modelling framework used in the analysis of the droplet evaporation events is valid only in the absence of a bulk-kinetic limitation on near surface composition, i.e. the particle must be assumed to be homogeneous in composition. Such a limitation was obvious for hygroscopicity measurements of trehalose, galactose and sorbitol at RH's lower than 80 %. To ensure the measurements are not compromised by bulk diffusion, we consider two important factors.

Firstly, the impact of viscosity on the hygroscopicity retrievals becomes very obvious when we consider the consistency and uncertainty in the raw hygroscopic growth curves determined from different droplets evaporating into differing RHs. Droplets drying into different RHs reach different compositions at different times, and will retain different amounts of water because of different drying rates. This leads to an artificially low MFS at a particular RH which then slowly returns to the equilibrium curve overtime. Thus, an inconsistency is apparent between retrieved hygroscopic growth curves (or MFS vs  $a_w$ ) when drying into different RHs. An example of this is shown in Figure S39.1, where we report unbinned hygroscopicity data for alanine (a non-viscous amino acid) and trehalose (viscous at RHs lower than 80%). It is clear here that the different portions of the hygroscopic curves retrieved from measurements at different RHs are consistent for alanine but not for trehalose. A further easy way to identify this retention of water in a particle that is not fully

equilibrated is simply to measure the much longer time-dependence in size once the initial evaporation of water has stopped. In droplets that have reached a bulk diffusion limitation, the existence of a kinetic limitation is apparent in a steadily decreasing size as water continues to leave over a timescale longer than 10 s.

**Fig S39.1 a) Unbinned hygroscopicity data for the compound alanine. b) Unbinned hygroscopicity data for the compound trehalose. At 50 % RH trehalose has a viscosity of  $3.8 \times 10^5$  Pa.s (Song et al. 2016).**



Secondly, we can determine the expected conditions under which we might expect problems to arise in retrieving hygroscopic growth curves from an evaporation measurement. Considering again trehalose at 80 % RH, an aqueous-trehalose droplet has a viscosity of 0.5 Pa.s, increasing to  $3.8 \times 10^5$  Pa.s at 50 % RH (Song et al. 2016). Therefore, as the RH of the gas phase for the evaporation measurement is lowered, we can expect the increasing viscosity/decreasing diffusivity to become increasingly important. By contrast, for aqueous-carboxylic acid droplets, the viscosity never gets above 1 Pa s even at the driest RHs considered here (Song et al. 2016).

With these known dependencies of viscosity on water activity, we can estimate the timescale for diffusional mixing within a droplet, assuming that this provides an estimate of the timescale for an evaporating droplet to form a homogeneous mixture. This timescale must be considerably shorter than the evaporation timescale for our hygroscopicity estimations to be valid. First, the Stokes-Einstein equation is used to estimate the diffusion constant of water at varying viscosity (varying RH).

$$D = \frac{k_B T}{6\pi r_{mol} \eta} \quad (1.1)$$

$D$  is the diffusion constant,  $k_B$  is the Boltzmann constant,  $T$  is temperature,  $r_{mol}$  is the molecular radius of water (taken as  $1.375 \text{ \AA}$ ) and  $\eta$  is the viscosity. It should be noted that equation (1.1) is likely to provide a significant underestimate of the diffusion constant due to the failure of the Stokes-Einstein equation. At a viscosity of 100 Pa s, the diffusion constant for water in sucrose is already more than one order of magnitude larger than estimated from the viscosity (Power et al. 2013). However, using diffusion constants estimated from (1.1) will provide an upper limit on the diffusional mixing timescale. The timescale for diffusional mixing,  $\tau$ , is then estimated using the expression

$$\tau = \frac{a^2}{\pi^2 D} \quad (1.2)$$

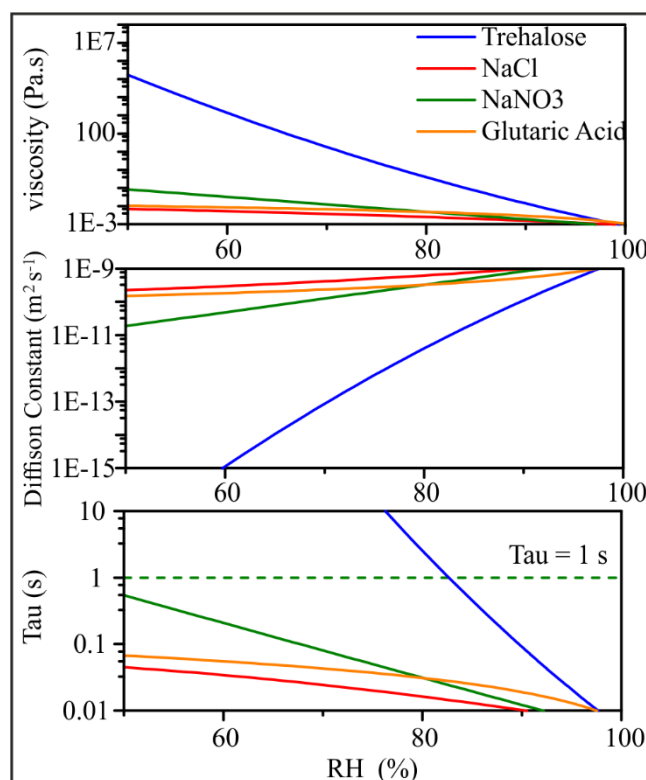
where  $a$  is the droplet radius (set as 10 microns in this calculation).

We compare the diffusional mixing timescales for aqueous droplets of trehalose, NaCl, NaNO<sub>3</sub> and glutaric acid in the newly added supplemental Figure S39.2 (and repeated below). Given that we have been able to report accurate hygroscopic growth curves for NaNO<sub>3</sub> down to 50 % RH (see Rovelli et al. 2016 and the

response to referee 2), it is clear that a final viscosity at 50 % of  $\sim 0.1$  Pa.s (Baldelli et al.) is insufficient to impede accurate measurement of the hygroscopicity. Indeed, this suggests that water transport in any aerosol droplet that maintains a viscosity lower than 0.1 Pa.s during drying should remain sufficiently fast to avoid a bulk diffusion limitation, permitting accurate hygroscopicity measurements. As an example of the diacarboxylic acids considered in this study, glutaric acid has a considerably lower viscosity at 50 % RH of  $\sim 0.01$  Pa.s (Song et al. 2016), indicative of what we might expect for all such similar systems. By contrast, aqueous-trehalose droplets cross the 0.1 Pa.s viscosity threshold at a water activity of  $\sim 0.85$  (Song et al. 2016), commensurate with the deviation and increased scatter in the hygroscopicity measurements reported above for this compound.

Based on the two considerations above and to indicate clearly the water activity ranges over which we consider the hygroscopicity measurements to be valid for trehalose (S30), galactose (S31) and sorbitol (S29), we have added a dashed line to indicate where the data appear to become kinetically limited. We have added the following words to the captions of these Figures: “Data taken at RHs lower than indicated by the dashed black line show increased error in hygroscopicity retrieval due to the imposition of a kinetic limitation on water transport.”

**Fig S39.2 a) Viscosity of Trehalose, NaCl, NaNO<sub>3</sub> and Glutaric Acid as a function of RH. b) Estimated diffusion constant as a function of RH. c) Timescale for diffusional mixing at the RH shown on x-axis. Dashed green line represents 1 second timescale for diffusional mixing.**



A. Baldelli, R. M. Power, R. E. H. Miles, J. P. Reid and R. Vehring *Effect of crystallization kinetics on the properties of spray dried microparticles*, *Aerosol Science and Technology*, 2016, 50:7, 693-704, DOI:10.1080/02786826.2016.1177163

R. M. Power, S. H. Simpson, J. P. Reid and A. J. Hudson, *The transition from liquid to solid-like behaviour in ultrahigh viscosity aerosol particles*, *Chemical Science*, 2013, 4, 2597, DOI: 10.1039/c3sc50682g

Y. Chul Song, A. E. Haddrell, B. R. Bzdek, J. P. Reid, T. Bannan, D. O. Topping, C. Percival, and C. Cai *Measurements and Predictions of Binary Component Aerosol Particle Viscosity* *J. Phys. Chem. A* 2016, 120, 8123–8137, DOI: 10.1021/acs.jpca.6b07835

### S40 Differences between Cyclic and Open Chain Sugar Conformer Thermodynamic Predictions

**Table S40.0: Table of UNIFAC groups for cyclic and open chain galactose and xylose.**

Compound	Open Chain (In Manuscript)	Cyclic
Galactose	$\text{CHO}(\text{CH}_1^{(\text{OH})})_4\text{CH}_2^{(\text{alc})}(\text{OH})_5$	$(\text{CH}^{[\text{alc}]})_4(\text{CH}_2^{[\text{OH}]})_1(\text{CHO}^{[\text{ether}]})_1(\text{OH})_4$
Xylose	$(\text{CH}_2(\text{OH}))_3\text{CH}_2^{(\text{alc})}\text{CHO}(\text{OH})_4$	$(\text{CH}^{[\text{OH}]})_4(\text{CHO}^{[\text{ether}]})_1(\text{OH})_4$

**Figure S40.0 Galactose and Xylose CK-EDB data as a function of MFS and water activity compared with predictions for both cyclic and open chain UNIFAC group thermodynamic predictions**

